

ELECTRON TRANSPORT AND TRAPPING

IN CRYSTALLINE SULPHUR

A thesis submitted to the

University of Leicester

by

David John Gibbons, M.A., M.Sc.

for the degree of Doctor of Philosophy

in the Faculty of Science

1965

BEST COPY

AVAILABLE

TEXT IN ORIGINAL IS
CLOSE TO THE EDGE OF
THE PAGE

CONTENTS

Abstract	4
Acknowledgments	6
<u>1. Introduction</u>	7
1.1 Structure and Properties of crystalline sulphur	11
1.2 Hole mobility and photoconductivity in orthorhombic sulphur	15
1.3 Electron mobility	19
<u>2. Theoretical treatment of transport mechanisms</u>	23
2.1 Theories of hopping conduction	23
2.1.1 Introduction	23
2.1.2 Limits of validity of band picture	24
2.1.3 The small polaron	28
2.1.4 Impurity band conduction and hopping between impurity centres	37
2.1.5 Comparison between hopping theories	38
2.1.6 Mobility on hopping model	40
2.1.7 Limits of applicability of various analyses	41

2.2	Release time from traps on hopping model	44
2.3	Trap-controlled mobility	48
2.4	Trap-controlled mobility in presence of point defects	51
<u>3.</u>	<u>Band widths in terms of molecular orbital theory</u>	<u>56</u>
3.1	Bonding in the sulphur molecule	56
3.2	The S ₈ molecular ions	66
3.3	Determination of orbital overlaps	68
3.4	Band widths in orthorhombic sulphur	71
<u>4.</u>	<u>Experimental methods</u>	<u>78</u>
4.1	Methods of crystal growth	78
4.2	Preparation of crystal specimens for transport and glow curve measurements	82
4.3	Electron and hole mobility measurements	85
4.3.1	Principle of the method used for measuring mobility	86
4.3.2	Electron mobility measurements	90
4.3.3	The electron gun	92
4.3.4	The specimen holder	94

4.3.5	The pulse equipment	96
4.3.6	The master pulse and field unit	98
4.3.7	Photoexcitation	100
4.4	Determination of electron lifetime by interrupted transits	102
4.5	Thermally stimulated conductivity	104
4.6	Depolarization measurements by space-charge probing	107
<u>5.</u>	<u>Experimental results</u>	<u>108</u>
5.1	Experimental results for electron mobility	108
5.1.2	Temperature dependence of mobility in (111) direction	110
5.1.3	Temperature dependence of mobility in principal directions	112
5.1.4	Electron mobility in region of monoclinic transition	113
5.2	Experimental results on transient space-charge limited currents	115
5.2.1	Accuracy of mobility determinations from transit time	121
5.2.2	Transient SCL currents in presence of trapped carriers	122
5.3	Experimental results for electron lifetime with respect to deep traps by interrupted transits	123
5.3.1	Temperature dependence of electron lifetime	125

5.4	Study of trap near 0.95 eV by polarization decay	127
5.5	Experimental results for thermally stimulated conductivity	130
5.6	Exciting molecular vibrational modes using a laser beam	135
6.	<u>Discussion of Experimental Results</u>	137
6.1	Interpretation of the Electron mobility results on a trap- controlled model	138
6.2	Trap-controlled mobility in presence of thermally generated point defects	140
6.3	Interpretation of the electron mobility results on a hopping model	143
6.4	Discussion of trapping phenomena	153
7.	<u>Conclusions</u>	156
Appendix:	Analysis of starting materials	159
References		161
Diagrams*		

* For the convenience of the reader a number of simple diagrams are included in the text. As a result, the figure numbers at the end are not all consecutive.

Abstract

Drift mobility techniques have been used to measure the transport of generated electrons in single crystals of orthorhombic sulphur grown from solution. The drift mobility was found to be the same for more than 20 specimens grown from starting materials of different degrees of purity, despite large differences in hole mobility measured on the same specimens. At 21°C, $\mu_e = 6.2 \times 10^{-4} \text{ cm}^2 \text{ V}^{-1} \text{ sec}^{-1}$ and was found to increase with temperature as $\exp(-\epsilon_a/kT)$, where $\epsilon_a = 0.167 \text{ eV}$. μ_e exhibited no measurable anisotropy. The transformation to the monoclinic modification is accompanied by a fall in mobility by a factor of about ten and an increased density of deep traps. The electron mobility results are shown to be consistent with an intermolecular hopping mechanism in which the electron interacts with one or more molecular vibrational modes. It is believed that this is the first time a strong case for a true hopping current has been presented. The polaron binding energy is shown to be 0.48 eV and the dimensionless electron-lattice interaction parameter, $\gamma \sim 18$.

The isolated S_8 molecule and its ions are examined theoretically in terms of molecular orbital theory and the study is extended in an estimate of the electron and hole bandwidths in the solid by an approximate method. A number of intramolecular and intermolecular orbital overlaps are calculated and the results are used in a discussion of the electron mobility.

The electron free lifetime at the surface and in the bulk was studied by a novel method involving interrupted electron transits.

The trapping spectrum was investigated by thermally stimulated conductivity and by an electron beam probing technique which was used to study the polarization decay. The results lend support to the hopping interpretation of electron transport.

A subsidiary study of space-charge perturbed electron currents provides experimental confirmation of a recent theoretical treatment by Papadakis.

Acknowledgments

The author would like to express his thanks to Professor E.A. Stewardson for the opportunity to work in his department.

It gives him great pleasure to record his appreciation of the active guidance and friendly encouragement generously given by Dr. W.E. Spear throughout the present investigation. He would also like to thank Dr. A.R. Adams for many useful discussions.

The author is grateful for a Senior Research Fellowship from the Xerox Corporation of America during the tenure of his stay.

1. Introduction

Sulphur is a particularly good example of an elemental molecular solid and it is surprising that in the past very little experimental work on the more fundamental aspects of charge transport in this material has been undertaken. In comparison with the polyphenyls, such as naphthalene and anthracene, and the charge transfer complexes, which have received far more attention, elementary crystalline sulphur should present a simpler material for a study of this interesting class of insulating solids. Recent work on the transport of generated holes and on the optical absorption and photoconductivity has stimulated renewed interest in orthorhombic crystals. It therefore seemed relevant to investigate the electron transport and also to attempt an interpretation of the experimental results from a fundamental point of view.

The aim of the present work was to investigate the transport and trapping of generated electrons in single crystals of sulphur grown

from solution, and to carry out a detailed analysis of the experimental results in terms of existing theories applicable to molecular solids.

After briefly reviewing the structure and properties of crystalline sulphur, a summary of previous work on carrier transport and photoconductivity is given in section 1.

An account of the various theoretical treatments of transport mechanisms in low mobility solids, with particular reference to theories of hopping conduction, is presented in section 2. A number of subsidiary results based on a hopping model are also derived. The implications of using a trap-controlled mobility model are examined, especially for the case where trapping centres are thermally generated point defects.

The groundwork for a more extensive band structure calculation is laid out in section 3. Bonding in the isolated S_8 molecule and in its ions is discussed in terms of molecular orbital theory, and a

number of molecular orbital overlaps are calculated. An approximate method is used to obtain an order of magnitude for the electron and hole bandwidths.

In section 4, the experimental methods are outlined. The way in which the crystals were grown and prepared for subsequent transport measurements is described and an account is given of the equipment used in the study of mobility and trapping effects.

Section 5 is devoted to experimental results for the temperature dependence and anisotropy of electron mobility. The same section includes the results for the electron free lifetime measured by interrupted transits. Further experimental investigations of deep electron trapping by conductivity glow curves and by depolarization techniques are described.

In section 6, the experimental results are discussed in terms of theories of hopping conduction and of trap-controlled mobility. A number of models are tested and it is shown that an intermolecular hopping mechanism provides the most consistent interpretation of the experimental results. From the analysis, a number of model parameters are derived and a comparison is made between these results and those estimated from the molecular orbital treatment.

1.1 Structure and Properties of Crystalline Sulphur

Orthorhombic sulphur, or S_8 , is the stable allotropic form at temperatures below 96°C . Large natural crystals can be found in volcanic regions widely distributed throughout the world and artificial crystals of high quality may be readily obtained from solution in the laboratory. The common crystallographic forms are shown in Fig.1.1.

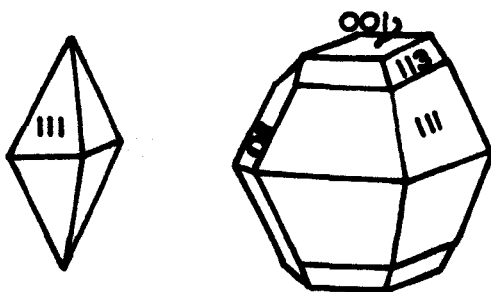


Figure 1.1

The most frequently occurring habit is the bipyramid, with well developed (111) faces, although the second pyramid, (113), the basal pinacoid, (001), and the brachydome (011) are common. The crystals are soft, ($H = 2$ on Moh's scale), and cleavage in the (001), (110), and (111) planes is imperfect. At room temperature their colour is pale yellow but as the temperature is raised the colour deepens. The high

coefficient of expansion ($\sim 70 \times 10^{-6}$) renders the crystals liable to fracture if subject to thermal shock and a good quality crystal may be easily damaged merely by being picked up between fingers.

Above 96°C at atmospheric pressure, orthorhombic crystals undergo a phase transformation to the tabular or acicular monoclinic allotrope known as S_{β} . The transformation is very slow and is frequently accompanied by a cloudiness developing in the crystal. If the heating is rapid the orthorhombic crystals may melt before the transformation takes place. The melting point of orthorhombic sulphur is 112.9°C and that of the monoclinic modification, 119.0°C .

Another allotropic modification, metastable at room temperature, is an orange-yellow rhombohedral variety known as Aten's sulphur, or Engel's sulphur. It is prepared by rapid solvent extraction of sulphur from the precipitate which is formed when a mineral acid is added to sodium thiosulphate solution. It reverts slowly to S_{β} at room temperature

in the course of a few days. Recent X-ray crystallographic studies (1961) by Caron and Donahue have shown it to be composed of S_6 molecules.

Warren and Burwell (1935), using X-ray diffraction techniques, showed the unit cell of S_8 to consist of a close packed structure of sixteen identical S_8 molecules. More refined measurements by Abrahams (1955) and a subsequent analysis by Caron and Donahue (1961) have provided accurate unit cell dimension and reliable parameters for the S_8 molecule. A simplified diagram of the unit cell and a photograph of a model of the structure are shown in figures 1.2 and 1.3 respectively.

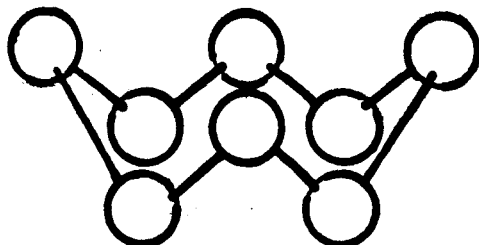


Figure 1.4

The S_8 molecule, (figure 1.4), is in the form of an eight membered puckered ring. The bond angle is $107^{\circ}54' \pm 36'$ and the torsional angle round the ring $98^{\circ}37' \pm 2^{\circ}9'$. The nearest neighbour distance round the ring is $2.048 \pm .002 \text{ \AA}$. Each molecule in the solid has eleven van der Waal's contacts, two of 3.33 \AA , four of 3.49 \AA , two of 3.63 \AA , one of 3.69 \AA and two of 3.74 \AA . These distances compare with the generally assigned van der Waal's diameter of about 3.7 \AA .

The crystal belongs to the orthorhombic holohedral class, mmm. At 25°C the unit cell dimensions were determined to be $a = 10.467 \pm .001 \text{ \AA}$, $b = 12.870 \pm .001 \text{ \AA}$, $c = 24.493 \pm .003 \text{ \AA}$. The unit cell belongs to space group $D_{2h}^{24} - Fddd$, the symmetry operations of which are three mirror glide planes at right angles with a translation of $\frac{1}{4}$ of the lattice spacing each way. According to Scott, McCullough and Kruse (1964) all molecular vibrations are active in the crystal although those not active in the isolated molecule would be expected to have very low intensity in the spectra of the crystal.

1.2 Hole Mobility and Photoconductivity in Orthorhombic Sulphur

The photoconductive and transport properties of orthorhombic sulphur seem to have received comparatively little attention. The only reliable transport measurements of holes are those reported by Adams and Spear, (1964). These authors measured the drift mobility of generated holes in artificial crystals grown from solution in CS_2 . The room temperature lattice mobility was found to be $10 \text{ cm}^2 \text{ V}^{-1} \text{ sec}^{-1}$ and the lifetime of holes with respect to deep traps was in the region of 10^{-5} sec. At lower temperatures the drift mobility became an activated process where the generated holes interacted with centres lying 0.19 eV above the valence band. Mobility values at room temperature ranged over two orders of magnitude and the corresponding density of these centres lay between 4×10^{14} and 10^{17} cm^{-3} for the various crystals. With increasing temperature a transition to a lattice controlled mobility was found. Figure 1.5 shows the experimental results for hole mobility as a function of temperature. Experimental evidence was presented to show that the

hole traps were probably associated with included solvent molecules. At temperatures above 96°C the transition to monoclinic sulphur was accompanied by a fall in hole mobility by a factor of about 30.

The data normally quoted for the photoconductive and optical properties of sulphur are based on the work of Kurrelmeyer (1927), and of Tartakovsky and Rekalova (1940). Figure 1.4 shows the spectral sensitivity of the photoconductivity obtained by these authors. A smooth response curve is shown which begins to rise at $6,500 \text{ \AA}$, reaches a maximum at $4,700 \text{ \AA}$ and then decreases steeply at shorter wavelengths. More recent work by Mead, (1964) and Spear and Adams (1965) extended the spectral range of the measurements and brought out the remarkable photoconductive response in the ultra-violet.

The large difference between the mobility of holes and electrons, to be described in later sections of this thesis, enabled Spear and Adams to investigate the optical generation efficiencies of holes and electrons separately by using pulse techniques. Their results are in substantial

agreement with the less detailed steady current measurements by Mead, (1964). Figure 1.7 shows the spectral dependence of absorption and the quantum efficiencies for generating both electrons and holes. The response falls into two parts; in the visible region, the hole response is similar to that reported by Kurrelmeyer; at $3,400 \text{ \AA}$ the ultra-violet hole response rises more rapidly than the absorption edge to another peak at $2,550 \text{ \AA}$ about four orders of magnitude larger than the response in the visible. The electron response behaves differently; at long wavelengths the generation efficiency is very small and, as the photon energy is increased, the quantum yield rises with the absorption edge before reaching a shoulder. At higher energies the hole and electron responses rise more or less together to near unit quantum efficiency.

An examination of the induced current pulse shape showed that throughout the range, carrier generation occurred only at the surface. The long wavelength hole response was ascribed to photon induced transitions between the valence band and filled localized surface states. In the

intermediate region the electron response was explained in terms of the interaction of excitons with deep donor states or filled electron traps at the surface.

The near unit quantum efficiency for both electrons and holes at 2,550 Å arises from direct band to band transitions. Careful analysis showed that the previously quoted value for the band gap of 2.6 eV based on the photoconductivity and absorption measurements by Kurrelmeyer must be rejected in favour of a value between 4.2 and 4.3 eV. Optical absorption near 2,500 Å is due to free carrier generation and, at slightly lower energies, the strong optical absorption may be attributed to exciton generation. The shape of that part of the absorption curve ascribed to exciton formation was consistent with a model by Toyozawa (1964) in which the exciton interacted linearly with lattice or molecular vibrational modes.

1.3 Electron Mobility

The background of previous work on electron conduction in sulphur presents a very confused picture. In 1948 von Hippel discussed the structure and conductivity in orthorhombic sulphur and used qualitative arguments to show that holes would not participate in the conduction process but that, after excitation, electron conduction should be possible.

On the basis of α -particle counting experiments in sulphur crystals Dean et al. (1960) made estimates for the mobility of electrons. Interpretation of these results was based largely on the assumption that this would be the only mobile carrier. They were able to assign a lower limit of $\mu = 0.1 \text{ cm}^2 \text{V}^{-1} \text{sec}^{-1}$ for the carrier mobility but it is not altogether clear now from their experiments whether or not this value should apply to electrons or holes.

The predictions of von Hippel were not substantiated by Adams and Spear (1964) who were able to observe the transport of generated

holes but not that of electrons. These authors used drift mobility techniques and hole transits up to $8\mu\text{sec}$ were observed by charge integration. Under these conditions no signal that could be associated with the drift of generated electrons was detected when the applied field was reversed. The lifetime of electrons with respect to deep traps was estimated to be less than 5×10^{-9} sec.

The preliminary results of the present investigation were published in 1964 and a reprint of the paper is included in the back cover of this thesis. Since publication, the results of two further independent investigations of electron transport in sulphur have appeared.

Transient space-charge limited current techniques were employed by Many et al., (1965), to study electron transport in natural single crystals. The electron mobility was found to be $6 \times 10^{-4} \text{ cm}^2 \text{ V}^{-1} \text{ sec}^{-1}$ at room temperature and to increase with temperature as $\exp(-\frac{0.2}{kT})$ in the range $250^\circ - 340^\circ \text{K}$. At higher temperatures the mobility

tended to level off at a value of about $2 \times 10^{-3} \text{ cm}^2 \text{V}^{-1} \text{sec}^{-1}$. It was concluded that the activation energy was associated with a trap dominated process, and an approximate value for the lattice mobility of $\mu_L = 2 \times 10^{-3} \text{ cm}^2 \text{V}^{-1} \text{sec}^{-1}$ was obtained. Theoretical reasons why this interpretation is not acceptable are given in sections 2.1.2 and 6.1.

The recent paper by Thornber and Mead, (1965), describes results for electron mobility in S_2 using drift mobility techniques. From their experiments they concluded that the electron mobility for various crystals lay in the range $0.4 - 4.5 \text{ cm}^2 \text{V}^{-1} \text{sec}^{-1}$ for applied fields below 10^4 V.cm^{-1} . These results were interpreted on a model of trap-controlled mobility. Two types of electron conduction were reported however and, in the same crystals, parallel transport in an "impurity band" could be observed at applied fields above 10^4 V.cm^{-1} . The measured values of μ_e within this band ranged from 9×10^{-5} to $1.2 \times 10^{-3} \text{ cm}^2 \text{V}^{-1} \text{sec}^{-1}$ at room temperature.

The results of Many and of Thornber are discussed in the light of the results obtained in the present investigation in Section 6.

2. Theoretical Treatment of Transport Mechanisms

2.1 Theories of Hopping Conduction

2.1.1 Introduction

A molecular crystal, such as sulphur, is characterized by strong covalent bonds between the atoms of which the molecules are composed and by very much weaker van der Waal's forces binding the molecules together. The intermolecular orbital overlaps are quite small relative to those in ionic or covalent solids and as a consequence the perturbations of the molecular energy levels by neighbour interactions are considerably reduced. Narrow bands are therefore to be expected in these crystals and the electron wavefunctions will be strongly centred on the molecular cores. Because of its localization, it is possible, although not necessary, for the electron to interact strongly with molecular or lattice vibrational modes. Consequently it may no longer be possible to treat these interactions as a small perturbation on the purely electronic band structure as in normal scattering theory. If the interactions are strong, then they must be treated in zero order

and the periodic lattice potential treated as a perturbation.

Carrier transitions to neighbouring sites may no longer be correlated in a wavelike manner and the band structure may be destroyed. The carrier proceeds then by a series of random phonon assisted site jumps, or "hopping".

It is constructive to examine the limits within which band motion and hopping would be expected to occur. In the following discussion, fundamental limitations arising from the uncertainty principle are used to indicate the range of applicability of the two approaches to carrier transport. Two slightly different formulations are employed and it is shown how they both lead to a similar limit.

2.1.2 Limits of Validity of Band Picture

The requirements of Heisenberg's uncertainty principle are of fundamental importance in connection with transport within a narrow band. One criterion for the band approach to be a good one is that

the uncertainty in the energy of a carrier due to scattering by lattice vibrations should not exceed the bandwidth, W .

$$\text{Thus} \quad W \geq \frac{\hbar}{\tau} \quad (2.1)$$

where τ is the scattering relaxation time. This enables a lower limit to be set on mobility for the band theory of conduction to apply.

$$\text{Since} \quad \mu = \frac{e}{m} \tau \quad (2.2)$$

inequality (2.1) yields

$$\mu \geq \frac{\hbar}{m \cdot W} \quad (2.3)$$

In terms of the Bloch tight binding scheme applied to a simple cubic lattice of period a , the energy, $E(k)$, of a carrier with propagation vector k is given by

$$E(k) = -2J(\cos k_x \cdot a + \cos k_y \cdot a + \cos k_z \cdot a) \quad (2.4)$$

where J is the exchange energy between an atom and one of its nearest neighbours, and k_x , k_y , k_z are the components of k along the principal axes of the crystal, (see, for example, Dekker, p257).

The zone limits are given by k_x , k_y , $k_z = \pm \frac{\pi}{a}$ and the bandwidth is simply

$$W = 12J \quad (2.5)$$

On the same model, the carrier effective mass at the band edge

is given by

$$\frac{1}{m^*} = -\frac{1}{\hbar^2} \frac{\partial^2 E(k)}{\partial k^2} = \pm \frac{2}{\hbar^2} J a^2 \quad (2.6)$$

We can then write $\frac{1}{m^* W} = \frac{a^2}{6 \hbar^2}$ and by substitution in inequality

(2.3) obtain

$$\mu \geq \frac{e a^2}{6} \quad (2.7)$$

For $a = 6 \text{ \AA}$, (approximately the average spacing between molecules in the case of the S_{α} lattice), this leads to mobilities in the region of $1 \text{ cm}^2 \text{ V}^{-1} \text{ sec}^{-1}$ as a lower limit for the band approach to apply.

An alternative formulation by Fröhlich and Sewell, (1959), takes into account the requirement that the electron within the band must have a mean kinetic energy which is larger than the uncertainty in energy resulting from the scattering process.

$$\begin{aligned} \text{Thus } (3/2)kT &\geq \frac{\hbar}{\tau} \\ &= \frac{e \hbar}{m^* \mu} \end{aligned} \quad (2.8)$$

If μ is expressed in $\text{cm}^2 \text{V}^{-1} \text{sec}^{-1}$ equation (2.8) leads to

$$\mu \geq \left(\frac{30}{m^*} \right) \cdot \frac{300}{T} \quad (2.9)$$

Inequality (2.9) is only valid when the bandwidth is not too small and thus the effective mass, m^* , is not too large. In terms of the tight binding scheme, the maximum velocity in a band, v_{max} , is given by

$$v_{\text{max}} = - \frac{1}{\hbar} \left(\frac{\partial E(k)}{\partial k} \right)_{k = \frac{\pi}{2a}} = \frac{W a}{6 \hbar} \sim \frac{W S}{k_{\text{D}}} \quad (2.10)$$

Here the lattice spacing a , is expressed in terms of the sound velocity, s , and the Debye temperature, Θ .

Whenever $v_{\text{max}} < s$, i.e. $W \lesssim k_{\text{D}}$, then absorption and emission of single acoustic phonons becomes impossible and the normal theory of acoustic phonon scattering of carriers within a band can no longer be applied. This limitation implies that, for normal band motion to prevail,

$$\frac{m^*}{m} \lesssim \frac{\hbar}{s a m} \quad (2.11)$$

Taken in conjunction with inequality (2.9) this leads to

$$\mu \geq \frac{30.s.a.m.}{\hbar} \cdot \frac{300}{T} \quad (2.12)$$

and with typical values of 3×10^5 cm.sec⁻¹ for s and 6 \AA for a

we obtain

$$\mu \geq \frac{30}{T} \quad (2.13)$$

A similar limitation is thus imposed where room temperature mobilities in the region of $0.1 \text{ cm}^2\text{V}^{-1}\text{sec}^{-1}$ would represent the lower limit for which the band approach is applicable.

2.1.3 The Small Polaron

When the bandwidth is small, the carrier may remain in the region of a lattice site for a time long compared with the period of lattice vibrations. As a result of electron lattice interaction, the surrounding lattice particles will be displaced to new equilibrium positions corresponding to a reduction of the total energy of the system. The induced lattice distortion will thus produce a potential well for the electron and, if the well is sufficiently deep, the electron

will occupy a bound state. The electron and its region of lattice distortion cannot move independently and any subsequent motion of the electron will be accompanied by the lattice deformation. The electron with its region of lattice distortion is known as a polaron.

Motion of a polaron in a band can occur when the distortion in band structure due to electron-lattice interaction is small compared with the electronic bandwidth. An analysis applied to a simplified model consisting of a linear chain of diatomic molecules by Siebrand (1964), following earlier work by Holstein, (1959), shows that the main result of electron lattice interaction is to reduce the polaron bandwidth. Yamashita and Kurosawa, (1958), showed that the wavefunction of a polaron could be expressed as the product of an electronic and a vibrational wavefunction. They showed that vibrational overlap integrals, (or Franck-Condon integrals,) entered the expression for the intermolecular exchange term for every mode of oscillation with which the electron interacts. Dispersion of vibrational frequencies is thus essential for carrier motion to take place.

A simple model was used by Friedman (1964), to demonstrate self-trapping due to the Franck-Condon effect, within the limits of approximation used by the above authors. Figure 2.2 shows the potential energy of a diatomic molecule and its negative ion as a function of the internuclear coordinate, x .

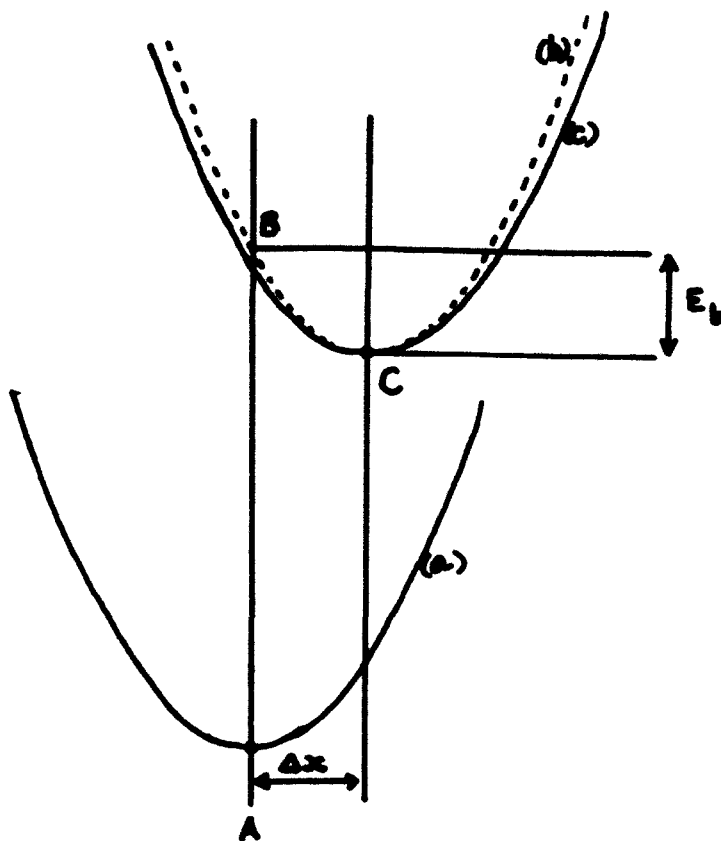


Figure 2.2

In the ground state, the atoms undergo small amplitude oscillations of frequency ω_0 about point A. The force constant, K , in the range of interest is assumed to be independent of x , and in terms of the reduced mass of the system, M ,

$$K = M \omega_0^2 \quad (2.14)$$

Curve b is the potential energy curve for the negative molecular ion; it is observed that the minimum at C is displaced relative to A by an amount Δx . Upon ionization, the internuclear separation will follow the path from B to C on curve b and the energy of the system will be reduced. If it is assumed that K is unchanged upon going from the neutral molecule to the negative molecular ion, then the configurational diagram of the molecular ion can be represented by (c) which has the same shape as (a). Under these conditions the polaron binding energy will be given approximately by

$$E_b = \frac{1}{2} K (\Delta x)^2 \quad (2.15)$$

The electron lattice interaction can now be described in terms of a dimensionless electron-lattice interaction parameter, γ , defined by

$$\gamma = E_b / \hbar \omega_0 \quad (2.16)$$

The purely electronic bandwidth, W , is reduced by vibrational interaction to Wx^F , where, at low temperatures,

$$F = \exp(-\gamma) \quad (2.17)$$

and at higher temperatures,

$$F \approx \exp \left[-\gamma \left(1 + \frac{2kT}{\hbar \omega_0} \right) \right] \quad (2.18)$$

It is clear from equation (2.18) that F , and therefore the polaron bandwidth decreases with increasing temperature.

If the polaron bandwidth is progressively reduced by vibrational interactions, a point will be reached where scattering introduces an uncertainty in the energy of the polaron comparable with the bandwidth. Band motion can no longer occur and the carrier will then proceed by a random hopping motion.

Yamashita and Kurosawa (1958), used time dependent perturbation theory to calculate transition probabilities of a carrier to a neighbouring molecular site. They considered only those transitions for which the vibrational quantum number of the molecule changed by ± 1 , and found that the transition probability was an increasing function of temperature. Their result is expressed in terms of the

modified zero order Bessel function,

$$I_0(z) = \frac{1}{2\pi} \int_0^{2\pi} \exp(z \cdot \cos x) dx \quad (2.19)$$

and the transition probability, P_Y , is given by

$$P_Y = \frac{2\pi}{\hbar} J^2 \left\{ -2\gamma(2s+1) \right\} \times I_0 \left\{ 4\gamma[s(s+1)]^{1/2} \right\} \quad (2.20)$$

where J is the intermolecular exchange energy between adjacent

molecules and $\frac{1}{s} = \exp\left(\frac{\hbar\omega_0}{kT}\right) - 1$. Here γ has the meaning already

defined by equation (2.16).

A similar calculation by Holstein (1959), considered transitions both where the vibrational quantum number changed by ± 1 and where the vibrational quantum number was unchanged. These were called 'non-diagonal' and 'diagonal' transitions respectively. It was shown that for temperatures below about half the Debye temperature, the diagonal transitions predominated and band motion occurred; the bandwidth was found to increase with decreasing temperature. Above this temperature, ($\sim \frac{\Theta}{2}$), non-diagonal transitions dominated and hopping transport occurred in which the transition probability increased

with temperature. Holstein obtained for the transition probability to neighbouring sites in the hopping region,

$$P_H = \frac{\omega_0 J^2}{\hbar^2 \omega_0^2} \left[\frac{2\pi}{2J \cos \theta \sinh \left(\frac{\hbar \omega_0}{2kT} \right)} \right]^{\frac{1}{2}} \exp \left[-2\gamma \tanh \frac{\hbar \omega_0}{4kT} \right] \quad (2.21)$$

where the symbols have the same meaning as given before.

Figure 2.3 demonstrates the expected variation of diffusion coefficient according to Holstein's analysis, plotted as a function of T^{-1} . As is shown in section 2.1.5, the diffusion coefficient is directly proportional to the transition probability, P . The curves are plotted for representative values of the model parameters, $J = \hbar \omega_0$ and $\gamma = 10$. The way in which the shape of this curve is changed by a different choice of these parameters is discussed in section 5.3.

A somewhat different approach by Toyozawa (1962), took into account the interaction of carriers with acoustic modes. The model considered was that of an elastic continuum in which the deformation extended over only a few unit cells. This contrasts with theories of the

large polaron, applicable to ionic crystals in particular, where the deformation is largely coulombic and extends over many lattice spacings.

Toyozawa used the result of Bardeen and Shockley that the perturbing potential for a carrier due to the dilatation is given by the local change in energy at the bottom of a band, $V(r) = E_d \cdot \Delta x$, where

Δx is the dilatation and E_d is the deformation constant. It was shown that if the electron-lattice coupling is large, localized states below the conduction band edge would arise. Two types of transport distinguished as hopping and drift motion, were discussed.

Figure 2.4 shows the relative positions of the available electron energy states plotted as a function of g^{-1} where g denotes the electron lattice coupling constant. For a simple cubic crystal of lattice

period a , g is given by

$$g = (1/6) \frac{E_d^2 \cdot m^*}{\hbar^2 C \cdot a} \quad (2.22)$$

where C is the compressibility of the crystal. It may be noted that large values of g are more likely in relatively soft crystals with

narrow bands. In figure 2.4 E_t and E_a denote the ground state and first excited state of the polaron respectively.

For large values of g , ($g \gg 1.49$), i.e. strong coupling, the excited self-trapping state also lies below the conduction band.

For small values of g , ($g \ll 0.903$), the normal band picture applies.

Two types of carrier motion in which self-trapping plays a significant role were distinguished.

- (a) In the range, $g \gg 1.49$, the electron makes transitions to neighbouring sites via the excited self-trapping state. In this region the process would be essentially adiabatic and the hopping activation energy would be equal to the excitation energy of the self-trapping state.
- (b) In the range, $1.49 \gg g \gg 0.903$, the electron moves by making a transition into the band where it is free to move until again being self-trapped in a localized state. This is known as drift motion.

In the case of strong coupling, (a), the hopping activation energy is given by

$$0.184 \frac{E_d^2}{M_s^2} < \epsilon < 0.25 \frac{E_d^2}{M_s^2} \quad (2.23)$$

where M is the mass of a unit cell and s is the velocity of sound.

In the intermediate coupling range, (b), the drift mobility activation energy is given by

$$0 < \epsilon < 0.184 \frac{E_d^2}{M_s^2} \quad (2.24)$$

2.1.4 Impurity band conduction and hopping between impurity centres

Mott and Twose, (1961), showed that in a partly compensated impurity semiconductor, if the density of impurities is high, the finite overlap of wavefunctions centred at impurity ions would give rise to a narrow band in which transport might occur. At sufficiently low temperatures, transitions between adjacent impurity sites would dominate thermal activation into bands and, depending on the density of impurities and the extent of vibrational interactions, either narrow

band carrier motion or hopping motion would be observed. In the hopping region, the analysis of Yamashita and Kurosawa was used to determine transition probabilities between adjacent impurity sites where their separation was random. The analysis has been applied particularly to experimental results obtained by Morin, (1958), and Heikes and Johnston, (1957), for electron conduction in doped crystals of transition metal oxides.

2.1.5 Comparison between Hopping Theories

An important factor, common to all theories of hopping conduction, is the activation energy associated with site jump probabilities. A direct quantitative comparison can be made between the analytic expressions of Yamashita and Kurosawa and Holstein since they are both based on essentially the same model.

The expression, P_Y , equation (2.20), obtained by Yamashita and Kurosawa for the site jump transition probability can be simplified in

the limit $\frac{\gamma k T}{\hbar \omega_0} \gg 1$ by using the asymptotic expansion for $I_0(z)$ where

$$I_0(z)_{z \rightarrow \infty} = (2\pi z)^{-\frac{1}{2}} \cdot e^z \quad (2.25)$$

Thus
$$P = \frac{1}{\hbar} \left(\frac{\pi}{2\gamma \hbar \omega_0} \right) \frac{J^2}{(kT)^{\frac{1}{2}}} \exp\left(-\frac{\gamma \hbar \omega_0}{2kT}\right) \quad (2.26)$$

A similar simplification was derived by Glarum, (1963), but it is important to note that the definition of γ used by Yamashita and Kurosawa differs from that employed by Holstein by a factor 2.

Holstein's definition is equivalent to equation (2.16) and is used throughout the present discussion; where necessary, corrections have been applied to the appropriate expressions for P_Y .

Equation (2.26) agrees with the corresponding simplification of the expression, P_H , equation (2.21), derived by Holstein, using the limit expansions for the hyperbolic functions. This high temperature expansion may be simplified further if E_b is substituted from equation (2.16), thus

$$P = \frac{1}{\hbar} \left(\frac{\pi}{2E_b kT} \right)^{\frac{1}{2}} J^2 \exp\left(-\frac{E_b}{2kT}\right) \quad (2.27)$$

A comparison between the full expressions, equations (2.20) and (2.21), valid for a wider temperature range is made in Figure 2.5 where the calculated values of P_Y and P_H are plotted as a function of $E_b/2kT$ with γ as a parameter. It may be seen that the two expressions are in substantial agreement for $\gamma \geq 7.5$.

2.1.6 Mobility on Hopping Model

If the site jump probability is known, then the diffusion coefficient, D , can be obtained from elementary diffusion theory.

If the spacing between molecular planes is a , then

$$D = a^2 P \quad (2.28)$$

where P is the probability per unit time that a carrier will make a transition to a neighbouring plane in one direction.

The Einstein relation between diffusivity and mobility,

$$D = \frac{\mu kT}{e}$$

can now be used to express the hopping mobility in terms of P ; thus

$$\mu = \frac{ea^2 P}{kT} \quad (2.29)$$

In the high temperature limit, using (2.27) for the jump probability,

$$\mu = \frac{ea^2}{\hbar} \left(\frac{\pi}{2E_b} \right)^{\frac{1}{2}} \cdot \frac{J^2}{(kT)^{3/2}} \cdot \exp\left(-\frac{E_b}{2kT} \right) \quad (2.30)$$

An extension of the analysis by Holstein to a three-dimensional array of polyatomic molecules was made by Siebrand, (1964). If the unit cell has more than one molecule, then the bands will have two or more branches which may or may not be degenerate. If the number of normal modes of the molecule is greater than unity, then the total polaron binding energy is equal to the sum of the binding energies of the various modes. Thus,

$$E_{b\text{total}} = \sum E_{bn} \quad (2.31)$$

Similarly, since the interaction parameter is, $\gamma_n = E_{bn}/\hbar\omega_n$, then

$$\gamma_{\text{total}} = \sum \gamma_n$$

2.1.7 Limits of Applicability of Various Analyses

In the derivations outlined above a certain number of conditions must be satisfied for the approximations used to be valid. The temperature at which band-type motion takes over from hopping was shown

by Holstein to occur at about $\frac{\Theta_{\text{Debye}}}{2}$ and thus equation (2.21) would only be valid in the range,

$$\frac{\hbar\omega_0}{2kT} \lesssim 1 \quad (2.32)$$

A number of subsidiary conditions derived by Holstein, and complementary to the requirement that the polaron binding energy be larger than the electronic bandwidth are expressed by inequalities, (2.33) to (2.35).

$$2J < (E_b)^{\frac{1}{2}} (\hbar\omega_0)^{\frac{1}{2}} \quad (2.33)$$

$$2J \ll E_b \quad (2.34)$$

$$J < (E_b)^{\frac{1}{4}} \left(\frac{2kT}{\pi} \right)^{\frac{1}{4}} \left(\frac{\hbar\omega_0}{\pi} \right)^{\frac{1}{2}} \quad (2.35)$$

The asymptotic expansions used to obtain the high temperature approximation given by equation (2.27) requires

$$\frac{JkT}{\hbar\omega_0} \gg 1 \quad (2.36)$$

Taken in conjunction with (2.32), this implies,

$$J^2 kT \gg E_b \quad (2.37)$$

The limits of applicability of Toyozawa's model, where acoustic modes are responsible for self-trapping, are not so clearly defined,

but it was shown that the self-trapped state is only stable provided,

$$E_d^2 \geq 2nJMs^2 \quad (2.38)$$

where n is the number of nearest neighbours. The conditions under which hopping and drift motion would be expected to occur have already been discussed.

2.2 Release Time from Traps on Hopping Model

If transport of carriers is predominantly by a hopping mechanism it is possible to derive an expression for the release rate of carriers in terms of the hopping probability, P . In this model it is assumed that trapping will occur when the transition takes place from a neighbouring site to a lattice defect or impurity centre. The equations of detailed balancing may then be used to express the release rate of carriers from a trap in terms of the site jump probability, P .

Suppose we have a density of molecular sites, N_m , of which n_m are occupied by an excess electron and a density of traps, N_t , of which n_t are occupied. Figure 2.6 shows an energy level diagram for these two possible electron states.

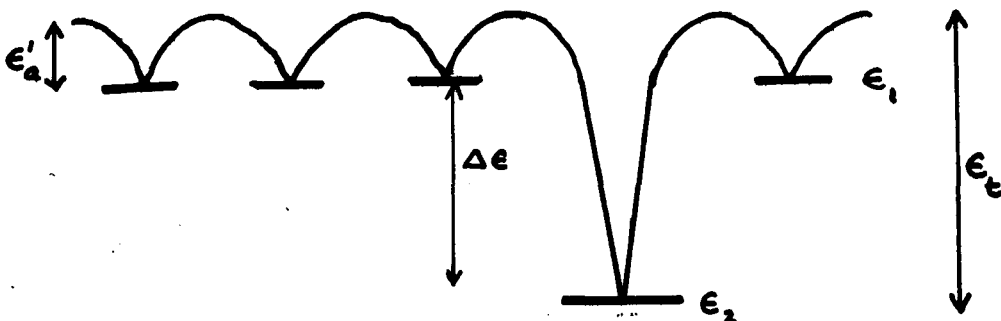


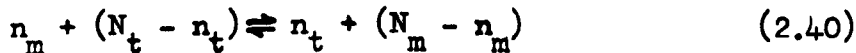
Figure 2.6

If the site jump probability into a trap is the same as that to a neighbouring molecular site, then the rate of trapping is given by

$$n_m \cdot P \cdot \frac{(N_t - n_t)}{(N_m - n_m)} \quad (2.39)$$

The rate of release of carriers from the n_t occupied traps is $A \cdot n_t$ where A is the rate constant for thermal release.

Assuming a bimolecular law for the interacting systems,



the equilibrium constant may be obtained by minimization of the free energy, (See Section 2.3).

$$\text{Thus} \quad \frac{n_m (N_t - n_t)}{n_t (N_m - n_m)} = \exp \left[- \frac{(\epsilon_1 - \epsilon_2)}{kT} \right] \quad (2.41)$$

where ϵ_1 and ϵ_2 are the energies of an electron on a molecular site and a trapping site respectively.

But from (2.39), in equilibrium

$$A n_t = n_m \frac{(N_t - n_t)}{(N_m - n_m)} \cdot P \quad (2.42)$$

and by comparison with equation (2.41) we obtain,

$$A = P \exp \left[- \frac{(\epsilon_1 - \epsilon_2)}{kT} \right] \quad (2.43)$$

Thus the thermal release time constant $\tau_r = 1/A$ is given by

$$\tau_r = \frac{1}{P} \exp \left(\frac{\epsilon_1 - \epsilon_2}{kT} \right) \quad (2.44)$$

An examination of expression (2.27) for P shows that it is of the form

$$P \propto (kT)^{-\frac{1}{2}} \exp \left(- \frac{E_b}{2kT} \right) \quad (2.45)$$

If the exponential term dominates, this can be approximated by

$$P = P_0 \exp - \left(\frac{\epsilon_a'}{kT} \right)$$

By substitution into (2.44) the thermal release time constant

will be given by

$$\tau_r = P_0^{-1} \exp \left(\frac{\epsilon_a' + \epsilon_1 - \epsilon_2}{kT} \right) \quad (2.46)$$

Thus the thermal activation energy for release from a trap is equal to $(\epsilon_a' + \epsilon_1 - \epsilon_2)$. On a simple diagram, if the molecular site is assumed to reside at a depth ϵ_a' below a "conduction level", then the activation energy for release from the trap is equal to the depth of

the trap, ϵ_t , as measured from this level, (figure 2.6)

The above analysis is applied to the interpretation of experimental results described in sections 5.7 and 5.8.

2.3 Trap Controlled Mobility

The thermal equilibrium distribution of carriers between two available energy states E_m and E_t may be derived in terms of the free energy of the carriers without invoking the mechanism by which the equilibrium is brought about. This is of importance in Section 2.2 in connection with calculating the release rate from traps and also for obtaining an expression for trap controlled mobility.

Consider the situation in which n_m electrons are distributed amongst N_m available states at energy E_m , and n_t electrons amongst N_t states at energy E_t .

The free energy, F_m , of the electrons at energy E_m is given

by

$$F_m = n_m E_m - kT \ln W_m \quad (2.47)$$

where W_m is equal to the number of ways in which the n_m electrons may be distributed among the N_m sites.

This is equal to $\frac{N_m!}{n_m! (N_m - n_m)!}$. A similar expression can

be written for the free energy of the electrons at an energy E_t .

Thus the free energy of the $n_t + n_m$ electrons is given by

$$F = F_m + F_t = n_m E_m + n_t E_t - kT \ln \left[\frac{N_m! N_t!}{n_m! n_t! (N_m - n_m)! (N_t - n_t)!} \right] \quad (2.48)$$

Using Stirling's approximation for $n!$ when n is large, the equilibrium condition may be obtained by minimizing F with respect

to n_t . Thus, by setting $\frac{\partial F}{\partial n_t} = -\frac{\partial F}{\partial n_m} = 0$,

$$\frac{n_m (N_t - n_t)}{n_t (N_m - n_m)} = \exp \left[\frac{(E_t - E_m)}{kT} \right] \quad (2.49)$$

If the drift mobility of electrons is dominated by a process in which E_m represents a state in which the electron is mobile and E_t a trapped state, then

$$\mu_{\text{drift}} = \mu \left(\frac{n_m}{n_m + n_t} \right) \quad (2.50)$$

where μ is the mobility of electrons in states E_m and the quantity in brackets represents the fraction of the time the electrons are mobile.

Hence, by (2.49)

$$\mu_{\text{drift}} = \mu \times \frac{1}{1 + \left(\frac{N_t - n_t}{N_m - n_m} \right) \exp \left(\frac{E_m - E_t}{kT} \right)} \quad (2.51)$$

If the density of carriers is very small compared with N_t and N_m ,

(which is nearly always the case in drift mobility measurements on

highly insulating solids), then

$$\mu_{\text{drift}} = \mu \times \left\{ 1 + \frac{N_t}{N_m} \exp \left(\frac{E_m - E_t}{kT} \right) \right\}^{-1} \quad (2.52)$$

A further simplification follows if the mobility is strongly trap

controlled, viz. if $N_t \exp \left(\frac{E_m - E_t}{kT} \right) \gg N_m$. Unity in the term in

brackets can then be dropped and we have

$$\mu_{\text{drift}} = \mu \times \frac{N_m}{N_t} \exp - \left(\frac{E_m - E_t}{kT} \right) \quad (2.53)$$

The mobility is thus an activated process at temperatures for

which this last approximation is valid, and as the temperature is increased

the influence of traps on mobility will become progressively unimportant,

as may be seen from an examination of equation (2.52).

2.4 Trap Controlled Mobility in Presence of Point Defects

The model to be described below was suggested by Silver, (1965), as a possible explanation of activated mobility. The derivations of a number of equations based on such an interpretation are briefly outlined here and one important condition under which the model would be expected to apply is mentioned.

The conduction process is envisaged in terms of a band model in which the electron interacts strongly with a dominant level of traps associated with point defects. If the density of defects is in thermal equilibrium at all temperatures then a modified form of the expression (2.53) for activated trap controlled mobility will result.

Consider a thermal equilibrium density, N_t , of defects at a potential energy ϵ_f higher than that of a completely ordered lattice; ϵ_f is thus equal to the heat of formation of a defect. Thus at any

temperature, T , if N_m is the density of lattice sites in the ordered state,

$$N_t = (N_m - N_t) \exp\left(-\frac{\epsilon_f}{kT}\right) \quad (2.54)$$

Provided the density of defects is not too high, this simplifies to

$$N_t = N_m \exp\left(-\frac{\epsilon_f}{kT}\right) \quad (2.55)$$

Now, if each point defect gives rise to a shallow electron trap of depth ϵ_t , the value of N_t from equation (2.55) can be used in the expression obtained for trap controlled drift mobility, equation

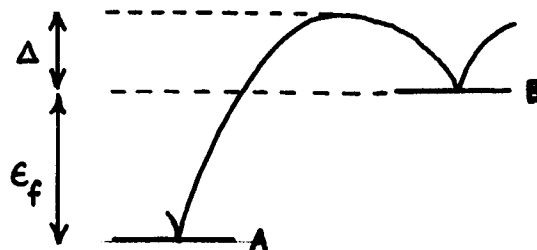
(2.53). Thus

$$\mu_d = \mu \times \frac{N_c}{N_m} \exp\left(\frac{\epsilon_t - \epsilon_f}{kT}\right) \quad (2.56)$$

It may be noted that equation (2.56) predicts that the drift mobility may either be independent of temperature or rise or fall with temperature according to whether $(\epsilon_t - \epsilon_f)$ is zero, positive or negative. If $\epsilon_f > \epsilon_t$, then the mobility will increase with temperature with an activation energy equal to the difference between the heat of formation and the trap depth.

It is constructive to examine the conditions under which such a process is likely to be observed. Clearly, in any measurements of mobility as a function of temperature it is important that a new equilibrium density of defects is established in a time short with the time interval between measurements. The kinetics of the process by which defects are formed will now be examined.

In general, the defects will represent metastable states; figure 2.7 is an energy diagram showing the potential barrier which must be overcome for a lattice site to become a point defect.



(2.7)

A represents the energy of the lattice in the completely ordered state.

The potential energy of a defect in a metastable position is shown at B where Δ is the depth of the potential well giving the defect some degree of stability.

The rate at which defects are formed thermally is given by the general kinetic equation,

$$-\frac{1}{N_m} \frac{\partial N_m}{\partial t} = \frac{1}{N_m} \frac{\partial N_t}{\partial t} = \nu \exp\left(-\frac{\epsilon_f + \Delta}{kT}\right) \quad (2.57)$$

where ν is a crystal lattice vibrational frequency.

Similarly, the rate at which defects are annealed out is given by

$$\frac{1}{N_t} \frac{\partial N_t}{\partial t} = \nu \exp\left(-\frac{\Delta}{kT}\right) \quad (2.58)$$

It may be seen that the forward and reverse rates are equal in the equilibrium condition given by (2.55).

Assuming an arbitrary initial distribution, the rate constant for establishing thermal equilibrium will be equal to the sum of the rate constants for the forward and reverse processes. Thus the time constant for establishing equilibrium will be given by

$$\tau_{\text{equil}} = \frac{1}{\nu} \left[\exp\left(-\frac{\Delta}{kT}\right) \right] \left[1 + \exp\left(\frac{\epsilon_f}{kT}\right) \right]^{-1} \quad (2.59)$$

A simplification to (2.59) is possible if the heat of formation, ϵ_f , is large compared with kT , thus,

$$\tau_{\text{equil}} \sim \frac{1}{\rho} \exp \left(- \frac{\Delta + \epsilon_f}{kT} \right) \quad (2.60)$$

The time constant for establishing an equilibrium density of defects is thus equal to the time constant for the process by which they are formed.

For this model to be applicable to a series of mobility measurements taken at different temperatures it is important that the time interval between measurements should be large compared with τ_{equil} given by equation (2.60). This criterion will be applied (Section 6.2) in the discussion of the experimental mobility results and the results of conductivity glow curve.

3. Band Widths in terms of Molecular Orbital Theory

3.1 Bonding in the Sulphur molecule.

As a first step towards a more complete understanding of the electronic structure of orthorhombic sulphur it is of value to examine the isolated molecule. Inspection of thermodynamic data shows that the single bond formation energy in S_8 is 2.72 eV , [Allen, (1959)], whereas the heat of sublimation at room temperature is only 0.13 eV per atom [Honig,(1962)]. Interactions between neighbouring molecules when they are condensed to form a solid are thus small compared with those between adjacent atoms in the molecule. We should expect a close correspondence between the electronic structure of the isolated molecule and the band structure of the solid. Further evidence that intermolecular forces play a relatively small part in determining the electronic structure is provided by infra-red absorption spectra of sulphur both in solution and in the solid state. The collected data by Scott et al,(1964), show that their molecular vibrational spectra are almost identical.

In the succeeding study, the X-ray structural determination of orthorhombic sulphur by Abrahams,(1955), and Caron & Donahue(1964) is used to provide the most accurate data for interatomic distances and the bond angles in the S_8 molecule. On the basis of these empirical data the bonding in the S_8 ring is discussed in terms of molecular orbital, (MO), theory and qualitative arguments are used to derive the electronic structure. Interatomic orbital overlaps are calculated using Slater 3s and 3p atomic wavefunctions and these results are used

in a detailed discussion of the available electron and hole states in the ionized molecule.

Sulphur atoms can form bonds in the following way. The outer shell electronic configuration of the sulphur atom is $3s^2 3p^4$ and the octet may be completed by the formation of a double bond, as in the S_2 molecule, or two single bonds, as in H_2S . Occasionally $3d$ orbitals may become involved in bond formation and the outer shell complement built up to 12 as in SF_6 . However, a normal covalency greater than two is uncommon except in the presence of strongly electronegative atoms such as F and O due to the large promotion energy usually associated with the use of d -orbitals.

The bond angle of 108° and the S-S bonding distance in S_8 of 2.048 \AA are very close to the tetrahedral angle of $109^\circ 28'$ and the single bond distance, 2.08 \AA , observed in other covalent sulphur compounds, [Pauling, (1950)]. It is normal to describe the bonding in terms of $3sp^3$ hybrid orbitals, [Cartmell & Fowles, (1961)]. Two orbitals are occupied by lone pairs and the remaining two are engaged in forming two single covalent bonds with neighbouring sulphur atoms. Because the lone pairs would show a tendency to utilize a greater proportion of the $3s$ orbital than the electrons which participate in the bonds, we might expect the sp^3 hybrids to be not quite equivalent. A compromise will be reached between the claims of the bonding and lone pair electrons for the $3s$ orbital such as to minimize the energy of the molecule as a whole. The bonds will strive to be as strong as possible by assuming a certain amount of s -character and be intermediate between pure p -bonds and tetrahedral bonds.

It is now possible to describe qualitatively the energy levels to be expected in an isolated S_8 molecule starting from a set of basis functions, ψ_1 , ψ_2 , ψ_3 , ψ_4 , centred on each sulphur atom. ψ_2 and ψ_4 are lone pair orbitals and, in the isolated atom prepared for bonding, represent states of lower energy than ψ_1 and ψ_3 . The latter will eventually overlap with similar orbitals on adjacent atoms to form the bonds.

Now consider eight isolated sulphur atoms initially at a sufficiently large distance apart for interactions between them to be negligible. Suppose furthermore that they are prepared for bonding by raising them all to an excited state corresponding to the hybridized wavefunctions described above. Orbitals ψ_2 and ψ_4 will be occupied by electrons with paired spins and, by Hund's rule, ψ_1 and ψ_3 will each contain one electron with parallel spins.

If the atoms are now brought closer together and their relative orientation is kept so that the angles in the molecule are maintained, significant energetic changes will be brought about by interactions between those states for which the orbital overlaps are large. The largest overlaps will be those between the bonding orbitals, ψ_1 and ψ_3 , and to a first approximation it is possible to neglect other interactions in describing the changes taking place to the isolated atomic energy levels as the molecule is built up.

In forming the bonds, the occupancy of orbitals ψ_1 and ψ_3 will be completed by shared electrons of opposite spin from adjacent

atoms. σ -bonds will be formed by the symmetric combination of wavefunctions on adjacent atoms. Two states will arise, one of energy lower than that in the atom, and one of higher energy, corresponding to the symmetric and antisymmetric combinations of wavefunctions. These states are denoted by $3sp^3\sigma$ and $3sp^3\sigma^*$ respectively. Stability of the bonds results largely from the lowering in energy of those electrons in the $3sp^3\sigma$ molecular orbitals.

As is shown presently, the overlaps between the lone pair orbitals ψ_2 and ψ_4 centred on adjacent atoms is only about 10% of that between bonding orbitals, and the atomic energy levels will consequently be perturbed considerably less. Molecular orbitals of π -symmetry will thus arise and, within this first order approximation, it can be assumed that the molecular orbitals are very similar to the isolated atomic orbitals.

Figure 3.1 shows how the atomic energy levels of the prepared isolated atoms are modified as they are brought closer together to form a molecule of S_8 . Interactions between the other atoms on the molecule will give rise to four bands of energy states. Bands of 32 discrete molecular energy levels, some of which may be degenerate in energy, will thus be formed. The lowest and highest bands, derived from $3sp^3\sigma$ and $3sp^3\sigma^*$ states respectively will both consist of eight levels, capable of accomodating 32 electrons altogether. The 'Aufbau Prinzip' can be used to show that the 48 outer shell electrons in the molecule will completely fill the lower three bands and leave the $3sp^3\sigma^*$ band unoccupied.

In the solid, neighbour interactions between nearby molecules will broaden the molecular energy levels into energy bands. Since these interactions can be treated as small perturbations on the energy states of the isolated molecule, the identity of the molecular energy configuration will be preserved.

An important consideration determining the molecular levels from which the electron band is derived is the relative position of any bands resulting from the overlap between higher energy atomic orbitals. In the present case it is necessary to take into account the relative positions of the bands derived from 4s and 3d atomic states. A plot of the spectroscopic levels for the isoelectronic sequence shows that in the isolated S^- ion the $3s^2 3p^4 4s$ level lies below the $3s^2 3p^4 3d$ level by about 5.6 eV. Since the orbital overlaps between 4s states are greater than those between 3d states, it is thus important to decide in sulphur whether the $4s\sigma$ molecular level lies above or below the $3sp^3\sigma^*$ level already discussed.

As far as is known no such calculation has been performed for orthorhombic sulphur. Recourse can be made however to a comparison between the crystalline forms of the other group VI(b) elements, selenium, tellurium and polonium. An examination of spectroscopic data shows that the p, d and s levels become progressively closer together in this sequence. A discussion of these solids by Gaspar, (1957), shows that the metallic conductivity in Po can be explained in terms of the d-band lying within the valence band. In Te and Se however the d-band

is relatively higher in energy and a recent calculation by Olechna & Knox, (1965) shows that the electron band in selenium is probably derived from overlapping 5s states. A similar calculation by Reitz (1957) shows that it is marginal whether the d- or the $sp^3\sigma^*$ band is the lower.

Since the atomic levels in the sequence Po.....S become progressively further apart it is to be expected that the 4s band in sulphur will lie above the band derived from $3sp^3\sigma^*$ states. In the succeeding discussion of the electron band it will be assumed that it arises from these latter molecular levels.

The electron band in the solid will thus be derived from the $sp^3\sigma^*$ molecular antibonding states, and the hole band from $3sp^3\pi^*$ lone pair states. Section 3.4 deals with a preliminary calculation of the electron and hole band widths, but before this can be done it is necessary to examine the isolated molecule on a more quantitative basis.

It is possible from the description of the bonding already given to calculate the hybridization parameters necessary to reproduce the observed bond angles. Once these parameters are known, the principal axes of all the orbitals can be calculated.

Consider a sulphur atom and its two bonds with neighbouring atoms in the S_8 ring, (figure 3.2). If a coordinate system is chosen so that the z-axis lies in the plane of the bonds and bisecting the angle between them, a one-electron hybrid orbital can be constructed as a linear combination of 3s and 3p atomic orbitals thus

$$\psi_1 = \alpha p_x + \alpha p_y + (\delta x \alpha) p_z + \beta s \quad (3.1)$$

Since the atomic 3s wavefunction is spherically symmetrical, the principal axis of ψ will make an angle of $\sin^{-1}(\frac{2}{2+\delta^2})^{\frac{1}{2}}$ with z. Using the experimental value for half the S-S-S bonding angle of $53^\circ 57'$ this leads to $\delta = 1.03$.

The normalization condition for ψ takes the form

$$2\alpha^2 + \delta^2\alpha^2 + \beta^2 = 1 \quad (3.2)$$

and thus ψ_1 , can be written as

$$\psi_1 = \alpha p_x + \alpha p_y + 1.03\alpha p_z + \sqrt{1 - 3.06\alpha^2} s \quad (3.3)$$

The remaining three hybrid orbitals are

$$\psi_2 = -\alpha p_x + \alpha p_y - 0.97\alpha p_z + \sqrt{1 - 2.94\alpha^2} s \quad (3.4)$$

$$\psi_3 = -\alpha p_x - \alpha p_y + 1.03\alpha p_z + \sqrt{1 - 3.06\alpha^2} s \quad (3.5)$$

$$\psi_4 = \alpha p_x - \alpha p_y - 0.97\alpha p_z + \sqrt{1 - 2.94\alpha^2} s \quad (3.6)$$

A further normalization condition requires $4\alpha^2 = 1$ and hence $\alpha = \pm \frac{1}{2}$.

If now the axes are rotated so that the axis of p lies along the principal axis of ψ we obtain

$$\psi_1, \psi_3 = 0.478s + 0.875p \quad (3.7)$$

$$\psi_2, \psi_4 = 0.515s + 0.857p \quad (3.8)$$

These orbitals may be compared with equivalent sp^3 hybrids in which

$$\psi = \frac{1}{2}s + \sqrt{\frac{3}{2}}p.$$

Wave functions ψ_1 and ψ_3 are bonding orbitals and are directed outwards from the atom towards nearest neighbours in the ring. ψ_2 and ψ_4 , which accommodate the unshared pairs, project outwards in a radial plane perpendicular to the plane of the bonds, see figure 3.3.

A simple calculation based on these hybridization parameters shows that one of the lone pair orbitals lies almost exactly in the median plane of the molecule and the other projects alternately upwards and downwards on adjacent atoms at angles of 111° to the median plane.

The orientation of these atomic orbitals with respect to four adjacent atoms in the S_8 ring is shown in figure 3.4.

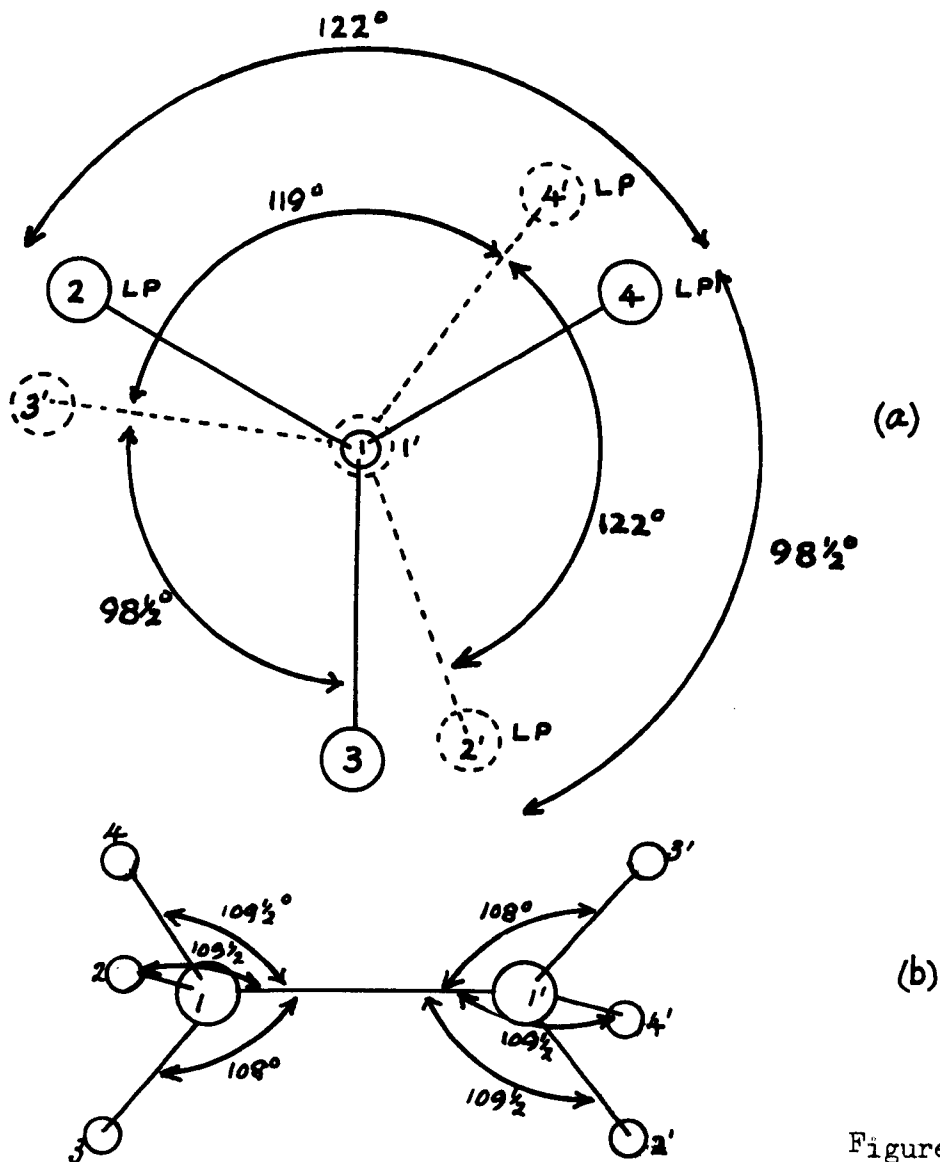


Figure 3.4.

The diagram (a) gives a view looking along a bond, and the principal axes of the four orbitals on each of the two bonded atoms are denoted by lines. Orbitals centred on the two middle atoms are distinguished by continuous lines and dashed lines respectively and are designated by unprimed and primed numerals, 1...4, in the two cases. The picture is completed by inclusion of the experimentally determined torsional angle of $98\frac{1}{2}^\circ$ [Caron & Donahue, (1961)]. Figure 3.4(b) gives a view looking along a direction perpendicular to the bond.

Atomic overlap integrals, $\langle \psi | \psi' \rangle$, were calculated by the general method described in section 3.3. The integrals were derived from the tabulated values prepared by Mulliken et al. (1949) where a single Slater neutral sulphur wavefunction with an orbital exponent of 1.817 A.U. was used. Using the notation of figure 3.4 the overlap matrix was calculated to have the following numerical values.

$$\langle \psi | \psi' \rangle = \begin{pmatrix} 11' & 12' & 13' & 14' \\ 21' & 22' & 23' & 24' \\ 31' & 32' & 33' & 34' \\ 41' & 42' & 43' & 44' \end{pmatrix}$$

$$= \begin{pmatrix} .572 & .073 & .066 & .073 \\ .073 & -.059 & +.087 & -.007 \\ .066 & .087 & -.009 & -.064 \\ .073 & -.007 & -.064 & +.084 \end{pmatrix}$$

It may be seen that the overlap between bonding hybrids, $\langle \psi_1 | \psi_{1'} \rangle$, is nearly an order of magnitude larger than that between any other pair of orbitals. In particular the overlaps between the lone pair orbitals, ψ_2 , ψ_4 , and the bonding orbitals directed towards the next atoms, ψ_3 , $\psi_{3'}$, are very small.

3.2 The S_8^- Molecular Ion

We are now in a position to discuss the S_8^- molecular ion.

In the LCAO approximation the molecular wavefunctions for the odd electron on the S_8^- molecular ion may be written, (unnormalized),

$$\phi_e = \sum_n (\psi_1 - \psi_{1'})_n = \sum \phi_n \quad (3.9)$$

where the notation of figure 3.4 is used. The overlap between molecular orbitals ϕ_n and ϕ_{n+1} on adjacent sites round the ring will determine the transition probability of the electron from n to $n+1$. Expressing ψ by $\psi = as + bp$, and using the values of hybridization parameters, a and b , already calculated, the molecular orbital overlap is obtained. The calculation yields $\langle \phi_n | \phi_{n+1} \rangle = 0.058$; this result is of considerable importance in discussion of the sulphur negative ion. In particular, the small value of this overlap indicates that the odd electron may be localized in an orbital between two sulphur atoms in the ring for a time which is long compared with the period of molecular vibrations.

If the electron is localized in the isolated ion between two sulphur atoms because of the small overlap between adjacent molecular orbitals, a strong repulsive interaction would be expected. Self-trapping by vibrational modes is likely and the motion of the electron round the ring would be accompanied by considerable distortion of the bonds. The molecule itself would thus behave in a similar way to the linear chain of diatomic molecules discussed by Holstein and described in Section 2.1. Transitions to neighbouring sites on the ring would occur in a series of random jumps in which absorption or emission of a number of vibrational quanta accompanies the transition. The

transition probability from adjacent sites would thus increase with temperature.

The behaviour of the S_8^- ion may be contrasted to the positive and negative ions of aromatic molecules such as benzene and the polyphenyls. In these planar molecules, the highest filled states and lowest empty states respectively are $p\pi$ and $p\pi^*$ molecular orbitals derived from pure p_z wavefunctions. Due to the fairly large overlaps between the parallel p_z orbitals centred on adjacent carbon atoms, the odd hole or electron on the molecular ion is delocalized round the ring in the π or π^* orbital. Vibrational interactions would be confined mainly to the symmetrical breathing mode and, although self-trapping by the whole molecule may be significant, it is not to be expected that self-trapping between neighbouring atoms will hinder the motion of the electron or hole round the ring. In the S_8^- ion, no π -orbital delocalization occurs and, as a consequence, strong localized configurational distortion within the ring would play a very much greater part in governing the motion of the electron.

If vibrational interactions are neglected, the wavefunction ϕ_e may be normalized by the condition $\langle \phi_e | \phi_e^* \rangle = 1$. Neglecting atomic orbital overlaps except those between ψ_1 and $\psi_{1'}$, (figure 3.4), the normalization constant for ϕ_e becomes

$$c_e = \frac{1}{2} (1 - \langle \psi_1 | \psi_{1'} \rangle)^{-\frac{1}{2}} = 0.38$$

Thus the normalized wavefunction for the odd electron on S_8^- is

$$\phi_e = 0.38 \sum_n (\psi_1 - \psi_{1'})_n$$

67a

Similarly, neglecting all overlaps between lone pair states, the normalized wavefunction corresponding to the highest antibonding $3sp^3$ state on S_8 is

$$\phi_h = 0.25 \sum_n (-1)^n (\psi_2 + \psi_4)_n$$

3.3 Determination of Orbital Overlaps

In section 3.1 a number of interatomic orbital overlaps were calculated to provide a basis for the discussion of electron and hole states in the isolated molecule. The general method by which these overlaps were obtained is outlined below.

In calculating integrals of the type $\langle \psi_1 | \psi_2 \rangle$, where ψ_1 and ψ_2 are pure 3s- or 3p atomic wavefunctions, much of the labour was saved by using the tabulated values of atomic integrals published by Kotani, (1963), and by Mulliken et al, (1949). These tables provide numerical values for the overlaps between Slater-type nodeless wavefunctions of the form $\psi_{3p_x} = \left(\frac{2\alpha^7}{15\pi} \right)^{\frac{1}{2}} x \cdot r \cdot \exp(-\alpha r)$ and $\psi_{3s} = \left(\frac{2\alpha^7}{45\pi} \right)^{\frac{1}{2}} r^2 \cdot \exp(-\alpha r)$. Provided the orbital exponent α is known, the values of $\langle \psi_1 | \psi_2 \rangle$ may be obtained by interpolation for any value of internuclear separation, r , up to $\alpha r = 24$. In practice, an accurate computation of the integral would involve initially a SCF calculation for ψ which is then expressed as the sum of two or more Slater-type wavefunctions with different values of α . Recent calculations by Clementi, (1964), provide such a basis set for neutral sulphur 3s- and 3p- atomic orbitals. In the calculations presented here however, approximate values of orbital overlap were obtained by using a single Slater wavefunction and appealing to Slater's rules for α .

If ψ_1 and ψ_2 are $3sp^3$ hybrid orbitals, and the z-axis is chosen to lie along the direction joining the two nuclei, these may be expressed in terms of s and p atomic wavefunctions,

$$\psi_1 = a_1 s_1 + b_{1x} p_{1x} + b_{1y} p_{1y} + b_{1z} p_{1z} \quad (3.12)$$

$$\psi_2 = a_2 s_2 + b_{2x} p_{2x} + b_{2y} p_{2y} + b_{2z} p_{2z} \quad (3.13)$$

where the coefficients a_i and b_{ij} are the hybridization parameters associated with orbitals ψ_i .

The overlap integral then takes the form,

$$\begin{aligned} \langle \psi_1 | \psi_2 \rangle &= a_1 a_2 \langle s_1 | s_2 \rangle + a_1 b_{2z} \langle s_1 | p_{2z} \rangle + \\ &+ a_2 b_{1z} \langle s_2 | p_{1z} \rangle + b_{1z} \cdot b_{2z} \langle p_{1z} | p_{2z} \rangle + b_{1x} b_{2x} \langle p_{1x} | p_{2x} \rangle + \\ &+ b_{1y} \cdot b_{2y} \langle p_{1y} | p_{2y} \rangle \end{aligned} \quad (3.14)$$

This may be written, using Mulliken's notation,

$$\begin{aligned} \langle \psi_1 | \psi_2 \rangle &= a_1 a_2 (3s3s\sigma) + (a_1 b_{2z} + a_2 b_{1z}) \times (3s3p\sigma) + \\ &+ b_{1z} b_{2z} (3p3p\sigma) + (b_{1x} b_{2x} + b_{1y} b_{2y}) \times (3p3p\pi) \end{aligned} \quad (3.15)$$

The computation of the integral is thus broken down into a calculation of the coefficients a_i and b_{ij} and of interpolating values of the integrals $(3s3s\sigma)$, $(3s3p\sigma)$ from the tables.

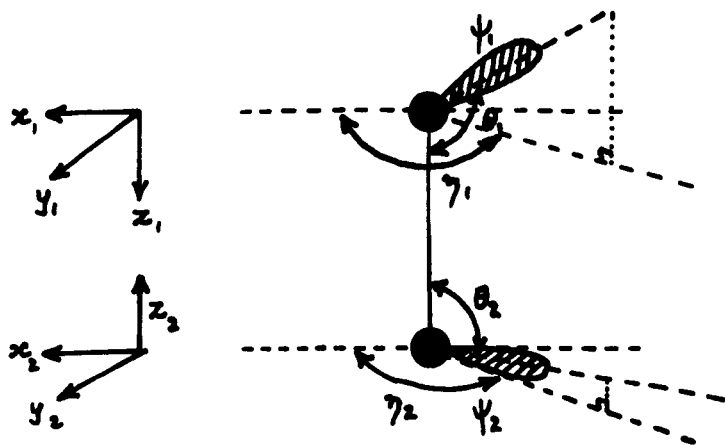


Figure 3.5

In practice the effort involved in calculating the coefficients b_{ij} is reduced if the angles made by the principal axes of ψ_i are expressed in spherical polar coordinates, θ_i and γ_i , (see figure 3.5). Thus if the wavefunction is available in the form

$$\psi_i = a_i s_i + b_i p_i, \quad \text{equation (3.7)}, \quad \text{the coefficients}$$

b_{ij} are given by

$$b_{ix} = b_i \cdot \sin \theta_i \cos \gamma_i \quad (3.16)$$

$$b_{iy} = b_i \cdot \sin \theta_i \sin \gamma_i \quad (3.17)$$

$$b_{iz} = b_i \cdot \cos \theta_i \quad (3.18)$$

Molecular orbital overlaps may be calculated along similar lines. In the LCAO approximation, a molecular orbital centred on atoms l and m is expressed as the sum of atomic orbitals, (*not normalized*),

$$\phi_{lm} = \psi_l \pm \psi_m \quad (3.19)$$

The overlap between ϕ_{lm} and ϕ_{uv} thus takes the form

$$\langle \phi_{lm} | \phi_{uv} \rangle = \langle \psi_l | \psi_u \rangle \pm \langle \psi_l | \psi_v \rangle \pm \langle \psi_m | \psi_u \rangle + \langle \psi_m | \psi_v \rangle \quad (3.20)$$

and the computation is reduced to that of four atomic orbital overlaps.

In the band structure analysis which follows in section 3.4 a number of representative overlaps of the type just described are computed. Since the odd electron in the S_8^- ion is effectively localized in a molecular orbital centred on two adjacent sulphur atoms in the ring, the $3sp^3$ molecular orbitals are expressed as a combination of two atomic orbitals as given above. Intermolecular overlaps, $\langle \phi_{lm} | \phi_{uv} \rangle$ were computed where adjacent atoms l, m , and u, v , are nearest neighbours on different molecules in the unit cell.

3.4 Band Widths in orthorhombic sulphur

In this section an attempt is made to estimate the widths of the bands appropriate to excess electrons and holes in orthorhombic sulphur. Use is made of the Bloch tight binding approach, [see for example, Dekker, (1959) p.257], in which the molecular wavefunctions for hole and electron bands are approximated by those calculated in section 3.2 for S_8 and the S_8^- ion. The intermolecular potential field is approximated by "muffin tin" potentials in order to obtain an order of magnitude for the bandwidths. The electron bandwidth is estimated in terms of the experimentally determined lattice mobility for holes.

Due to the small overlaps, the binding energy between the molecules of a crystal such as sulphur is characteristically very small compared with the bonding and excitation energies of the free molecule, and the motion of an excess carrier can be formulated in terms of the tight binding approach. This approximation uses as basis functions the Bloch momentum eigenfunctions of the crystal lattice.

One-electron crystal wavefunctions, Ψ , are constructed as a linear combination of molecular wavefunctions, ϕ , which are identical except for orientation. The periodicity of the structure requires that Ψ be constructed by taking the symmetric and antisymmetric combinations of the molecular wavefunctions over all the molecules in the unit cell.

The Bloch sum is then given by

$$\Psi(k) = \sum_{\ell=0}^{N-1} \exp(ik \cdot r_{\ell}) \left[c_1 \phi_1(r-r_{\ell}) \pm c_2 \phi_2(r-r_{\ell}-r_2) \pm c_3 \phi_3(r-r_{\ell}-r_3) \pm \dots \right] \quad (3.21)$$

where the constants c_1, c_2, \dots are phase factors and ϕ_2, ϕ_3, \dots are the molecular wavefunctions with position vectors r_2, r_3, \dots relative to the one at the origin, ϕ_1 ; the sum is extended over the 16 molecules in the unit cell, and N is the number of unit cells in the crystal.

Following Katz et al(1963), the crystal wavefunction is then written as

$$\hat{\Psi}(k) = \sum_{N=1} \exp(ikr_{\ell}) \left[\phi(r-r_{\ell}) \pm \phi(r-r_{\ell}-r_2) \pm \phi(r-r_{\ell}-r_3) \pm \dots \right] \quad (3.22)$$

where the substitutions $c_2 = \exp(ikr_2)$, $c_3 = \exp(ikr_3)$... have been made.

In a calculation of the band structure of anthracene, LeBlanc, (1961), showed that in the case of the hole band the wavefunctions to be employed are those appropriate to an electron in the highest filled orbital of the neutral molecule. For the electron band, however, the ϕ_e must be the one electron wavefunction for the odd electron in the ground state of the isolated mononegative ion. An exactly similar behaviour would be expected in sulphur and the calculations which follow are based on this result.

For electron or hole bands respectively the molecular wavefunctions are expressed as the antisymmetric combinations of eight $3sp^3\sigma^*$ hybrid orbitals or eight $3sp^3\pi^*$ orbitals. The complete molecular wavefunction for the odd electron on the S_8^- ion is thus given by

$$\phi_e = \sum_{2n} c_n (-1)^n \phi_n \quad (3.23)$$

where

$$c_e = \frac{1}{4} \left(\frac{1}{1 - \langle \psi_i | \psi_i \rangle} \right)^{1/2} = 0.38 \quad (3.24)$$

and the sum, \sum_n , extends over the 8 atoms in the molecule.

However, within the limits of the present approximation, since the probability of an electron or hole making a transition from one molecule to another is much greater between those orbitals which are nearest in the unit cell, the only interactions which are taken into account are those for which the atoms on adjacent molecules are separated by 5.5 Å or less. This approximation is equivalent to writing the molecular orbital as

$$\phi_e = c_e (-1)^n \left\{ \psi_n - \psi_{n+1} \right\} \quad (3.27)$$

where the atoms n , $n+1$ are nearest neighbour atoms to a similar pair on a neighbouring molecule.

The interaction between the odd electron or hole and the remaining electrons can be treated by the Hartree equation. The crystal field can be approximated by the sum of Hartree terms,

$$V(r) = \sum_n V_n(r - r_n) \quad (3.28)$$

where V_n is the potential of an isolated neutral molecule. V_n can be expressed in a similar way as the sum of eight terms appropriate to the sulphur atoms on the molecule.

The energy is a many valued function of k and the eigenvalues of $\hat{\Psi}$ are

$$E(k) = \text{const} - \sum_s E_s \cos k \cdot r_s \quad (3.30)$$

where
$$E_s = \langle \phi_{n+s} | V | \phi_n \rangle \quad (3.31)$$

A simplification can be introduced if it is assumed that $V(r)$ is approximately constant except in a small region close to the atomic nuclei. The potential field then takes the form of a "muffin-tin", [Ziman, (1963)], This approximation allows us to write,

$$E_s \sim V \langle \phi_{n+s} | \phi_n \rangle \quad (3.32)$$

An examination of the calculations by Katz et al. for anthracene shows that despite the rather crude model, this may be quite a good approximation for a molecular crystal. It should serve reasonably well for a discussion of the bands to a first order approximation.

Orthorhombic sulphur has 16 molecules in the unit cell and, although the orientation of the important overlaps between adjacent molecules relative to the $+x, +y$ and $+z$ axes may be different, the set of 20 relevant atomic overlaps are the same for all molecules. Table 3.1 shows the approximate relative positions of the centres of the neighbouring molecules in terms of the unit cell dimensions a, b and c . Four different orientations of the environment about any molecule are possible and these are designated by 1, 2, 1' and 2' in the table. The molecular orbital overlaps for electron states in four cases and for hole states has been calculated. It might be expected that a more complete calculation would yield values of the same order of magnitude for the remaining overlaps.

TABLE 3.1

Environment of molecule and M.O. Overlaps

<u>Environment</u>				<u>Overlap</u>	
1	2	1'	2'	<u>Electrons</u>	<u>Holes</u>
$-\frac{c}{4}$	$+\frac{c}{4}$	$+\frac{c}{4}$	$-\frac{c}{4}$	-	3×10^{-2}
$\frac{a-b}{4}$	$\frac{a+b}{4}$	$-\frac{a-b}{4}$	$\frac{a-b}{4}$	1.6×10^{-4}	4×10^{-2}
$-\frac{a-b}{4}$	$-\frac{a+b}{4}$	$\frac{a-b}{4}$	$\frac{a+b}{4}$	1.6×10^{-4}	4×10^{-2}
$\frac{2a+c}{4}$	$-\frac{2a+c}{4}$	$+\frac{2a-c}{4}$	$-\frac{2a-c}{4}$	9.0×10^{-4}	5×10^{-2}
$-\frac{2a-c}{4}$	$\frac{2a-c}{4}$	$-\frac{2a+c}{4}$	$+\frac{2a+c}{4}$	9.0×10^{-4}	5×10^{-2}
$\frac{a+b}{2}$	$\frac{a-b}{2}$	$\frac{a+b}{2}$	$-\frac{a-b}{2}$	-	3×10^{-2}
$-\frac{a+b}{2}$	$-\frac{a-b}{2}$	$-\frac{a+b}{2}$	$\frac{a-b}{2}$	-	3×10^{-2}
$\frac{a+b-c}{4}$	$-\frac{a+b+c}{4}$	$\frac{a+b+c}{4}$	$\frac{a-b-c}{4}$	-	4.5×10^{-2}
$\frac{a-b+c}{4}$	$\frac{a+b-c}{4}$	$-\frac{a-b+c}{4}$	$-\frac{a+b-c}{4}$	-	4.5×10^{-2}
$-\frac{a+b+c}{4}$	$-\frac{a-b-c}{4}$	$-\frac{a+b-c}{4}$	$\frac{a+b+c}{4}$	-	4.5×10^{-2}
$-\frac{a-b-c}{4}$	$\frac{a-b+c}{4}$	$\frac{a-b-c}{4}$	$-\frac{a-b+c}{4}$	-	4.5×10^{-2}

The band structure is given by

$$\begin{aligned}
 E(k) = E_a \cos k \cdot \frac{c}{4} + 2E_b \cos k \cdot \left(\frac{a-b}{4}\right) + E_c \left[\cos k \cdot \left(\frac{2a+c}{4}\right) + \cos k \cdot \left(\frac{2a-c}{4}\right) \right. \\
 \left. + 2E_d \cos k \cdot \left(\frac{a+b}{2}\right) + E_e \left[\cos k \cdot \left(\frac{a+b-c}{4}\right) + \cos k \cdot \left(\frac{a-b+c}{4}\right) \right. \right. \\
 \left. \left. + \cos k \cdot \left(\frac{a-b-c}{4}\right) + \cos k \cdot \left(\frac{a+b+c}{4}\right) \right] \right] \quad (3.33)
 \end{aligned}$$

where E_a, E_b, \dots are the intermolecular exchange integrals between the one at the origin and the nine nearest neighbouring molecules.

Simplifications to the above expression can be made for certain directions of k -space. Consider k parallel to a^{-1} , i.e. $k \cdot b = k \cdot c = 0$. Then,

$$\begin{aligned}
 E(k_a, 0, 0) = E_a + 2E_b \cos k \cdot \frac{a}{4} + 2E_c \cos k \cdot \frac{a}{2} \\
 + 4 E_d \sin^2 \frac{ka}{4} + 4 E_e \cos k \cdot \frac{a}{4} \quad (3.34)
 \end{aligned}$$

The energy bands for electrons are plotted (figure 3.6) in the reduced zone scheme given by $-\pi \leq k \cdot a \leq +\pi$.

The bandwidth of the lowest electron and highest hole bands are given in terms of the intermolecular potential V in table 3.2 where a representative value for the overlaps of $10^{-3}V$ is assigned to each of E_a, E_b, \dots for electron bands, and the calculated values for holes. The normalization conditions for ϕ_e and ϕ_h has been introduced, and the appropriate overlaps in (3.31) and (3.32) for holes and electrons are those listed in table 3.1 multiplied by c_e^2 and c_h^2 respectively, where $c_e = 0.38$ and $c_h = 0.25$.

<u>TABLE 3.2</u>	
<u>Approximate band widths in a⁻¹ plane</u>	
<u>Electrons</u>	<u>Holes</u>
$5 \times 10^{-3} V c_e^2$	$4 \times 10^{-1} V c_h^2$

An estimate can be made for V in terms of the experimentally determined lattice controlled mobility for holes. Using the condition for band-type motion described in section 2.1, (Fröhlich & Sewell, 1959).

$$\frac{m_h^*}{m} \geq \frac{30}{\mu} \cdot \frac{300}{T} \quad (3.35)$$

it must be concluded that $m_h^* \geq 3m$ for $\mu_h = 10 \text{cm}^2 \text{V}^{-1} \text{sec}^{-1}$ at $T = 300^\circ \text{K}$

$$\text{Since } \frac{1}{m^*} = -\frac{1}{\hbar^2} \left(\frac{d^2 E(k)}{dk^2} \right) \quad (3.36)$$

the principal xx component of the diagonalized effective mass tensor is given by

$$\frac{1}{m_x^*} \sim -\frac{1}{\hbar^2} \left(\frac{d^2 E(k_a)}{d^2 k_a^2} \right) \quad (3.37)$$

Thus $V \lesssim 31.7 \text{eV}$. The estimated maximum values for the electron and hole bandwidths are thus $2 \cdot 10^{-2} \text{eV}$ and 0.8eV respectively.

No claim is made^{as} to the accuracy of this estimate since a number of crude approximations have been made. However, the arguments do indicate that the electron bandwidth is considerably narrower than the hole bandwidth and furthermore that the electron bandwidth may well be narrow compared with kT . The above discussion could provide a starting point for a more complete calculation of the bands on a more quantitative basis.

4. Experimental Methods

4.1 Methods of Crystal Growth

Single crystals of orthorhombic sulphur were grown from solution in CS_2 at room temperature by a method similar to that described by Adams and Spear, (1964). Nearly all the crystals were grown in the bipyramid habit from a deep trough of saturated solution. With care it was found possible to produce large clear single crystals with well developed faces. Figure 4.1 shows a number of crystals grown by this method. Similar methods were also employed to grow crystals from other solvents and a few remarks are made at the end of this section about these crystals.

A saturated solution at room temperature was prepared in a closed container by allowing the solvent to stand in contact with crystalline sulphur for about 20 hours with occasional shaking.* At the end of this time the solution was filtered rapidly through a fluted filter paper into a covered dish. Supersaturation was avoided by adding a small amount of additional solvent to the filtrate at this stage.

Large bipyramid crystals from CS_2 were prepared by pouring the solution to a depth of 2 - 6 cm into a glass crystallization dish. A lid was placed over the dish and the rate of solvent evaporation could be adjusted by leaving a small opening just beneath the cover at the side. Diurnal temperature fluctuations were minimized by

* Analysis of the starting materials is to be found in the Appendix.

lowering the dish into a large dewar flask containing several litres of water, so that the water just covered the bottom of the dish. A diagram of the apparatus is shown in Figure 4.2. Crystals up to 8 cm across could be grown in the course of about a week at room temperature.

As the solvent evaporated, the progress of crystal growth was followed by inspection through the glass cover plate. From time to time, the larger crystals were removed from solution; it was found that crystals of greater perfection could be obtained by doing this, rather than allowing all the solvent to evaporate. Encrustations on the crystal faces due to rapid evaporation of CS_2 were avoided by immediately rinsing them in a larger beaker of toluene for a few seconds. Excess toluene was afterwards removed by lightly touching the crystal surface with a filter paper.

Generally, each time crystals were removed, a sufficient quantity of additional CS_2 was added to the remaining solution to redissolve any residual crystals. If this was not done, it was found that very many small crystals were formed during the subsequent period of growth.

A number of attempts were made at obtaining crystals from other solvents. With two exceptions, the method used was substantially the same as that already described. Methylene iodide produced small crystals at room temperature in the course of a month and a number of these proved suitable for transport measurements; their form was similar to some of the smaller crystals grown from CS_2 . Crystals grown from turpentine tended to be less than 1mm across and did not

appear until the solvent had become resinous. Toluene and carbon tetrachloride yielded opalescent crystal flakes about 50μ thick which were very fragile but a number of small well-formed bipyramid crystals were obtained from benzene.

Selenium monochloride and sulphur monochloride proved to be good solvents but, owing to their reactivity with moist air, the method of crystal growth from these solvents had to be modified slightly. The crystallization dish was placed on a platform in a desiccator containing silica gel; the solvent evaporated and escaped slowly through a tube containing coarse grains of silica gel fitted in the lid of the desiccator. After removing from the solution, the grown crystals were washed rapidly in benzene or toluene.

The crystals grown from selenium monochloride were strongly coloured, the colour varying from light brown to bright orange for various crystals, suggesting that some reaction of the sulphur with the solvent had taken place. Well formed crystals up to 1.8 cm across were grown from sulphur monochloride however; no other solvent apart from CS_2 produced crystals of such size and with such good faces. Their colour was not always quite as bright yellow as those grown from CS_2 .

4.2 Preparation of Crystal Specimens for Transport and Glow Curve Measurements.

Single crystal specimens were prepared for transport and conductivity glow curve measurements in the form of thin parallel sided platelets. Before cutting any crystal, the orientation of the various faces was determined by an examination of its morphology; generally the largest were the (111) faces and specimens of this orientation proved the easiest to prepare. Where possible, one natural face was retained as one face of the finished specimen.

Specimens of (111) orientation were prepared by mounting the crystal with a selected (111) face downwards in the recess on a small brass grinding jig, using phenylsalicylate as an adhesive. Damage to the crystal due to thermal shock was avoided by taking the adhesive only just to its melting point and by preheating the crystal. Specimens of various thicknesses in the range 50 - 500 μ were prepared using jigs with different depths of recess, by grinding away the unwanted portion of the crystal. A diagram of a crystal mounted for grinding is shown in Figure 4.3(a). The initial stages of grinding were performed on a glass plate, using grades 120 and 4F carborundum powder mixed to a paste with water. Minute scratches were removed from the ground surface by polishing with 6 μ diamond paste on a soft polishing cloth, using teepol as a lubricant. The specimen was rinsed carefully in water before being removed from the jig and then washed in ethyl acetate.

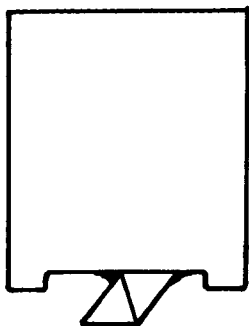


Figure 4.3(a)

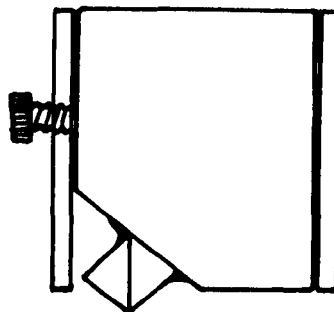


Figure 4.3(b)

Specimens of any other orientation were mounted on a special jig, the construction of which was such that the cutting angle was correct for the required orientation. Figure 4.3(b) shows how the recess in the jig tilted the crystal to the appropriate angle. Three jigs were constructed so that principal axial sections might be ground by mounting a crystal on a (111) face. After one face had been correctly ground and polished, the crystal was removed from the special jig and ground to a suitable thickness using the method described above for (111) specimens.

The specimen thickness was measured by using a miniature optical lever thickness gauge [Spear, Adams & Henderson, (1963)]. This enabled the thickness to be probed at a number of points to an accuracy of about 1μ . Generally the thickness uniformity over an area of 0.5 cm^2 was in the region of 5μ .

Owing to the reactivity of sulphur, the number of possible electrode contact materials which could be employed was severely limited. Three types of contact were used successfully, the choice depending on the particular measurements which were to be undertaken.

- (a) Aquadag suspension of colloidal graphite in water was used as the top contact for transport measurements in the electron bombardment equipment. This was applied in the form of a thin layer by means of a small camel hair brush.
- (b) Silver paste, (Johnson Matthey & Co., number 36 FST), was used as the bottom contact in all the transport measurements. Silver paste was also used to affix the crystal to its support so as to provide good thermal continuity.
- (c) Evaporated gold was used for both the bottom and top contacts in the thermal glow curve measurements and also as the top contact for transport measurements using photoexcitation. Thin semi-transparent conducting contacts were applied by evaporating gold in vacuo from a small tungsten spiral at about 10 cm distance until the resistance on an adjacent glass test slide had fallen to about 20 ohms per square. The evaporation was effected at a pressure of 10^{-5} torr; it was found that the lowest resistance layers were produced on the sulphur at high rates of evaporation. Somewhat thicker layers of gold were used as a bottom contact.

After preparation of contacts, the specimen was mounted on a thin glass microscope cover slip and 46 SWG copper wire connectings attached by silver paste or Aquadag.

Figure 4.4 shows a finished specimen mounted ready for use.

Special precautions had to be exercised in the mounting of specimens for the conductivity glow curve measurements. These measurements required taking the specimens to liquid nitrogen temperature and care was needed to avoid introduction of strain due to the large difference in expansion between the glass cover slip and the crystal. For this reason the specimen was held in position at one side only by a small drop of nitrocellulose cement. The wire connections were held in contact with the gold electrodes with a spot of Aquadag, and sufficient flexibility in the wires was provided to allow for movement of the crystal.

4.3 Electron and Hole Mobility measurements

Electron and hole drift mobilities were measured using the pulse techniques which had been developed in these laboratories in the past few years and had been used in previous work on the selenium allotropes and Cds, [Spear(1960), Spear, Lanyon & Mort(1962)]. The drift mobility of holes was measured in substantially the same way as that described by Adams & Spear(1964), and an extension of the method appropriate to the measurement of much lower mobilities was used for electrons.

Electron beam excitation was used for all measurements of hole transport, and also for electrons at low temperatures. However, particularly at high temperatures where the specimens tended to sublime if kept in high vacuum, electron mobilities were also measured using photoexcitation by a short flash from a discharge tube.

In the succeeding description of the experimental method only brief reference is made where the details have already been described. Any modification which was incorporated is dealt with in greater detail, and a separate section is devoted specifically to measurements of electron mobility.

4.3.1 Principle of the method used for measuring mobility

The single crystal specimen is prepared in the form of a thin parallel-sided platelet and is provided on opposite faces with thin large-area ~~conducting~~ contacts, T and B, (figure 4.5).

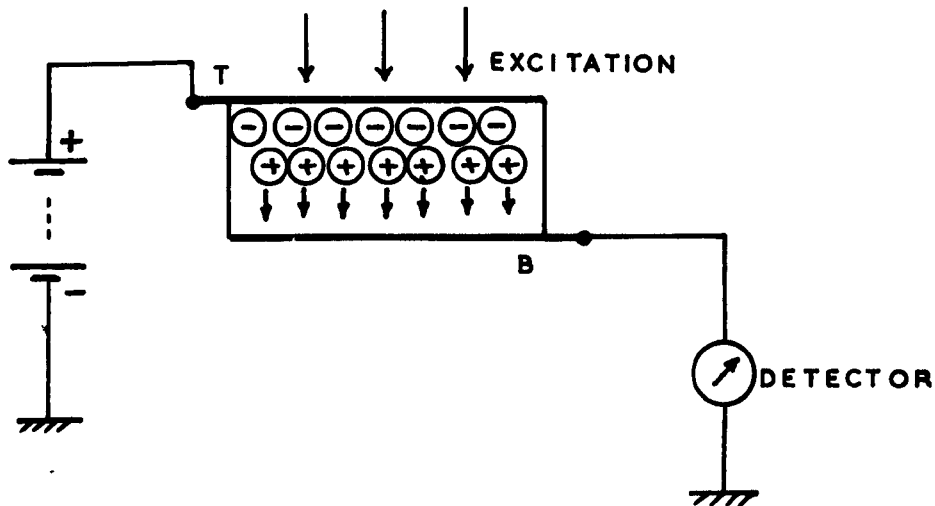


Figure 4.5

Free carriers are generated near the top face, T, by a short excitation pulse of strongly absorbed light or electrons incident through the semi-transparent top electrode. Carriers of opposite sign are separated in the presence of an applied electric field. Depending on the polarity, either electrons or holes are drawn into the bulk of the crystal towards the bottom electrode. In the absence of deep trapping and space-charge effects the steady drift of one sign of carrier gives rise to a constant displacement current which may be readily detected in the external circuit. When the carriers arrive at the bottom electrode, B, the current falls rapidly to zero and their mobility can be determined from measurements of the transit time, t_t , at various values of applied field.

The field applied across the specimen is usually pulsed; experience has shown that this reduced the build-up of internal space charges due to injection. The excitation is arranged to occur near the centre of this pulse.

When the transit time is short, as in all the previous investigations for which this method has been described, somewhat greater detection sensitivity is achieved by displaying the charge displacement rather than the current. The basic circuits used for measurements of either the displacement charge or the displacement current are shown in figure 4.6 together with the idealized pulse shape obtained by the two methods.

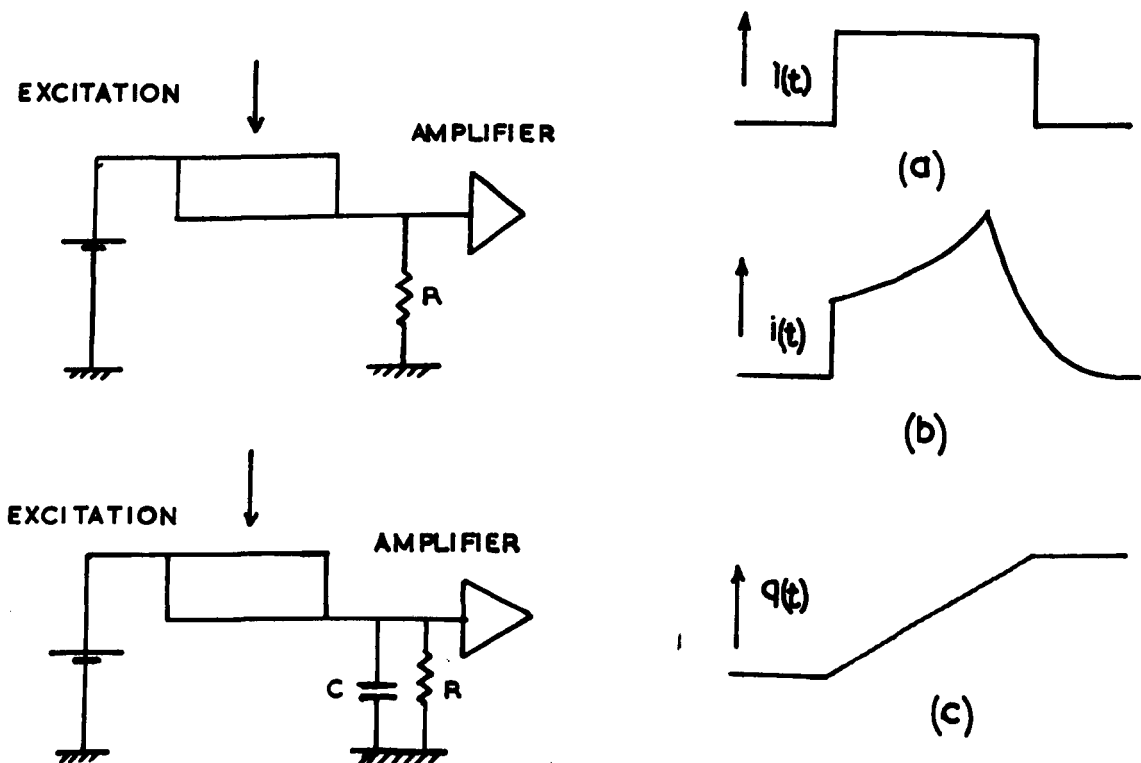


Figure 4.6

The drift mobility, μ , is obtained from the relation

$$\mu = \frac{d^2}{V \cdot t_t} \quad (4.2)$$

where V is the potential applied across the specimen of thickness, d . In practice μ is obtained by measuring t_t as various values of applied potential, V , and determining μ from the slope of a linear plot of t_t^{-1} against V .

In the present investigation of electron transport, particularly at low temperatures where the induced currents were small, greater precision in measurements of μ was achieved by increasing the excitation level sufficiently for the induced currents to be limited by the space charge of mobile carriers. The current pulse shape then had the form shown in figure 4.6(b) and the transit time, t_t' was measured to the peak value of the current. The mobility was then obtained from the modified form of equation (4.2) appropriate to transient space-charge limited currents described in section 5.2 :

$$\mu = k \frac{d^2}{V \cdot t_t'} \quad (4.3)$$

Here k is a constant depending on the excitation level and lying between 0.8 and 1.0.

For the observation of well defined transit times it is essential for the excitation pulse to be short compared with t_t .

A limitation on the method for determining drift mobilities arises when the lifetime of drifting carriers with respect to deep

traps is short compared with the transit time; in this context 'deep' refers to traps from which the thermal release time constant is long compared with t_t . No discontinuity in the current may be seen at $t = t_t$ if deep trapping is severe, and the mobility can then no longer be measured by these techniques. In practice, this limitation eventually determines the lowest temperature at which mobilities may be measured since, in general, an increasingly larger number of traps become 'deep' within the above definition as the temperature is lowered.

In all the measurements, particular care was taken to avoid the build-up of an internal space-charge field due to trapped carriers. Space-charge neutralization was achieved in the interval between field pulses by further exciting the specimen with a succession of pulses in the absence of an applied field. This process generated free carriers which moved under the influence of the space-charge field and recombined with trapped carriers of opposite sign. By examining successive displacement currents in the opposite direction during the discharging cycle it was thus possible to provide a check on the efficiency with which neutralization was being achieved.

4.3.2 Electron Mobility Measurements

It was found more convenient in measurements of electron mobility to observe the displacement current due to drifting carriers [figure 4.6(a)], rather than the charge, [figure 4.6(c)], because of the much longer transit times involved. Broader excitation pulses could also be used and the pulsing circuits developed specifically for electron transport measurements are described in succeeding sections. The lower drift velocities of the generated electrons made it necessary to incorporate more sensitive detection equipment than that which was used for holes and also to take particular care to ensure good low frequency response in the circuits.

For all electron transport measurements, using both electron beam and light flash excitation, the specimen was connected in the circuit shown in figure 4.6(a).

Stray capacity, effectively in parallel with the specimen, was minimized by feeding the output directly to the earthed input resistance of a cathode follower mounted beneath the specimen holder. The input resistance, R , could be switched in four steps from 10^6 to 10^3 ohms. In practice, to maintain an adequate signal-noise ratio, R was kept as large as possible consistent with obtaining an adequate high frequency response, usually 10^6 or 10^5 ohms. No coupling capacitors were used and the cathode follower output was fed directly to a Keithley ultra-low noise amplifier type 103. This amplifier

had a frequency response extending from 100 kc/sec to 0.1 c/sec and the output was coupled to the d.c. input of a type 'L' plug-in unit on a Tektronix 541A oscilloscope. The maximum overall sensitivity was 5×10^{-11} amp per cm deflection on the CRT screen and transits due to the motion of fewer than 10^6 electrons were readily observable.

4.3.3 The Electron Gun

A demountable electron gun and specimen chamber was used in all experiments in which free carriers were generated by means of electron pulse excitation. Since the details of this method have been described elsewhere, [Spear,(1960), Spear & Mort,(1963)], only a brief description will be given here.

The gun consisted of a 0.1mm dia. tungsten hairpin cathode, K, centred behind a modulator electrode, M; (figure 4.7). A sliding 'O' ring seal was provided to allow the filament to be aligned accurately behind the modulator aperture while the gun was operating. A cylindrical first anode, A_1 , was held at +300 volts with respect to cathode by means of a small dry battery, and the intensity of the electron beam was controlled by application of a variable negative bias to M. Final acceleration of the beam was effected by the second anode, A_2 , at earth potential. The cathode of the gun was kept at a negative potential in the range from 10 to 35 kV provided by a Brandenburg stabilized EHT generator, type MR/100R/1. A short magnetic lens M, was used to centre and focus the beam on to the specimen.

The beam was located accurately by focusing it just within the edge of a 3mm dia phosphor-coated aperture, P, held directly above the specimen. Unnecessary heating of the specimen under steady bombardment was avoided by carrying out all initial beam adjustments with a moveable vane, V, in position just above the crystal.

The gun and specimen chamber were evacuated to a pressure below 10^{-4} torr by an oil diffusion pump and rotary backing pump. A Penning gauge and control unit was used to monitor the pressure.

4.3.4 The Specimen Holder

The same specimen holder was used for all electron and hole transport measurements, see figure 4.7 . The holder was designed to provide a convenient means of accurately controlling the specimen temperature in the range -100° to $+120^{\circ}$ C and at the same time to screen the specimen from spurious electrical pickup and stray radiation.

The specimen, (figure 4.4), was mounted in close contact with the upper end of a 1" dia. copper rod, R. Thermal continuity between the rod and the specimen was effected with a thin film of silicone pump oil. R was thermally isolated from the rest of the system by a 3" length of thin-walled stainless steel tubing, S. A chromel-alumel thermocouple was held in contact with the thin glass cover slip on which the crystal was mounted at a distance of about 1mm.

Cooling or heating of the specimen was brought about by immersing the lower end of the copper rod into a Dewar flask containing liquid at a suitable temperature. Times between 15 and 25 minutes were usually required for the specimen temperature to reach equilibrium. The specimen temperature was determined by measuring the thermocouple EMF with a Pye Instruments Precision Potentiometer using ice for the reference junction.

Temperatures above 80° C were maintained by means of a heated oil bath and, below this temperature and down to 0° C, water or ice was used. Lower temperatures were maintained either by a mixture of solid CO_2 and acetone or by one of the range of 'Arcton' refrigerants,

(ICI Ltd., Liverpool). The latter enabled the temperature to be held at a number of fixed points with considerable accuracy, if necessary for prolonged periods.

Vacuum seals were provided to bring the thermocouple leads and specimen connections through the base plate. Efficient screening of the specimen from stray radiation and electrical interference was effected by a small detachable brass lid. An aperture was incorporated in the top of the lid immediately above the specimen to permit the entry of exciting radiation.

4.3.5 The Pulse Equipment

After initial adjustments under low intensity continuous bombardment, the beam was cut-off by applying a steady negative bias to M. For measurements of hole transport, a short positive square pulse was applied to the modulator to drive the gun on. The beam pulse generator consisted essentially of a mercury-wetted contact high speed relay which was used to discharge a coaxial delay line. To avoid effects due to lead inductance and stray capacity, the coaxial connection to the gun was terminated by a 75 ohm resistor mounted inside the gun housing. A series of interchangeable delay cables enabled the pulse width to be varied in the range 6 - 300 nsec.

Excitation pulses which could be conveniently produced by this method were generally too short to be used for measurements of electron transport. Occasionally it was possible to replace the delay line with a condenser and thereby obtain an exponentially decaying pulse up to 10μ sec long, but greater flexibility was achieved by using a transistorized multivibrator to modulate the beam. This was coupled in to the cathode circuit which made it possible to switch over without difficulties from short pulse excitation, (delay line), to longer pulse excitation.

Both generators, which were mounted near the gun at -EHT potential, were phased and triggered with light flashes. Lenses were used to focus the light output from neon discharge lamps on to

phototransistors incorporated in the generator driving circuits. This made it possible to trigger the two beam pulse generators independently, and at the ~~same~~ time it eliminated all high voltage capacitors connected between EHT and earth. This new method of triggering was found to be considerably more convenient when the EHT supply was switched on or off since no precautions were needed to avoid capacitative surges. As no signals due to residual EHT ripple appeared across the generator inputs, optical triggering provided the additional advantage of more accurate timing of the pulse circuits.

The light flashes were synchronized with the field pulse from a master pulse unit to be described in the next Section.

4.3.6 The Master Pulse and Field Unit

During measurements of electron and hole mobilities, and of electron free lifetime by the method of interrupted transits, (Section 4.4), it was important to have a convenient source of trigger pulses, phased with the 50 c/sec mains, and occurring at predetermined intervals of time. A master pulse unit providing facilities for excitation and discharge, and at the same time generating correctly timed field pulses was designed and constructed.

The main purpose of the master unit was to provide an additional series of 50 c/sec excitation pulses occurring just before the field pulse was applied, (figure 4.8). These were required to achieve space-charge neutralization, and the last pulse in the series was arranged to occur during the field. After a predetermined time interval the sequence was repeated, and a number of auxillary trigger outputs were provided to coincide with this time interval.

Accurate timing was achieved by incorporating a number of binary dividers operating from the 50 c/sec mains input. The switched divider output was used to operate a gate circuit and produce at 50 c/sec a burst of 8 trigger signals at fixed time intervals. This group of signals was used to trigger the excitation at fixed intervals lying between 160msec and 5 sec. Timing of the field pulse was adjusted so that the last excitation pulse in the group of 8 occurred near the centre of the field pulse. A switch was incorporated so that the number of discharge pulses could be increased,

if necessary, by using continuous 50 c/sec excitation.

A block diagram of the master pulse unit is shown in figure 4.9, and the relative positions of the various pulse outputs in figure 4.8.

For experiments on interrupted transits, (to be described in greater detail in section 4.4), a separate trigger output was provided to coincide with the beginning of the field pulse. This pulse was used to trigger an external double-pulse generator.

Low impedance field pulses were generated with a mercury-wetted-contact high speed relay in series with a dry battery source. The relay coil was driven from a multivibrator circuit so that pulses between 3 and 16 msec could be produced by changing time constants in the circuit. The battery voltage source was built from a number of dry batteries in series so that, by using suitable tapings, voltage outputs from zero to 540 volts in 1.5 volt steps could be obtained in three switched ranges.

4.3.7 Photoexcitation

Measurements of electron drift mobilities at high temperatures, and of transient space-charge limited currents, were performed by means of photoexcitation. Since transit times in the millisecond range were involved, it was possible to use the light output from a triggered xenon discharge tube to generate free carriers.

A Dawe Instruments Transistor Strobotorch, type 1202 D, complete with tube supplies and trigger facilities was used to drive a Wotan XIE 15W discharge tube at the end of a short high voltage lead. Separate measurements indicated that the duration of the flash was in the region of 4μ sec. The tube was fixed a few inches away from the specimen which was mounted on the same holder as that used in the electron bombardment gear, (section 4.3.4). The arrangement is shown in figure 4.10. Transparent conducting gold top electrodes were fitted to all specimens used in this series of measurements.

The flash tube was triggered externally at about 1 c/sec from one of the master pulse unit auxillary outputs so that the light flash was phased with the 50 c/sec mains and occurred within the field pulse. An additional flash was employed in the interval between field pulses to maintain space-charge neutrality.

Frequently at low applied fields, the transit time was longer than the available field pulse, (16 msec), and, under these conditions,

it was necessary to use a steady field. The excitation was still triggered externally at the same rate, but space-charge neutralization was achieved by manually reducing the applied field to zero for a few seconds.

The specimen was connected via a cathode follower and high gain amplifier to an oscilloscope in exactly the same way as that used for electron beam excitation.

4.4 Determination of Electron Lifetime by Interrupted Transits

The exceptional properties of electrons in orthorhombic sulphur made it possible to determine their free lifetime by a very direct method.

The technique depended on measuring the displacement current of electrons after short pulse excitation and of interrupting the transit by momentarily reducing the applied field to zero; the field was restored to its original magnitude after a predetermined time interval. The time of interruption was varied in the range $50 \mu\text{sec} - 100 \text{msec}$ and the ratio of conduction currents before and after interruption was used to determine the carrier lifetime directly.

Information about the spatial distribution of traps was provided by interrupting the transit when the charge cloud had travelled various distances across the specimen. Since the process of carrier trapping in the absence of a field is basically one of diffusion into traps, the temperature dependence of free lifetime was also measured in order to determine the dependence of diffusion coefficient on temperature.

The field pulses for this series of measurements were obtained by amplifying the output from a Nagard double pulse generator. A low impedance amplifier providing pulses up to 250 V was constructed using three EL38 beam tetrodes in parallel, designed to operate from a negative stabilized 300 V supply. The pulse output was taken from a common 1000 ohm anode load, one end of which was at earth potential.

Additional delay and trigger circuits were used to phase the light flash with the field pulses. Between each pair of field pulses a number

of additional light flashes were provided to maintain space-charge neutrality. All units were triggered and phased with the 50 c/sec mains from the master pulse unit described in Section 4.3.6.

The relative positions of the field and excitation pulses and a block diagram of the experimental arrangement are shown in figures 4.11 and 4.12 respectively.

If i_0 is the initial value of conduction current, the current will decay to i_t , where

$$i_t = i_0 \exp(-t_i/\tau) \quad (4.4)$$

after interrupting the field for a time t_i . Here τ is the mean lifetime of electrons with respect to deep traps. If i_t/i_0 is measured as a function of t then τ may readily be obtained from the slope of a semi-logarithmic plot.

In practice, to avoid signals due to switching transients, i_t was measured at a fixed time interval after restoring the field; this time was usually chosen to coincide with the arrival of carriers at the bottom electrode. In some extreme cases it was necessary to determine i_t by taking differences between the output signal in the absence and in the presence of excitation.

4.5 Thermally Stimulated Conductivity

In the course of the present investigation on electron transport it became of interest to investigate the trapping spectrum to test one proposed interpretation of the results.

The method of thermally stimulated conductivity, or conductivity glow curves, was used to gain, at least, a qualitative idea of the trap distribution. One aim of this study was to investigate the possibility that one or more of these trapping centres were associated with point defects whose density might be altered by different heating or cooling schedules, (see section 2.4).

The method is similar to that employed to investigate the thermoluminescence of phosphors. To measure thermally stimulated conductivity, the specimen is prepared in the form of a thin platelet provided on opposite faces with thin conducting contacts. After cooling to liquid nitrogen temperature, the specimen is irradiated through the semi-transparent top electrode with strongly absorbed ultra-violet radiation to generate free carriers just within the surface. Depending on the polarity, carriers of one sign are drawn towards the bottom electrode in the presence of an applied field. Some carriers reach the bottom electrode to be subsequently extracted and the remainder become trapped in the bulk of the specimen.

After irradiation for some time, a steady state is reached in which either the internal field due to trapped carriers exactly balances the applied field or, alternatively, all the traps become filled. At

this stage irradiation is discontinued and the specimen is heated at a steady rate. Carriers are progressively released from traps by thermal excitation as the temperature is raised and the displacement current due to their movement in the applied field may be measured with a sensitive current indicator. The presence of discrete trapping levels is indicated by a series of current maxima as the crystal is heated. From the position, magnitude and shape of these peaks it is possible to calculate the density and depth of the trapping centres.

The specimen holder used for measurements of thermally stimulated conductivity is shown in figure 4.13. The crystal was mounted inside a small blackened copper enclosure in thermal contact with the top of a long copper rod. A nichrome heating coil was wound near the upper end of the rod. The crystal enclosure fitted inside an evacuated chamber provided with a synthetic silica window so that the crystal could be irradiated. A small front-silvered glass mirror reflected the radiation on to the specimen. The temperature was measured with a fine chromel-alumel thermocouple mounted directly in contact with the crystal at one side; a spot of Aquadag was used to ensure good thermal contact between the junction and the specimen. The specimen contact lead to the current indicator was taken through a shielded polythene vacuum seal.

During both irradiation and heating, the specimen current was monitored with an Ekco vibrating reed electrometer. The output from this was fed to a Kipp pen recorder. By changing the scale sensitivity and input resistance to the electrometer in the range from 10^8 to 10^{12}

ohms, it was possible to obtain a 10 inch deflection the recorder with currents ranging from 10^{-8} to 10^{-15} amp.

The specimen was cooled by immersing the lower end of the copper rod in a flask of liquid nitrogen. After thermal equilibrium had been established, ultra-violet radiation from a mercury discharge lamp was directed on to the specimen through a Kodak 18B Wratten filter. A constant field was maintained across the crystal from a dry battery supply. Irradiation was discontinued when the conduction current reached a steady value.

Heating at an approximately constant rate was effected by removing the liquid nitrogen reservoir and by passing a constant current through the heating coil. Heat transfer to the crystal was assisted by introducing dry gas, (90% N_2 , 10% H_2), at a pressure of about 10 torr just before the heating cycle began. From time to time the heating current was increased manually to maintain the heating rate as nearly constant as possible. The progress of the heating was monitored on a Varian pen recorder and synchronism between the time scales on the two recorders was achieved with markers at regular time intervals.

4.6 Depolarization measurements by space-charge probing

It was of considerable interest to measure the release rate of carriers from a prominent electron trap near 0.95 eV reported by Dean, Royce & Champion, (1960), Adams & Spear, (1964) and by Thornber & Mead, (1965). An electron beam probing technique was used to measure the polarization due to electrons trapped in the crystal bulk as a function of time and temperature.

The specimen was polarized in the presence of an applied field by bombarding it with 30 kV electrons for a time long enough for the induced electron current to reach a steady value. The applied field was then reduced to zero and, at various time intervals after polarization, the space-charge field was probed with a short 30 kV electron pulse. The magnitude of the charge displacements in the field of the trapped electrons was assumed to be proportional to the number of trapped electrons. A semi-logarithmic plot of discharge pulse height as a function of time thus enabled the release rate from traps to be determined.

5. Experimental Results

5.1 Experimental Results for Electron Mobility

The drift mobility techniques described in section 4.3 were used to measure the mobility of electrons in more than 20 single crystal specimens over the temperature range -80°C to $+113^{\circ}\text{C}$. Crystals were grown from starting materials of different degrees of purity and results were obtained with both electron beam and light flash excitation. Parallel measurements of hole mobility were made on all specimens at room temperature to provide a comparison with the results for electrons. In the region of the transition temperature to the monoclinic modification, (section 1.1), the behaviour was studied in detail. Anisotropy of electron mobility was investigated by taking a number of measurements on specimens cut from single crystals in different orientations. Preliminary results of this study were reported by Adams, Gibbons & Spear, (1964).

It was found possible to obtain useful measurements of both electron and hole mobilities on all crystals grown from solution in CS_2 . Of those from other solvents, only the ones grown from methylene iodide provided specimens with sufficiently long carrier lifetime for mobility measurements. The majority of crystals were prepared from 6N ultra pure sulphur or from laboratory reagent quality. Four grades of CS_2 were employed ranging from the BDH product used for infra-red spectroscopy to BDH 'Analar', M & B Reagent Quality and BDH 'Technical'. Chemical analyses of these starting materials is to be

found in the Appendix.

Identical mobility results were obtained with both light flash and electron beam excitation. Specimen thicknesses ranged from 66 to 344 microns and, under applied fields from 2.6×10^3 to 3.3×10^4 V.cm⁻¹, electron transit times from 270 μ sec to 50 msec were measured on various specimens. A typical electron transit current pulse is shown in figure 5.1 for low intensity light flash excitation in a specimen 200 microns thick. The short initial spike corresponds to the movement of holes to the top electrode. Electron and hole transit measurements on the same specimens established that in spite of the long electron transit times, the total negative charge transported across the crystal was very nearly equal to that for holes. This, in conjunction with the observation that the pulse is substantially rectangular in shape indicates that surprisingly little deep electron trapping occurs in the crystal volume during transit.

The suggestion, [Adams & Spear(1964)], that the apparent absence of an observable electron displacement might be due to a very short lifetime with respect to deep traps is clearly incorrect in view of the present work. However, the presence of a number of deep electron traps has been confirmed by a method of space charge probing and by thermally stimulated conductivity to be described in later sections of this thesis.

A number of electron transits were measured under space-charge limited conditions by increasing the intensity of excitation. One

such transit is shown in figure 5.2. The rise in current towards the end of the pulse is similar to that reported for iodine by Many et al. (1961) and measurements of transit times on the same specimens at both high and low intensity excitation showed that the appropriate theoretical expressions, equations (4.3) and (4.2), in section 4.3.1 lead to the same values of mobility. At low temperatures the use of high intensity excitation was found to offer considerable advantages in detection since the displacement currents tended to be rather small.

At no stage in the course of the present investigation of electron transport was the high mobility of electrons reported by Thornber & Mead, (1965), observed. Electron bombardment excitation pulses as short as 6 nsec were employed in conjunction with wide band amplifiers, but no signals that could be associated with the high velocity drift of generated electrons were seen.

5.1.2 Temperature Dependence of Mobility in (111) Direction

Figure 5.3 shows the temperature dependence of mobility for seven specimens of (111) orientation grown from ultra-pure (UP) and Laboratory Reagents (LR). The electron mobility is $6.2 \pm 0.6 \times 10^{-4} \text{ cm}^2 \text{V}^{-1} \text{sec}^{-1}$ at 21°C and the transport is an activated process over the entire temperature range. The remarkable feature of the results is that, within experimental error of about 10%, the mobility values for all specimens fall on a common curve. This is in striking contrast to their hole mobility in the trap controlled temperature range which is listed on the figure. In agreement with previous results by Adams & Spear, (1964), these measurements show order of magnitude differences in μ_h between crystals; this is not unexpected as $\mu_h \propto N_t^{-1}$ at a given temperature, [equation (2.53), section 2.3] .

The gradient of the average curve in figure leads to a constant activation energy of $0.167 \pm .005 \text{ eV}$ over the entire temperature range from 193°K to 386°K .

The present mobility results for electrons, in comparison with those for holes, point therefore to an essentially different mechanism of transport. The electrons interact with centres whose density is evidently a fundamental property of the crystals. The extremely small and consistent value of μ_e would certainly be in accord with an intermolecular hopping mechanism but, from these results alone, it is not possible at this stage to exclude other models. An alternative

possibility that the centres may be thermally generated point defects must be considered in the light of the experimental evidence for traps and their behaviour at different heating and cooling rates described in sections 2.4 and 5.5. Consideration must also be given to a model in which the centres are shallow electron traps due to an impurity which has a tendency always to enter the crystal in a constant proportion during the process of growth.

A detailed discussion of the alternative interpretations of these important electron mobility results is reserved for section 6.

5.1.3 Temperature Dependence of Mobility in Principal Directions

It appeared of considerable interest to attempt a correlation between the structural anisotropy and the electron transport. A number of specimens were prepared from large single crystals so that the mobility could be measured in the three principal directions. Specimens of (100), (010) and (001) orientation were all cut from crystals grown from CS_2 and, since none of these forms was present on most of the grown crystals, they were all prepared with two ground and polished faces.

Figure 5.4 shows the results for the electron mobility in the principal directions plotted as a function of temperature. The solid line, which is identical to that shown in figure 5.3 for the (111) direction, is drawn on the same graph for comparison.

It is seen that, within experimental error, there is no observable anisotropy either in mobility or in activation energy. This is an unexpected result when consideration is given to the very different orientation of the molecules in the (001) direction relative to the other two.

5.1.4 Electron Mobility in region of Monoclinic Transition

Since the orthorhombic allotrope of sulphur undergoes a structural transformation to the monoclinic modification at 96°C it was of interest to investigate the influence of this structural change on the electron transport.

The electron mobility was measured on a number of crystals in the range of temperatures above the transformation point. It immediately became apparent that the rate of transformation varied from crystal to crystal. It was possible, on one crystal, to measure mobility up to the melting point of orthorhombic sulphur without any observable deviation from the curve of figure 5.3. Since this crystal eventually melted at 114° it can be inferred that no transformation had taken place in the course of several hours heating above 96° and these results are presented in figure 5.3 to extend the range of measurements for orthorhombic sulphur up to 113°C .

Other crystals, however, did undergo changes in the same period of time. The results are shown in figure 5.5. It is seen that mobility values fall significantly below the curve for orthorhombic crystals and that, on subsequent cooling, considerable hysteresis in the mobility arises. The arrows on the diagram show the order in which the measurements were taken. It was not found possible to follow the recovery of mobility on cooling beyond the last experimental point because the lifetime of carriers with respect to deep traps became progressively shorter as the experiment continued. If the crystal

was held above 96°C for a time only just long enough for a fall in mobility to be observable, then almost complete recovery to the orthorhombic values took place on cooling.

Examination of crystals which had been heated above 96°C for several hours showed them to be almost completely opalescent.

A steady value of $\mu_e \approx 2 \times 10^{-4} \text{ cm}^2 \text{ V}^{-1} \text{ sec}^{-1}$ was reached after six hours heating in the range 99° - 109°C. These results are similar to those for holes, [Adams & Spear, (1964)], where a fall in mobility by a factor of 30 was observed above the transformation temperature.

On subsequent cooling no change in μ_e was observed until the transformation temperature was reached; below this point the mobility increased towards the orthorhombic values. Throughout the experiment the induced electron current towards the end of the pulses became smaller until eventually no discontinuity at $t = t_t$ was observable. This demonstrates that an important effect of taking sulphur through its transformation point is the introduction of deep traps, the density of which increases both on heating and on cooling.

5.2 Experimental Results on transient space-charge

limited currents

Although transient SCL currents were used together with experiments at lower excitation intensities for the determination of electron mobilities, these measurements were confined mainly to the determination of transit times. In the present study a number of subsidiary measurements were made to provide experimental evidence in sulphur for the behaviour predicted theoretically by Many et al. (1961) and by Papadakis, (1965). Most features of the analysis were found by Many to fit the experimental results on photogenerated holes in single crystals of iodine and, to provide a comparison between the behaviour of SCL currents in these two molecular crystals, a series of additional measurements were performed in sulphur.

Many observed SCL currents by generating free carriers near the top face of platelet specimens by intense light flash excitation and by following the motion of one sign of carrier to the bottom electrode in the presence of an applied field, (figure 4.6(a), section 4.3.1). An alternative method was occasionally employed in which intense steady illumination was used to generate carriers near the surface, and their progress through the crystal was observed after sudden application of the field.

In the drift mobility measurements employed by Spear care is normally taken to prevent the space-charge of drifting carriers from modifying the internal field. However, if the excitation intensity

is increased sufficiently, the generated reservoir of mobile carriers near the surface may be drawn out of this region under SCL conditions. As a result, in stead of a constant carrier drift velocity, the leading edge of the charge cloud will be accelerated by the field of the carriers behind. If the reservoir is maintained, the displacement current due to the drifting carriers will fall when the leading edge of the charge cloud arrives at the bottom electrode; the current will drop more or less rapidly to a value appropriate to steady SCL currents, see figure 5.6.

If the space-charge reservoir is not maintained, then a similar perturbation of the internal field will be brought about by the packet of drifting carriers. The leading edge will be accelerated and the trailing edge will be retarded by the space-charge field. After the first carriers arrive at the bottom electrode the displacement current will drop to zero in a time dependent on the spread of the charge packet during transit. According to the analysis by Papadakis, the shape and duration of the transient current pulse should depend on the ratio, β , of the applied field, E , to the space-charge field, $\frac{4\pi Q}{\epsilon\epsilon_0}$; where Q is the total injected mobile charge per unit area. Figure 5.7 shows the computed pulse shape for three values of the parameter β .

As the applied field is increased, the ratio of the peak to the initial value of current response, j_t/j_0 , should decrease since $\beta \propto E$ for a given injected charge, Q . A similar decrease should be observed with a reduction of excitation intensity and a transition from a square law to a linear dependence of j_0 on E would be expected

at low levels.

Oscillograms of the transient current response in sulphur for several values of applied field after high intensity flash excitation are shown in figure 5.8(a). The initial value of photocurrent density j_0 , is plotted in figure 5.9 as a function of applied voltage for three sulphur specimens of different thicknesses. It is seen that the V^2 dependence of j_0 on V predicted by Many appears to be obeyed over two orders of magnitude of current density.

Although the shape of the current pulse became almost rectangular when the experiment was repeated at lower excitation densities, an almost square-law dependence of j_0 on V was still observed. One such low intensity run is marked 'L' on the graph. This behaviour was not observed by Many in iodine and his analysis does not predict such a result. The reason for these differences became apparent in continuing the investigation.

The experimentally determined values of j_0 and j_t enable β to be determined. A plot of j_t/j_0 for various values of β is given in figure 5.10.* Theory predicts that for complete space-charge limitation $\beta = 1$ and that for a given injected charge, β rises monotonically to large values with increasing applied field. Figure 5.11 shows the ratio j_t/j_0 measured on one specimen as a function of applied field. This analysis leads to figure 5.12 which gives the

* The author is indebted to Mr. A.C Papadakis of the G.P.O. Research Station, London, for supplying the computer results from which figure 5.10 and table 5.1 were prepared.

experimentally determined variation of β with field.

The surprising result of this analysis is that β does not follow the predicted behaviour. In particular, it is seen that β passes through a minimum somewhere near the middle of the range and at no value of applied field is the current completely space-charge limited. The results suggest that account should be taken of the dependence of the injected charge, Q , on the applied field.

Two methods are available for determining Q . Since E is known, Q may be derived from the β values already obtained as

$$Q = \frac{e E}{4 \pi \beta}$$

Alternatively, Q may be obtained from the total area beneath the current pulse. Figure 5.13 shows the values of Q obtained by the two methods as a function of applied field plotted on the same graph.

It is seen that good agreement is obtained between the two independent determinations of Q . This lends support to the assumption that the rise in current pulse towards the end of transit is related to the injected charge, Q , according to the theory outlined by Papadakis. However, it is very clear that a fairly complicated dependence of Q upon E obtains.

Qualitative agreement with the results of figure 5.13 can be achieved on the basis of a simple model.

Immediately after excitation, the generation region contains a very high density of both holes and electrons, and before the holes

are all extracted, carrier recombination would be expected to reduce the number of electrons in the space charge reservoir near the electrode. Since the hole mobility is several orders of magnitude greater than that of electrons, a calculation can be based on the assumption that the electrons are immobile for the time it takes the holes to recombine or leave the crystal.

Consider a thin sheet of holes generated at a distance x beneath the specimen surface. The time taken for this sheet to reach the top electrode is

$$t_x = \frac{x}{\mu E_a}$$

where E_a is the average local field in which the holes are moving.

The number of holes reaching the electrode, to be subsequently extracted, is given in terms of a mean recombination lifetime, τ , by

$$\begin{aligned} Q &= Q_0 \cdot \exp\left(-t_x/\tau\right) \\ &= Q_0 \cdot \exp\left(-x/\mu E_a \tau\right) \end{aligned} \quad (5.1)$$

Assuming an initially uniform ionization density, the mean distance through which all such sheets drift is equal to $w_0/2$ where w_0 is the excitation depth. Hence the number of free electrons remaining in the crystal, which can be equated to the number of holes reaching the top electrode, is given by

$$Q = Q_0 \cdot \exp\left(-w_0/2\mu E_a \tau\right) \quad (5.2)$$

In practice, the average value of E_a changes from the applied field

E , at $t = 0$ to approximately $E(1 - \frac{1}{2\beta})$ when all the holes have left the crystal or recombined. Here β has the value determined from the experiments above. Using $\bar{E}_a \approx E/2$, equation (5.2) yields

$$Q = Q_0 \cdot \exp(-w_0/\mu E \tau) \quad (5.3)$$

This last expression gives a curve which qualitatively agrees with the results of figure 5.13. By careful curve fitting the average recombination lifetime, τ , can be obtained. The solid line in figure 5.13 shows the best fit between equation (5.3) and the experimental points using $w_0 = 10^{-4}$ cm and $\tau = 5 \times 10^{-5}$ sec.

This value of τ may be compared with the results of section 5.3 where $\tau = 7 \times 10^{-5}$ sec for the surface region was obtained by a different method. The good agreement between the two values suggests that the analysis described here provides a satisfactory explanation of the dependence of Q on E .

We are now in a position to explain the approximately square-law dependence of electron current on applied field at all excitation levels. It may be seen on examination, that for fields greater than about 10^3 V.cm^{-1} , the curve of figure 5.11 may be approximated fairly well by a straight line, A. Thus within the range of interest equation (5.3) can be written

$$Q = kQ_0 (E - E')$$

where E' is a constant equal to about 10^3 V.cm^{-1} . Provided E is not too small this leads to

$$\begin{aligned} j &= Q \cdot \mu \cdot E \\ &\approx kQ_0 \cdot \mu \cdot E^2 \end{aligned}$$

5.2.1 Accuracy of Mobility Determinations from Transit Time

It is valuable to re-examine the results of mobility determinations utilising transient SCL currents. The results of figure 5.12 show that in this series of measurements, which was typical of those used for mobility determinations, the value of β varied from 2.2 to 3.5 as the field was changed. The theoretical computations shown in Table 5.1, indicate that the ratio t'_t/t_t varies from 0.85 to 0.89 in this range of β . This causes the plot of $1/t'_t$ against E to become slightly curved. However, in practice, the experimental errors involved in a single measurement of t'_t are in the region of 10% and are therefore sufficient to mask the effect. For most mobility determination an average value of 0.87 for t'_t/t_t was used and the mobility was determined from the slope of a linear plot of $1/t'_t$ against E.

β	t'_t/t_t
2.00	.845
2.25	.856
2.50	.865
2.75	.874
3.00	.881
3.25	.888
3.50	.893
3.75	.899

5.2.2 Transient SCL Currents in the Presence of Trapped Carriers

All of the experimental results for which the analysis presented above was applied were obtained on crystals substantially free from trapped carriers. Care was taken to achieve space-charge neutralization by the use of discharge pulses in the way described in section 4.3.1.

It was of interest to investigate qualitatively the influence of a space-charge of trapped carriers on the transient SCL current pulse. A number of excitation pulses in succession at 10 c/sec were allowed to fall on the specimen which was initially space-charge free. A multiple exposure of the resulting oscilloscope traces of the current pulses is shown in figure 5.8(b).

It is seen that, with successive pulses of excitation, the total charge transported across the specimen becomes smaller, while the transit time becomes progressively longer. On a number of specimens it was found that the equilibrium density of trapped space-charge caused the transit time to increase by about 12%. Apparently the influence of the mobile and the trapped space-charges on the transit time are very nearly equal and opposite; the transit time then becomes equal to t_t .

5.3 Experimental Results for electron lifetime with respect to deep traps by Interrupted Transits

A particularly striking feature of the electron transit current after low level excitation is the remarkably flat top exhibited by the pulse even though transits lasting several milliseconds were observed. This indicates that, for the duration of the transit, very little deep trapping takes place in the crystal bulk. The method of interrupted transits, described in section 4.4, enabled the electron free lifetime to be determined directly and, furthermore, provided the opportunity for studying the lifetime at various distances from the region of generation beneath the surface.

The temperature dependence of electron diffusion coefficient was also measured by performing a series of measurements of the electron free lifetime at various temperatures.

A photograph of an interrupted transit current pulse is shown in figure 5.14. All measurements of current after reapplication of the field were performed after at least $400 \mu\text{sec}$, so that switching transients had a negligible effect on the accuracy. In some extreme cases when the current was very small, the amplifier recovery was taken into account by making measurements both with and without excitation pulses.

Measurements on one crystal at room temperature gave the results shown in figure 5.15. The ratio of electron conduction currents before and after interrupting the applied field is plotted semi-logarithmically as a function of the interruption time, t_1 . The various curves are

plotted for different distances travelled by the generated cloud of carriers, x , before the field was reduced to zero. The slope of the curves is proportional to the electron free lifetime, τ .

The results clearly show that for $x \gg 38 \mu$ the electron lifetime can be described in terms of a single time constant, τ_f . For $x \lesssim 38 \mu$ however, τ is not independent of time, t_i , and the initial part of the current decay is more rapid. All values of τ converge for large t_i towards the constant value, τ_f , obtaining near the centre of the specimen. For this particular specimen τ_f was determined to be 4.4 msec, and measurements on other crystals showed values up to 17 msec.

It is interesting to make estimates of the trap density which would lead to this value of lifetime on the basis of a hopping model. If we assume that the electron 'hops' into a trap and, further, that the electron has equal probabilities of hopping into a trap or of hopping on to a molecular site, (figure 2.6), τ_f is given by

$$\tau_f = \frac{1}{P} \cdot \left(\frac{N_m}{N_t} \right) \quad (5.4)$$

Here P is the hopping probability defined by equation (2.27) and N_m, N_t are the densities of molecular sites and of traps respectively.

Since $P = 4.4 \times 10^9 \text{ sec}^{-1}$ at room temperature, (see section 6.3), and $N_m = 5 \times 10^{21} \text{ cm}^{-3}$ the above measured value of $\tau_f = 4.4 \text{ msec}$ corresponds to $N_t \approx 2 \times 10^{14}$ traps per cc.

It appears that the electron lifetime may be determined by two processes in the region near the electrode. It may be seen that the

initial rate of electron current decay is more rapid near the region of generation and it is very probable that, simultaneously with deep trapping, a certain amount of recombination with trapped holes takes place. Since a proportion of the generated holes would be extracted under the influence of the applied field, recombination could only account for a fraction of the reduction in electron density before all the trapped holes had recombined. Beyond this stage, the electron density would decrease exponentially by deep trapping.

A modified version of the experiment was used to determine the recombination lifetime in the region of generation. The excitation pulse was arranged to occur at predetermined time intervals before the field was applied. The initial value of conduction current pulse, i_0 , on application of the field was determined for various periods of time, t , between the excitation and field pulses. i_0 was plotted semi-logarithmically as a function of t .

The decay was not exponential, (figure 5.16), but the slope of the current decay curve at $t = 0$ was used to derive the initial value of recombination lifetime. The results led to $\tau = 7 \times 10^{-5}$ sec at $t = 0$. The very much shorter lifetime in the generation region suggests that the density of recombination centres near the surface is at least two orders of magnitude higher than the density of traps in the bulk.

5.3.1 Temperature dependence of Electron Lifetime

The preliminary investigation described above showed that a constant lifetime with respect to deep traps, τ_p , could be assigned to

generated electrons at distances greater than about 38μ from the surface. A number of determinations of τ_f at different temperatures in the range -33°C to $+57^\circ\text{C}$ were made by interrupting the drift of the electron cloud at the centre of a specimen 155μ thick.

Values of $\log(\tau_f)$ for this specimen are plotted in figure 5.17 as a function of $10^3/T$. It may be seen that there is a greater scatter of points than the corresponding set of measurements of mobility, largely because of the greater complexity involved in the measurements. The slope of the line gives the diffusion activation energy of $0.21 \pm .02\text{eV}$.

Since the diffusivity is related to the drift mobility by the Einstein equation, $D = \frac{\mu kT}{e}$, when the factor kT is taken into account these results lead to a slightly lower value of $0.19 \pm .02\text{ eV}$ for the mobility activation energy. This is in good agreement with the value determined from drift mobility measurements, (section 5.1.2) and lends support to the initial assumption that an electron 'hops' into a trap from a neighbouring molecular site.

This last conclusion is of importance when the depth of a trap is calculated on a hopping picture in terms of its release time by thermal excitation. The theory outlined in section 2.2 is supported by the above result and is used to interpret the experimental results for deep traps in the next section.

5.4 Study of Trap near 0.95eV by Polarization Decay

The electron beam probing technique described in section 4.6 was used to examine the rate of polarization decay at various temperatures. Of particular interest was a careful examination of the level of electron traps near 0.95eV reported by Adams & Spear, (1964), since this trap was too deep for study by the method of thermally stimulated conductivity.

A number of specimens were prepared from different batches of grown crystals and they all yielded similar results. The electron beam probe pulse was 100 nsec long and displacement charges due to the motion of generated holes in the field of the trapped electrons were measured at various intervals of time after polarization. After each probe pulse the specimen was completely discharged and repolarized to saturation in the presence of an applied field by 15 excitation pulses each lasting $200 \mu\text{sec}$.

Charge displacements during probing were compared with those obtained 20 msec after polarization. The experiment was repeated at various temperatures in the range 21°C to 40°C .

Difficulties were experienced with some specimens. The decay of polarization was not always exponential over the entire range. In the millisecond time range the decay was more rapid and in the range of several hours the decay was slower. To overcome these effects which were due to thermal release from neighbouring trapping levels, (see section 5.5), the temperature range was limited to about 20°C and time

intervals were restricted at each temperature so that the range of polarization decay covered less than one order of magnitude.

The space-charge decay for a typical crystal at three temperatures is shown in figure 5.18. The time constant for thermal release, τ_r , at 21°C was 104 minutes. The activation energy calculated from these curves by $\tau_r \propto \exp(\epsilon_t/kT)$ yielded $\epsilon_t = 0.95 \pm .02$ eV in good agreement with the value of $\epsilon_t = 0.94$ eV reported by Adams & Spear, (1964), the value 0.95 eV by Thornber & Mead (1965) and the value 0.92 eV by Dean & Royce, (1960).

A comparison can be made between the trap depth calculated by these means and that calculated from the release rate on the basis of a hopping model as described in section 2.2. On the assumption that an electron 'hops' into a trap from a neighbouring molecular site, the release time constant is given by equation (2.44),

$$\tau_r = P^{-1} \exp\left(\frac{\Delta\epsilon}{kT}\right) \quad (5.5)$$

where $\Delta\epsilon$ denotes the energy difference between the molecular site and the deep trapping level (figure 2.6). From the experimental mobility values, (section 6.3), the probability of hopping between molecular sites is $P = \left(\frac{kT}{ea^2}\right) \times \mu_e = 4.4 \times 10^9 \text{ sec}^{-1}$ at 21°C. Over a small temperature range this can be written as

$$P = P_0 \cdot \exp\left(-\frac{\epsilon_a'}{kT}\right) \quad (5.6)$$

where $\epsilon_a' = 0.18$ eV. Substituting P and the measured value of τ_r into equation (5.5) then leads to $\Delta\epsilon = 0.78$ eV and ϵ_t is therefore

$$0.78 + 0.18 = 0.96 \text{ eV.}$$

The remarkably close agreement between the predicted and observed values of ϵ_t lends support to the initial assumption that the thermal release can be described in terms of a hopping model.

5.5 Experimental results for thermally stimulated conductivity

The electron trapping spectrum was measured on eight crystals using the method outlined in section 4.5.

At low temperatures, virtually noise-free conductivity peaks were readily observable at a variety of heating rates in the range $0.1 - 0.5^{\circ}\text{C}.\text{sec}^{-1}$. Above about 220°K however, the currents tended to be particularly noisy, and in some specimens it was found impossible to obtain any accurate measurements of conductivity. The noise was probably associated with the different expansion coefficients of the specimen and the contact, since contacts of vacuum deposited gold on both sides of the specimen tended to reduce the noise. The specimens always became progressively more noisy as they were cyclically heated and cooled, and the most detailed studies of the peaks appearing above about 220°K were obtained on newly prepared samples.

Altogether measurements were made on 8 crystals taken from three separate batches; all exhibited the same series of four prominent conductivity peaks. A representative conductivity glow curve is shown in figure 5.19 where the linear pen recording of current has been reproduced on a logarithmic scale. No additional peaks were observed on any other crystals.

A number of methods are available for estimating trap depths from the position, magnitude and widths of the observed peaks. A critical comparison of these methods as applied to Cds has been made by Dittfield & Voigt(1964) and a general review is to be found in the dissertation

of Heijne(1961). Only two methods were employed here, the first based on an analysis by Randall & Wilkins,(1945), and the second suggested by Broser & Warminsky,(1952).

The analysis by Randall & Wilkins considers the general kinetic equations for the conduction current as a function of time in the absence of retrapping, while the specimen is heated at a constant rate. The result shows that within the range of heating rates used here, the glow curve peak occurs when the time constant for thermal release from the trap is in the region of 1 second. Thus the trap depth, ϵ_t , is given by

$$\epsilon_t = kT_m \ln(\nu_0) \quad (5.7)$$

where T_m is the temperature at which the peak occurs. The frequency factor, ν_0 , is characteristically $10^{10} - 10^{14} \text{ sec}^{-1}$ for most wide band solids with neutral trapping centres.

If this result is modified for a hopping model, the analysis of section 2.2 shows that the thermal release time constant, τ_r , is given by

$$\tau_r = P^{-1} \exp\left(\frac{\Delta\epsilon}{kT}\right) \quad (5.8)$$

where $P \approx P_0 \exp(-e'_a/kT)$. The experimental mobility results yield a value of $5 \cdot 10^{12} \text{ sec}^{-1}$ for P_0 and if $\tau_t = \Delta\epsilon + e'_a$ is measured from a 'conduction level' lying 0.18eV above the molecular site, (section 6.3), equation (5.7) becomes

$$\epsilon_t = kT_m \ln(P_0) \quad (5.9)$$

It is thus seen that the depths of trap calculated from equations (5.7) and (5.9), will be very similar.

The analysis by Broser & Warminsky applies to crystals in which replenishment of charge from the electrodes is possible. It is shown that the current maximum occurs when the quasi-Fermi level for electrons passes through the trapping level. Since this analysis assumes that the mobility is independent, or nearly independent, of temperature, it is necessary to modify the expressions to take into account the activated electron mobility obtaining in sulphur.

If we write $\mu = \mu_0 \cdot \exp(-\epsilon_a/kT)$, the experimental mobility results yield $\mu_0 = 0.44 \text{ cm}^2 \text{V}^{-1} \text{sec}^{-1}$. The expression for the trap depth, measured from a 'conduction level' now 0.17 eV above the molecular site, then becomes

$$\epsilon'_t = kT_m \cdot \ln \left\{ \frac{N_c \cdot e \cdot \mu_0}{\sigma_m} \right\} \quad (5.10)$$

where N_c is the effective density of states in the conduction band, e is the electronic charge and σ_m is the value of conductivity measured at the glow curve maximum.

On a hopping picture, N_c in the above expression must be replaced by the density of molecules, $N_m = 5 \cdot 10^{21} \text{ cm}^{-3}$.

Using these methods, the values of ϵ'_t determined from the peaks are given in table 5.2.

Table 5.2

Approximate trap depths determined from glow curve peaks

Peak	Randall & Wilkins (ϵ_t)		Broser & Warminsky (ϵ_t')
	$\beta_0 = 10^{12} \text{ sec}^{-1}$	$\beta_0 = 3 \cdot 10^{12} \text{ sec}^{-1}$	$\mu_0 = 4.4 \text{ cm}^2 \text{ V}^{-1} \text{ sec}^{-1}$
1	0.36 eV	0.37 eV	-
2	0.43 eV	0.44 eV	0.39 eV
3	0.59 eV	0.60 eV	-
4	0.74 eV	0.76 eV	0.77 eV

No peaks were observed corresponding to traps lying in the range 0.27 - 0.36 eV.

An important aim of these studies was to test the possibility that the density of traps might be altered by annealing or rapid quenching. The total charge released from the two traps at 0.37 eV and 0.44 eV was measured after different cooling rates from room temperature. In some cases the specimen was cooled somewhat and held at this temperature before being quenched by rapid cooling to 100°K.

Table 5.3 shows the experimental results for the peak at 0.44 eV. The small peak at 0.37 eV was too small to make accurate measurements but within a factor 2 this remained constant for all the runs.

Table 5.3

Glow curve peak amplitude after different cooling schedules

<u>Holding temperature</u>	<u>Holding time</u>	<u>Cooling time to 100°K</u>	<u>Peak height</u>
+21°C	(new specimen)	90 mins	3.8×10^{-12} A
+21°C	48 hours	12 min	3.8×10^{-12} A
-23.5°C	20 mins	10 min	3.5×10^{-12} A
-58°C	4½ hours	10 min	3.9×10^{-12} A
-128°C	40 mins	6 min	3.3×10^{-12} A

The results show that the height of the conductivity glow curve peak at 0.44 eV is independent of the cooling rate to within about 10%.

The results of this experiment have an important bearing on the interpretation of the electron mobility results discussed in section 6.2.

5.6 Exciting Molecular Vibrational Modes using a Laser Beam

It will be shown in section 6.3, that the most consistent interpretation of the electron mobility results is based on an intermolecular hopping mechanism in which the electron interacts strongly with one or more vibrational modes of the molecule. Under these circumstances, the mobility should be enhanced if these molecular vibrations can be excited with highly absorbed radiation at the appropriate wavelength. The analysis of section 6.3 shows that one of the modes with which the electron interacts strongly may be the e_g fundamental stretching mode of the S_8 molecule. This gives rise to a strong peak in the infra-red absorption spectrum of S_8 at 193 cm^{-1} ; the half-width of this peak is about 10 cm^{-1} .

Vibrational modes at this wavelength were excited by using the pulsed output from a water vapour laser,[†] [Crocker, Gebbie, Kimitt & Mathias, (1964)]. The output power in two narrow peaks at 186 and 182 cm^{-1} was 8.10^{-4} and 6.10^{-2} watts respectively and the pulse duration was about 10^{-5} sec.

Triggering facilities were provided so that, in measurements of electron mobility by the methods described in section 4.1, the laser

[†] This experiment was carried out with the kind cooperation of Mr. L. Mathias and Mr. A. Crocker in the IR laser research division of SERL, Baldock, England.

pulse was phased to occur when the electrons had travelled about half way across the specimen. The IR radiation was allowed to reach the crystal through a fine evaporated gold grid back electrode.

The electron pulse height and transit time were carefully examined for any change in amplitude or duration due to absorption of the laser output. Within the limits of detectability of 0.5% in transit time and of 0.1% in electron current, no effect was observable.

This experiment must be regarded as inconclusive. Should an effect have been observed it would have provided valuable support for the suggested interpretation of electron transport and also given information concerning the vibrational mode with which the electron interacts. The negative result could be explained by the dispersion of vibrational frequencies which would reduce the lifetime of the excess phonon by other modes. If this effective lifetime is short then a much higher intensity IR beam would be needed to change significantly the density of phonons at this particular frequency from its thermal equilibrium value.

Should a laser become available in the future providing a strong output at either this wavelength or at 214.5 cm^{-1} , (a_1 fundamental breathing mode), it would be interesting to repeat this experiment. Examination of the IR absorption spectrum shows that this latter peak is very sharp and therefore a stronger perturbation of the thermal equilibrium phonon density may be possible under excitation.

6. Discussion of Experimental Results

In this concluding section of the thesis the experimental results are discussed in terms of the theoretical models applicable to low mobility solids. The results for electron mobility and its temperature dependence are particularly significant and a critical examination of the various possible mechanisms of transport provides a reliable foundation for an extension of the same fundamental principles to trapping phenomena. The electronic structure of the solid in terms of the preliminary molecular orbital calculations is used to provide a semiquantitative background against which the analysis is developed, and an approximate method is used to estimate the extent of vibrational interactions.

The extremely small and consistent values of electron mobility and the observation that the mobility is an activated process over more than two orders of magnitude provides the basis for a discussion of the transport mechanism in terms of three models. Analysis of the mobility results in terms of these models is critically examined in the next three sections and a further discussion of various trapping phenomena is to be found in section 6.4.

6.1 Interpretation of the electron mobility results on a trap-controlled model

A mechanism of trap-controlled mobility is essentially a band model in which the electrons interact with shallow traps below the conduction band. For the time being, the trap density is assumed constant,

As shown in section 2.3,

$$\mu_{\text{drift}} = \mu_L \cdot (N_c/N_t) \cdot \exp(-\epsilon_t/kT)$$

in the strongly trap-controlled mobility range.

It is possible to estimate the maximum value of the ratio (N_c/N_t) obtaining in sulphur on the basis of the experimentally determined values, $\mu_{\text{drift}} = 7 \cdot 10^{-4} \text{ cm}^2 \text{ V}^{-1} \text{ sec}^{-1}$ at 300°K and $\epsilon_t = 0.17 \text{ eV}$. According to the limitation imposed by the uncertainty relation described in section 2.1 a lower limit of $\mu_L \sim 1 \text{ cm}^2 \text{ V}^{-1} \text{ sec}^{-1}$ can be assigned for a band model to apply.

The result turns out to be

$$N_c/N_t \lesssim 0.6$$

The limiting value of $\mu_L \sim 1 \text{ cm}^2 \text{ V}^{-1} \text{ sec}^{-1}$ implies a narrow band in which N_c must be very near the density of molecules in the crystal. Clearly the suggestion that the traps may be the result of an included impurity or structural defect must now be rejected. It thus appears that the model would only apply to a solid in which every molecule was capable of acting as an electron trap.

The logical conclusion of this analysis therefore leads to an essentially different mechanism of electron transport. Localized electron states below the conduction band might arise as a result of vibrational interactions; according to the analysis by Toyozawa (section 2.1.2) a type of thermally activated drift motion could result. However, it is also possible for motion between localized states to occur without activation into a band provided the molecular orbital overlaps corresponding to these states is not vanishingly small. In this case, as a result of finite overlaps, a narrow band would be formed and either narrow band carrier motion or hopping conduction would occur without activation into an adjacent band. Again the role of vibrational interactions might be important and, as a result, further localization of the electron in a self-trapped state would take place.

It is interesting how the application of a trap-controlled mobility interpretation to the present results leads immediately to a model of electron transport in which vibrational interactions play an important role. However, the deductions made in this section are sufficiently modified to invalidate the above conclusion if the traps arise as a result of thermally generated point defects, and this model is now considered.

6.2 Trap-Controlled Mobility in Presence of thermally generated Point Defects

This model is still essentially a band picture but the shallow traps with which the electron interacts are now capable of changing in density as the crystal temperature is altered. As shown in section 2.4 this leads to an activated drift mobility in the strongly trap-controlled temperature range, given by

$$\mu_{\text{drift}} = \mu_L \left(\frac{N_c}{N_m} \right) \cdot \exp\left(-\frac{\epsilon_t - \epsilon_f}{kT} \right)$$

where ϵ_f is the heat of formation of the defect. In this case the experimentally determined activation energy is $(\epsilon_t - \epsilon_f) = 0.17\text{eV}$ and the analysis of the preceding section can be used to show, as before, that $(\frac{N_c}{N_m}) \lesssim 0.6$. Since $N_c \sim N_m$ for narrow bands this result is no longer unreasonable and it is necessary to examine carefully the implications of such a model.

On the basis of experiment it is possible to assign approximate values to ϵ_t and ϵ_f . An important requirement is for the trapped electron to be released from the defect centre by thermal excitation, rather than by the ionized defect relaxing into an ordered lattice position. Thus we can write,

$$\omega \cdot \exp(\epsilon_t/kT) \ll \nu \exp(\Delta/kT)$$

where ω and ν are crystal lattice vibrational frequencies and Δ is the excitation energy for annealing a defect.

$$\text{Hence } (\epsilon_t - \Delta) \ll kT \ln(\nu/\omega)$$

Since ν and ν_0 would be expected to be of the same order this can be rewritten,

$$\epsilon_t - \Delta \lesssim kT \sim 0.03\text{eV}$$

Further estimates can be based on the rate at which a thermal equilibrium density of defects is established after a change of temperature. In section 2.4 it is shown that the time constant for this process is given by

$$\tau_e = \nu^{-1} \exp\left(\frac{\epsilon_f + \Delta}{kT}\right)$$

The measurement of mobility as a function of temperature shown in figure 5.3 were performed at time intervals between 10 and 30 minutes after each temperature change. Thus the model would apply to the present experimental results only if $\tau_e \ll 10^3 \text{sec}$ which leads to $(\epsilon_f + \Delta) \ll 0.89 \text{ eV}$ for $\nu = 5.10^{12} \text{sec}^{-1}$.

We thus have three equations,

$$\epsilon_t - \epsilon_f = 0.17\text{eV}$$

$$\epsilon_f + \Delta \ll 0.89\text{eV}$$

$$(\epsilon_t - \Delta) \lesssim 0.03\text{eV}$$

from which it may be deduced $\epsilon_t \ll 0.55\text{eV}$, $\epsilon_f \ll 0.38\text{eV}$, $\Delta \lesssim 0.52 \text{ eV}$.

By similar arguments, a lower limit can be assigned to ϵ_t . Thus by making the estimate $N_t \lesssim 10^{-2} N_m$ for a band model to apply, and using $N_t = N_m \exp(-\epsilon_f/kT)$, it is shown that $\epsilon_f \gtrsim 0.12 \text{ eV}$ and hence $\epsilon_t \gtrsim 0.29\text{eV}$.

It is now possible to employ the data obtained for the electron trapping spectrum by experiments on thermally stimulated conductivity, (section 5.5). The only trapping levels which were found to be present in the range $0.29\text{eV} \lesssim \epsilon_t \lesssim 0.55\text{eV}$ were shown to be those at 0.37eV and 0.44eV . Neither of these levels was changed in density by different cooling and annealing schedules.

On the basis of the conductivity glow curve results it can thus be concluded that the present electron transport model cannot be substantiated. A simple calculation shows that the annealing time for these two traps should increase to at least 10^3 sec when the specimen is cooled to temperatures between -35° and -80°C . If they were capable of being annealed, the effect of different cooling and annealing times should have been readily observable within the range of the experiment.

6.3 Interpretation of the Electron Mobility Results on

Hopping Model

With the preliminaries of sections 6.1 and 6.2 settled, it now remains to attempt an interpretation of the electron mobility results in terms of an intermolecular hopping mechanism. The extremely small and consistent values of activated mobility are certainly in accord with such a mechanism. In this section the experimental results are fitted to the theoretical analyses by Holstein and Yamashita and Kurosawa and a number of model parameters are derived from the experimental results. From an examination of the limits of validity of the analysis and the infra-red absorption spectrum of S_x , estimates are made of the energies of the molecular vibrational modes with which the electron interacts strongly. The results are compared with an approximate value of the polaron binding energy using the simplified model suggested by Friedman. A fit of the experimental results to Toyozawa's model, in which self-trapping arises by interactions with acoustic vibrational modes, is also attempted. The conclusions of this analysis are discussed in terms of the physical nature of the interactions to be expected in sulphur.

The experimental mobility results of figures 5.3 and 5.4 show that the electron mobility for all crystals is equal to $6.2 \pm 0.6 \times 10^{-4} \text{ cm}^2 \text{ V}^{-1} \text{ sec}^{-1}$ at 21°C and its temperature dependence can be expressed by

$$\mu = \mu_0 \cdot \exp(-\epsilon_a/kT) \quad (6.1)$$

where $\epsilon_a = 0.167 \pm .005 \text{ eV}$ and $\mu_0 = 0.45 \pm .05 \text{ cm}^2 \text{ V}^{-1} \text{ sec}^{-1}$.

Since the temperature dependence of μ is exponential over the entire range, it is possible to describe the results on a hopping picture, using the high temperature limit approximation, equation (2.30),

$$\mu = \frac{ea^2}{\hbar} \left(\frac{\pi}{2E_b} \right)^{\frac{1}{2}} \frac{J^2}{(kT)^{\frac{3}{2}}} \exp \left(- \frac{E_b}{2kT} \right) \quad (2.30)$$

If the factor $(kT)^{-3/2}$ is taken into account, this leads to $E_b/2 = 0.20$ eV. Thus the polaron binding energy is $E_b = 0.40$ eV.

However, as shown below, a small adjustment to this value of E_b is necessary if the full expression, (2.21) is used for P , rather than the asymptotic expansion, (2.26), implicit in (2.30).

In terms of the site jump probability, P , the mobility is given by equation (2.29) thus,

$$\mu = \frac{ea^2}{kT} \cdot P \quad (2.29)$$

From the experimental mobility values, $P = 4.4 \times 10^9 \text{ sec}^{-1}$ at 21°C , where an average spacing between molecular sites of $a = 5.95 \text{ \AA}$ has been used. If the mobility is expressed by equation (6.1), and account is taken of the extra term kT in equation (2.29), then P can be written,

$$P = P_0 \cdot \exp \left(- \frac{E_a'}{kT} \right)$$

where $P_0 = 5.1 \times 10^{12} \text{ sec}^{-1}$ and $E_a' = 0.18$ eV. It may be seen that for all temperatures below the melting point of S_{80} at 386°K , the electron is localized on a molecule for many periods of molecular vibration.

The intermolecular exchange energy, J , appearing in equation (2.30) can now be derived from the experimental mobility values.

Using $a = 5.95 \text{ \AA}$ as before, the result is $J = 0.05 \text{ eV}$. It may be noted that this value is somewhat larger than the approximate value calculated in section 3.4.

It is constructive to examine the electron lattice interaction in greater detail. In section 2.1, it was shown that the polaron binding energy, E_b , can be expressed in terms of a dimensionless electron-lattice interaction parameter, γ ,

$$E_b = \gamma k \omega_0$$

where the molecular vibrational modes are assumed to have the same frequency ω_0 . If, for the moment, it is assumed that the electron interacts predominantly with only one vibrational mode, then values of γ and $k\omega_0$ can be assigned consistent with the experimentally determined value of E_b .

A plot of the full theoretical expressions for hopping probability, P_Y , equation (2.20) and P_H , equation (2.21) for various values of the interaction parameter γ are shown in figure 2.5. From these curves and equation (2.29) it is possible to derive the form of the temperature dependence of mobility; these results are shown in figure 6.1 for four values of γ . It may be seen that for $\gamma = 10$ the deviation from an exponential law is too great for the experimental mobility values to be fitted. For $\gamma \approx 15$ the theoretical expression can be fitted to the experimental curve provided $k\omega_0 = E_b$ is adjusted to obtain the observed value of the activation energy. Table 6.1 shows the values of E_b found necessary to obtain a fit for various values of γ .

Table 6.1

γ	E_b (eV)	$\hbar\omega_0$ (eV)
∞	0.40	0.000
50	0.44	0.009
35	0.45 ₅	0.013
20	0.47 ₅	0.024
18	0.48	0.027
15	0.49	0.033

From the table it can be seen that $\gamma \gtrsim 15$ implies that $\hbar\omega_0 \leq 0.033$ eV.

The infra-red absorption spectrum for one of the crystals grown in this laboratory from solution in CS_2 is shown in figure 6.2 †. According to the assignments by Scott, McCullough & Kruse, (1964), the peak at 0.0265 eV corresponds to the a_1 symmetrical breathing mode of the S_8 molecule and the peaks at 0.0291 eV, 0.238 eV, 0.0186 eV and 0.0093 eV to e_1 , e_2 and b_2 stretching modes. It seems possible therefore that the electron interacts with one or more of these fundamental vibrational modes of the molecule. Table 6.2 shows the values of γ derived from these magnitudes of $\hbar\omega_0$ consistent with the calculated values of E_b given above.

† This absorption spectrum was kindly measured by Dr. D.M Adams of the Department of Chemistry at Leicester University, using an R.I.I.C FS520 automatic recording IR interferometer.

Table 6.2

<u>Vibrational mode</u>	<u>$1/\lambda$ (cm⁻¹)</u>	<u>$\tau\omega_0$(eV)</u>	<u>γ</u>	<u>E_b(eV)</u>
e ₂ fundamental	75.5	.0093	47	0.44
e ₂ fundamental	151	.0186	25	0.47
e ₁ fundamental	193	.0238	20	0.47 ₅
a ₁ fundamental	214.5	.0265	18	0.48
b ₂ fundamental	236	.0291	17	0.49

From these calculated values it is now possible to test whether expression (2.21), used in the interpretation of the mobility results, falls within the limits of validity as laid down by Holstein. These limits are expressed by equations (2.32) to (2.35) in section 2.1.6.

The low temperature limit for hopping to occur is given by (2.32), thus

$$\frac{\tau\omega_0}{2kT} \lesssim 1$$

This implies that, for the analysis to be valid down to 197°K, (the lowest temperature for which the electron mobility was measured), $\tau\omega_0 \lesssim .034$ eV. Thus all the values shown in table 6.2 fall within the requisite range. However further requirements for the analysis to be valid are given by inequalities, (2.33) to (2.35), thus

$$2J < (E_b)^{\frac{1}{2}} (\tau\omega_0)^{\frac{1}{2}} \quad (2.33)$$

$$2J \ll E_b \quad (2.34)$$

$$J < (E_b)^{\frac{1}{2}} \left(\frac{2kT}{\hbar}\right)^{\frac{1}{4}} \left(\frac{\tau\omega_0}{\hbar}\right)^{\frac{1}{2}} \quad (2.35)$$

It can be shown that (2.33) is satisfied for all values of $\tau\omega_0 \geq .023$ eV.

With both the approximate value of $J \sim 10^{-3}$ eV calculated in section 3.4 and the derived value of $J = .05$ eV from the above analysis, inequality (2.34) can be satisfied. Requirement (2.35) is the most stringent and this is fulfilled if $\hbar\omega_0 \geq .025$ eV.

If it is assumed that the electron interacts with only one vibrational mode, all the requirements of the Holstein analysis can be fulfilled for the a_1 breathing mode at .0265 eV and the b_2 fundamental at .0291 eV.

The conclusion that a fundamental stretching mode may play a part in self-trapping of the electron is not unexpected. However, no account has yet been taken of the more probable circumstance that more than one vibrational mode may be involved. In this case, the effective value of $\hbar\omega_0$ is given by (2.31) thus

$$(\hbar\omega_0)_{\text{eff}} = \frac{\sum \gamma_n \hbar\omega_{0n}}{\sum \delta_n} \quad (6.2)$$

and the above limits would apply where $.025 \text{ eV} \lesssim (\hbar\omega_0)_{\text{eff}} \lesssim .034 \text{ eV}$.

Thus the estimate $\gamma \sim 19$ must be regarded as the maximum value that any individual γ_n might assume. Higher energy modes can thus be brought within the bounds of validity of the analysis, but from the present experimental data it is not possible to draw any further conclusions about the individual values of γ_n and $\hbar\omega_{0n}$.

The large polaron binding energy, $E_p = 0.48$ eV, can be discussed in terms of the simplified model employed by Friedman, (1964).

Consideration of the S_0^- ion in section 3.2 showed that, due to the small overlaps between $3sp^3\sigma^*$ molecular orbitals centred on adjacent

pairs of atoms in the ring, the electron may interact locally with one or more vibrational modes. If the electron is confined between two sulphur atoms for a time long compared with the period of molecular vibrations, ($\sim 10^{-12}$ sec), then the contribution by skeletal stretching modes to the binding energy, E_{bs} , can be expressed in terms of the change in separation, Δx , of the two atoms when the molecule is ionized. The relation between bond length and bond order, R , can be fitted to the quadratic expression,

$$x = .03R^2 - .29R + 2.34 \quad (6.3)$$

where the bond length, x , is measured in \AA , and values of x for single, double and triple bonds have been taken from Pauling, (1950). Thus since the bond order will change from 1 to approximately $\frac{1}{2}$ in the presence of the excess electron, the bond length will increase by approximately $\Delta x = 0.12 \text{\AA}$. E_{bs} is then given by equation (2.15), thus

$$E_{bs} = \frac{1}{2}k (\Delta x)^2$$

Using the value of stretching force constant, $k = 2.37 \text{ mdyne/\AA}$, determined from the molecular vibrational spectra of S_8 by Scott et al. (1964), this yields,

$$E_{bs} \sim 0.10 \text{ eV}$$

Following Siebrand, (1964), since it is not possible to use this method for estimating the contributions to E_b from torsional and bending vibrational modes, it is assumed that these will be of the same order. Thus

$$E_b \sim 0.2 \text{ eV}$$

When consideration is given to the very approximate nature of the above calculation, the agreement with the previous estimate of $E_b = 0.48$ eV from the mobility results is fairly good.

It is interesting to note an implication of the present model. Since it is assumed that the electron will reside on a site between to adjacent sulphur atoms in the ring for a time long compared with the period of molecular vibrations, the electron will not only 'hop' between adjacent molecules in the solid, but it will also 'hop' round the ring. If the analysis by Holstein can also be applied to the isolated molecule, this means that the parameters, γ , and, $\hbar\omega_0$, will also apply to hopping from site to site within the molecule. However, from a comparison of the values of orbital overlap calculated in sections 3.1 and 3.4, it can be seen that the probability of hopping from site to site round the ring will be at least two orders of magnitude higher than that between adjacent molecules in the solid. Intermolecular transitions in the solid are thus not likely to be influenced strongly by hindered transitions round the ring and none of the previous conclusions concerning electron mobility needs to be modified.

Unfortunately, experimental verification of this behaviour of the odd electron in the isolated S_8^- molecular ion is lacking, and the justification for it must rest on the calculated values of orbital overlap. Certainly this behaviour would be in accord with the suggested interpretation of electron transport, and furthermore it allows fair agreement to be obtained between the two estimates of

polaron binding energy, E_p .

So far the self-trapping of the electron has been described in terms of interactions with molecular vibrational modes; from purely physical considerations these interactions would be expected to be the most important. If the electron interacted predominantly with acoustic lattice modes, however, the analysis by Toyozawa, (section 2.1.2), would apply. It is important to test this possibility.

According to analysis, the mobility activation energy, ϵ_a , in the hopping region is given by

$$0.184 \frac{E_d^2}{Ms^2} \lesssim \epsilon_a \lesssim 0.25 \frac{E_d^2}{Ms^2}$$

where E_d is the deformation potential constant, M is the mass of a unit cell, and s is the velocity of sound.

From measurements of the shift with temperature of the optical absorption edge by Dean & Royce, (1960), Moss, (1952), and by Bass, (1953), the value of E_d is calculated to be about $3.7 \text{ eV} \cdot \text{cm}^{-1}$. Using $s = 3.5 \times 10^5 \text{ cm} \cdot \text{sec}^{-1}$ this leads to $0.005 \text{ eV} \lesssim \epsilon_a \lesssim 0.007 \text{ eV}$. Agreement with experiment is thus very poor, as might be expected.

Somewhat better agreement is obtained, however, if the crystal structure is approximated by a cubic lattice having only one molecule per unit cell. In this case, on Toyozawa's theory, displacements of one molecule with respect to its neighbours might be responsible for self-trapping; physically this would appear to be a more reasonable assumption since the wavefunction for the odd electron does not extend very far through the unit cell. In terms of this modified model, the

activation energy is then given by

$$0.08 \text{ eV} \lesssim E_a \lesssim 0.10 \text{ eV}$$

This result is close to the experimental value of 0.17 eV, and in view of the uncertainty in the exact value of E_d , it must be regarded as good agreement.

The hopping models both of Holstein, in which molecular vibrational modes are involved, and of Toyozawa in which acoustic modes are involved, can thus be fitted to the experimental results. It is necessary to enquire whether this agreement is fortuitous or whether any physical reason can be found for the coincidence. An important question hinges on the type of distortion in the solid which gives rise to the change in band gap with temperature. If the changes arise mainly by distortions within the S_8 ring, and furthermore the same distortions are brought about when the solid is compressed, then a parallel can be found between the two approaches, since the interactions in both cases are effectively with molecular vibrational modes. If, however, the shift in band gap with temperature arises largely through changes in equilibrium separation of the molecules, then the agreement between the two theories would appear to be accidental.

These questions cannot be answered unequivocally on the basis of the presently available experimental data on sulphur. However, from the physical nature of the interactions to be expected in a molecular solid, it would not be unreasonable to reject the Toyozawa model.

6.4 Discussion of Trapping Phenomena

One of the most remarkable features of the experimental results on trapping is the long electron lifetime with respect to deep traps. However, this result is readily accounted for in terms of the hopping picture discussed in the previous section, if it is assumed that trapping can only occur when a hopping transition from an ordered molecular site into a trap takes place. Unlike a band picture where the electron would be free to make large excursions through the lattice with a mean kinetic energy of $\frac{3}{2}kT$, the electron in sulphur spends most of its time localized on molecular sites. From the experiments of section 5.3 it is shown that the free lifetime within the bulk is in the region of 10msec at room temperature, and, on the basis of a hopping picture, the density of deep traps is therefore about 10^{14} cm^{-3} . Such densities are not unexpected for relatively pure crystals free from a large number of lattice defects.

It must be emphasised, however, that the long lifetime cannot be regarded as evidence for hopping: a similar result would be expected on a strongly trap-controlled transport mechanism. In this latter case the electron would spend most of its time in shallow traps, and for only a small fraction of the time would it be free to interact with deeper centres. The arguments against such a model must rest with the analysis already discussed in sections 6.1 and 6.2.

The temperature dependence of electron lifetime provides an important result. Since the derived value of mobility activation energy from these experiments was the same, within experimental error,

as that determined from the drift mobility measurements, strong evidence is supplied in support of the assumption that electron transitions into the deep traps involve no potential barrier in addition to that which already exists between ordered molecular sites. These results therefore provide experimental justification for the analysis of trap density, (section 5.3), and of the release time from traps on a hopping model, (section 2.2), in which it is assumed that no such additional barrier exists.

Thermally stimulated conductivity investigations were conducted mainly to test whether the density of deep traps could be changed by different cooling or annealing schedules. The most important result of these experiments has already been used in a discussion of one possible mobility model, (section 6.2). Quantitatively, the calculated trap depths must be treated as only approximate because a very much greater variety of measurements would have been necessary to determine the depths with greater confidence than about 0.05 eV. However, it is clear that four discrete trapping centres in the range 0.27 - 0.77 eV were present in all the crystals. No experimental evidence was found for exponential distributions of traps as proposed by Thornber & Mead, (1965). These authors interpreted the rise in optical absorption near the fundamental absorption edge in terms of electron transitions from the valence band to a distribution of vacant centres lying below the conduction band. The present experimental results cannot substantiate this interpretation.

The trap near 0.95 eV is most interesting since its presence has been reported by several investigators in natural crystals as well as those grown from solution in CS₂. The close agreement between the depth calculated from the release time at room temperature and that determined from the temperature dependence of release rate provides additional support for the interpretation of electron transport.

The positions of the various traps in relation to the electron energy of an ordered molecular site are shown in figure 6.3.

7. Conclusions

Orthorhombic sulphur provides a good example of an insulating molecular solid in which transport of generated electrons takes place by an intermolecular hopping mechanism. It is shown that the most consistent interpretation of the experimental mobility results is based on a model in which the electron interacts strongly with one or more molecular vibrational modes. From an analysis of the experimental results, the polaron binding energy is found to be

$$E_b = \sum_n E_{bn} = 0.48 \text{ eV and the interaction parameter, } \gamma = \sum_n \gamma_n \sim 18.$$

The experimental results justifying this interpretation of the transport mechanism are summarized as follows:

- (1) The extremely small and consistent values of μ_e on more than 20 crystals prepared from starting materials of different degrees of purity, indicate that the electron mobility results are a fundamental property of the crystals. In the contrast to this, the room temperature hole mobilities on the same specimens show large variations.
- (2) Mobility is an activated process over the entire range from 193° to 386°K
- (3) The measured trap depth at 0.95 eV, and that calculated from the release rate on a hopping model are in close agreement.
- (4) The density of traps in the region, $0.27 \text{ eV} < \epsilon_t < 0.55 \text{ eV}$ is independent of cooling and annealing schedules.

The first three results enumerated above provide direct evidence in favour of a hopping model; the fourth enables a possible alternative mechanism to be eliminated. Further support for a hopping mechanism is provided by a number of theoretical studies, the principal features of which are enumerated as follows:

- (5) The approximate widths of electron and hole bands calculated from molecular orbital theory indicate that the electron band is sufficiently narrow .
- (6) Values of E_p calculated on the basis of a simple model compare reasonably well with the value derived from experiment.
- (7) Analysis on a model of trap-controlled mobility leads to the conclusion that every molecule must be capable of acting as a trap.

It is shown that the experimental studies of electron free lifetime and of deep trapping, although they do not provide additional evidence for a hopping mechanism, are consistent with such a model. Experimental values for the electron lifetime range from about 5×10^{-5} sec in the region of generation to about 10^{-2} sec in the bulk; such values would be expected with a density of recombination centres greater than $2 \times 10^{16} \text{ cm}^{-3}$ at the surface and a density of deep traps of about 10^{+14} cm^{-3} in the bulk.

Five discrete levels of electron traps were identified at 0.37 eV, 0.44 eV, 0.60 eV, 0.76 eV and 0.96 eV. These correspond to depths below an ordered molecular site of 0.19 eV, 0.26 eV, 0.42 eV, 0.58 eV and 0.77 eV respectively.

A strong case in favour of a hopping mechanism is presented here. Additional experimental and theoretical studies could usefully be undertaken to provide further insight into the processes taking place in the solid. If a high intensity source of infra-red radiation at the appropriate wavelength became available, the possibility of exciting molecular vibrational modes, sufficiently to enhance the electron mobility, presents an attractive direct test of the model and, furthermore, it should provide information on which modes are involved in self-trapping of the electron. A detailed theoretical study of the S_8 molecule would enable a more exact band structure calculation to be undertaken. This would not only provide accurate data for the electron and hole bandwidths but it would enable the extent of vibrational interactions to be calculated in a more precise way. There is a possibility of theoretically treating the isolated S_8 molecule as a very simple example of a "one dimensional" array of atoms in which vibrational interactions play an important part in localization of an excess electron.

AppendixAnalysis of Starting MaterialsA Analysis of CS₂ used as solventAnalar Reagent, BDH

Specific gravity, (20°C)	1.262 to 1.265
Distillation range	95% distils between 46° and 47°C
Acidity, (as SO ₂)	0.001% max
Non-volatile matter	0.003% max
Hydrogen sulphide, (H ₂ S)	0.00015% max
Sulphur dioxide, (SO ₂)	0.00025% max

Reagent Grade, M & B

Specific gravity, (20°C)	1.260 to 1.264
Distillation range	95% distils between 46° and 47°C
Acidity	Neutral to litmus
Non-volatile matter	0.01% max
Foreign sulphur compounds	No reaction

B Analysis of sulphur used as starting materialL. Light & Co., 6N Purity(UP)

Ca	0.2	ppm
Cu	0.1	ppm
Mg	0.05	ppm
Si	0.02	ppm
Ag	0.01	ppm
Na	0.1	ppm

BDH, Laboratory Reagent,(LR)

Ca	0.6	ppm
Na	0.8	ppm
K	0.5	ppm
Cl	7	ppm

References

- Abrahams, J.C.(1955) Acta.Cryst., 8 , 661
- Adams, A.R., Gibbons, D.J. & Spear, W.E.(1964) Solid State
Commun. 2 , 387
- Adams, A.R. & Spear, W.E.(1964) J.Phys.Chem.Solids, 25 , 1113
- Allen, T. (1959) J.Chem.Phys., 31 , 1039
- Bass, A.M. (1953) J.Chem.Phys., 21 , 80
- Broser, I. & Warminsky, R. (1952) Z.Phys., 133 , 340
- Caron, A. & Donahue, J. (1961) Acta.Cryst., 14 , 548
- Cartmell, E. & Fowles, G.W.A. (1961) 'Valency and molecular structure',
Butterworths
- Clementi, E. (1964) J.Chem.Phys., 40 , 1944
- Crocker, A., Gebbie, H.A., Kimmitt, M.F. & Mathias, L.E.S.(1964)
Nature,(London), 201 , 250
- Dean, P.J., Royce, B.S.H. & Champion, F.C.(1960) Proc.Phys.Soc.B,
(London), 75 , 119
- Dekker, A.J. (1962) 'Solid State Physics', Macmillan
- Dittfeld, H.J. & Voigt, J. (1963) Phys.stat.sol., 3 , 1941
- Friedman, L. (1964) Phys.Rev., 133 , A 1668
- Fröhlich, H. & Sewell, G.L.(1959) Proc.Phys.Soc.(London), 74 , 643
- Gáspár, R. (1957) Acta.Phys.Hung., 7 , 289
- Glarum, S.H. (1963) J.Phys.Chem.Solids, 24 , 1577
- Heijne, L. (1961) Philips Res.Rep.Suppl., 4 , 97
- Heikes, R.R. & Johnston, W.D. (1957) J.Chem.Phys., 26 , 682
- von Hippel, A. (1948) J.Chem.Phys., 16 , 372

- Holstein, T. (1959 *Annals of Physics*, 8 , 325)
- Honig, R.E. (1962) *R.C.A.Review*, 23 , 567
- Katz, J.I., Rice, S., Choi, S. & Jortner, J. (1963) *J.Chem.Phys.*, 39 , 1683
- Kotani, M., Ameniya, A., Ishiguro, E. & Kimura, T.(1963) 'Tables of
molecular integrals', Maruzen & Co.
- Le Blanc, O.H. (1961) *J.Chem.Phys.* 35 , 1275
- Kurrelmeyer, B. (1927) *Phys.Rev.*, 30 , 893
- Many, A., Simhony, M., Weisz, S.Z. & Levinson, J. (1961)
J.Phys.Chem.Solids, 22 , 308
- Many, A., Simhony, M. & Grushkevitz, Y.(1965) Private communication
- Mead, C.A. (1964) *Physics letters*, 11 , 212
- Morin, F.J.(1958) *Bell syst.tech.J.*, 37 , 1047
- Moss, T.S.(1952) 'Photoconductivity in the elements', Butterworths
- Mott, N.F. & Twose, W.D.(1961) *Advances in Physics*, 10 , 107
- Mulliken, R.S. Reike, C.A., Orloff, D. & Orloff, H. (1949), *J.Chem.
Phys.* 17 , 1248
- Olechna, D.J. & Knox, R.S.(1965) Private communication
- Papadakis, A.(1965) *Conf.Solid State Phys.*, Bristol, England.
- Pauling, L.(1950) 'The nature of the chemical bond', Oxford Univ.Press
- Randall, J.T. & Wilkins, M.H.F.(1945) *Proc.Roy.Soc.*, A 184 , 390
- Reitz, J.R.(1957) *Phys.Rev.*, 105 , 1233
- Scott, D.W., McCullough, J.P. & Kruse, F.H.(1964)*J.Mol.Spectr.*,13, 313
- Siebrand, W.(1964)*J.Chem.Phys.*, 41 , 3574
- Silver, M.(1965) Private communication
- Spear, W.E.(1960) *Proc.Phys.Soc.(London)*, 76 , 826
- Spear, W.E. & Adams, A.R.(1965) *J.Phys.Chem.Solids*,(In Press)

- Spear, W.E., Adams, A.R., & Henderson, G.A. (1963) *J.Sci.Insts.*, 40, 332
- Spear, W.E., Lanyon, H.P.D. & Mort, J. (1962) *J.Sci.Insts.*, 39, 81
- Spear, W.E. & Mort, J. (1963) *Proc.Phys.Soc.(London)*, 81, 130
- Tartakovsky, P.S. & Rekalova, G. (1940) *Zh.eksper.teor.Fiz.*, 10, 1025
- Thornber, K.K. & Mead, C.A. (1965) *J.Phys.Chem.Solids*, 26, 1489
- Toyozawa, Y. (1962) in 'Polarons & Excitons' (ed.Kuper, C.G. & Whitfield, G.D.)
Oliver & Boyd, p.211
- Toyozawa, Y. (1964) *Tech.Rept.Inst.Solid State Phys.*, Univ. Tokyo, A 119
- Warren, B.E. & Burwell, J.T. (1935) *J.Chem.Phys.*, 3, 6
- Yamashita, J. & Kurosawa, T. (1958) *J.Phys.Chem.Solids*, 5, 34
- Ziman, J.M. (1963) 'Electrons in Metals', Taylor & Francis

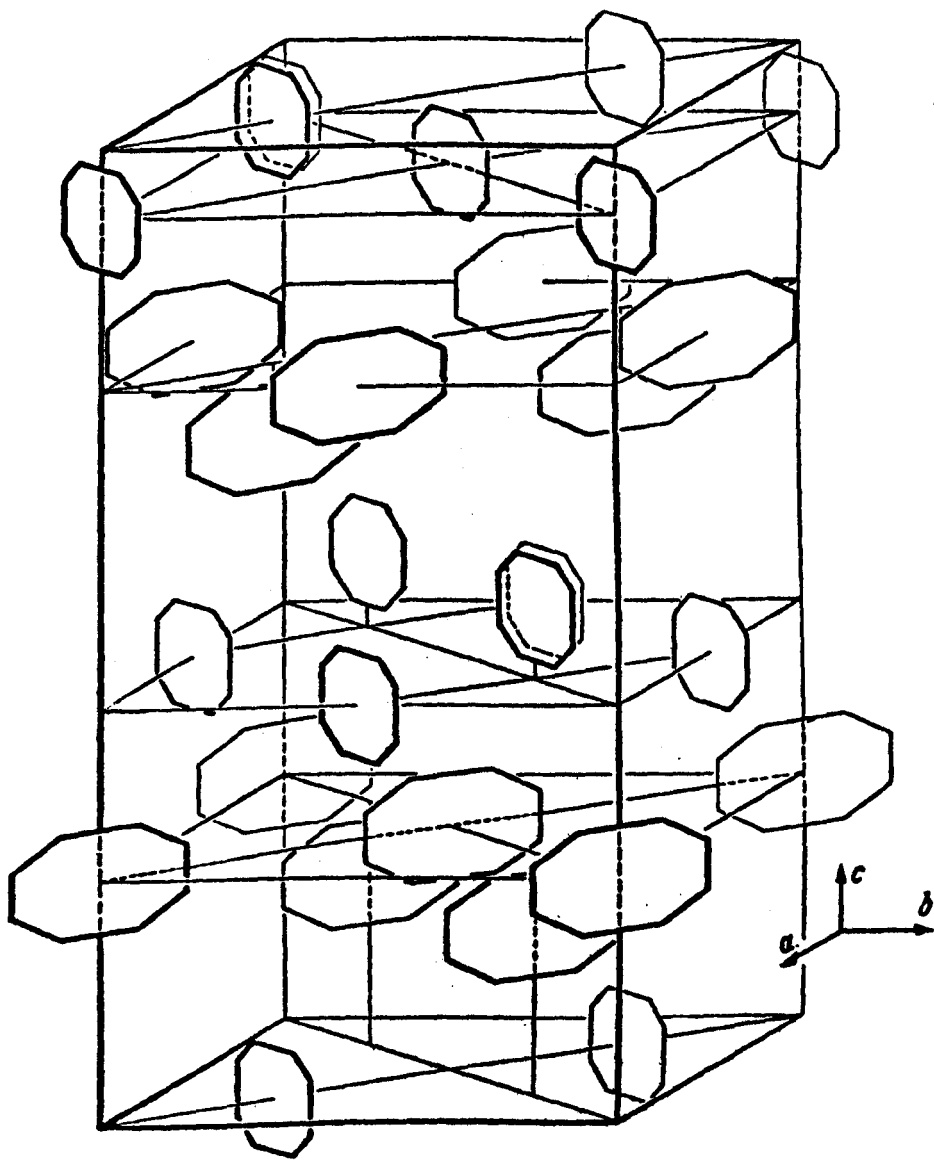
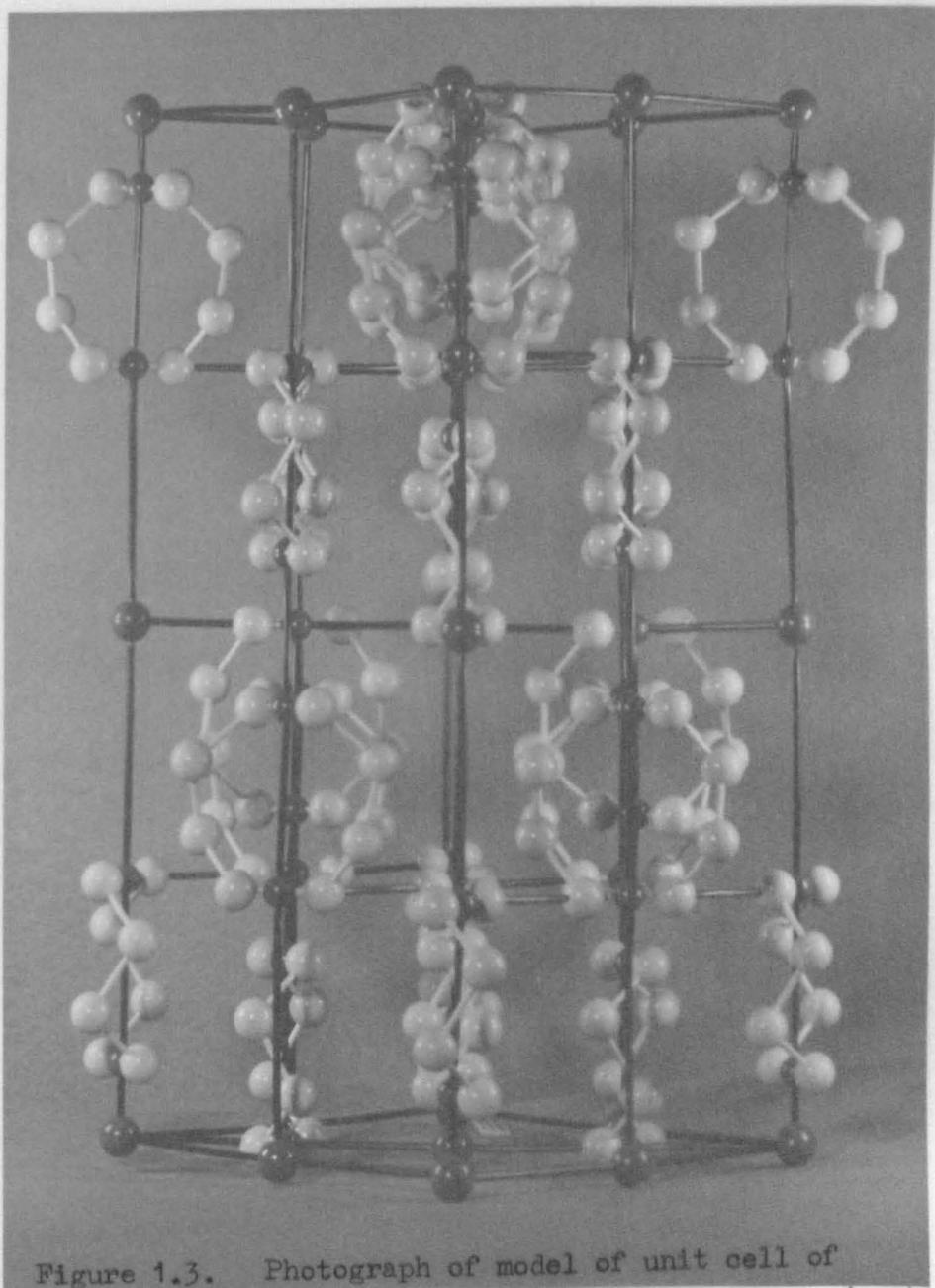
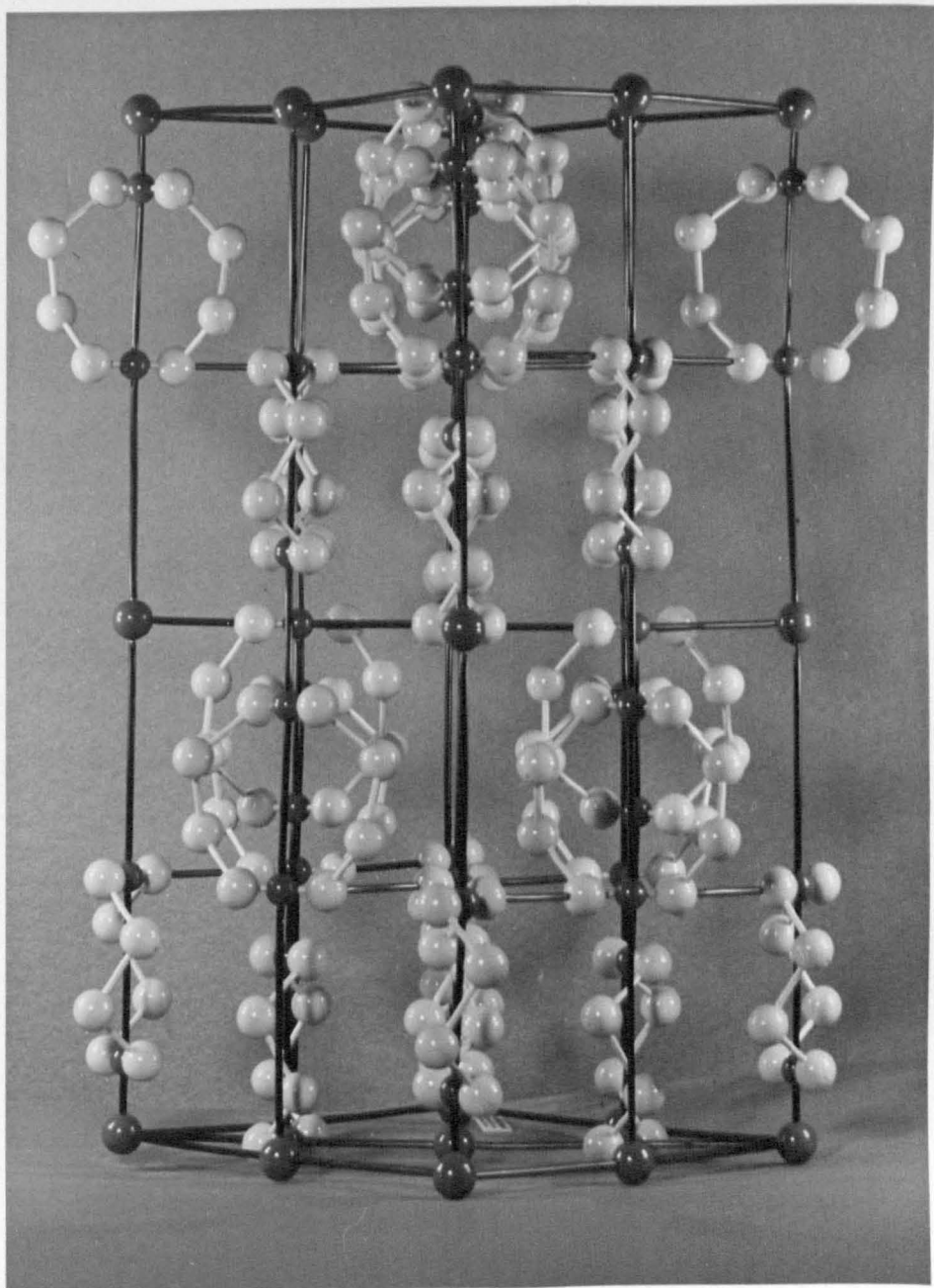


Figure 1.2 Simplified diagram of unit cell of orthorhombic sulphur.





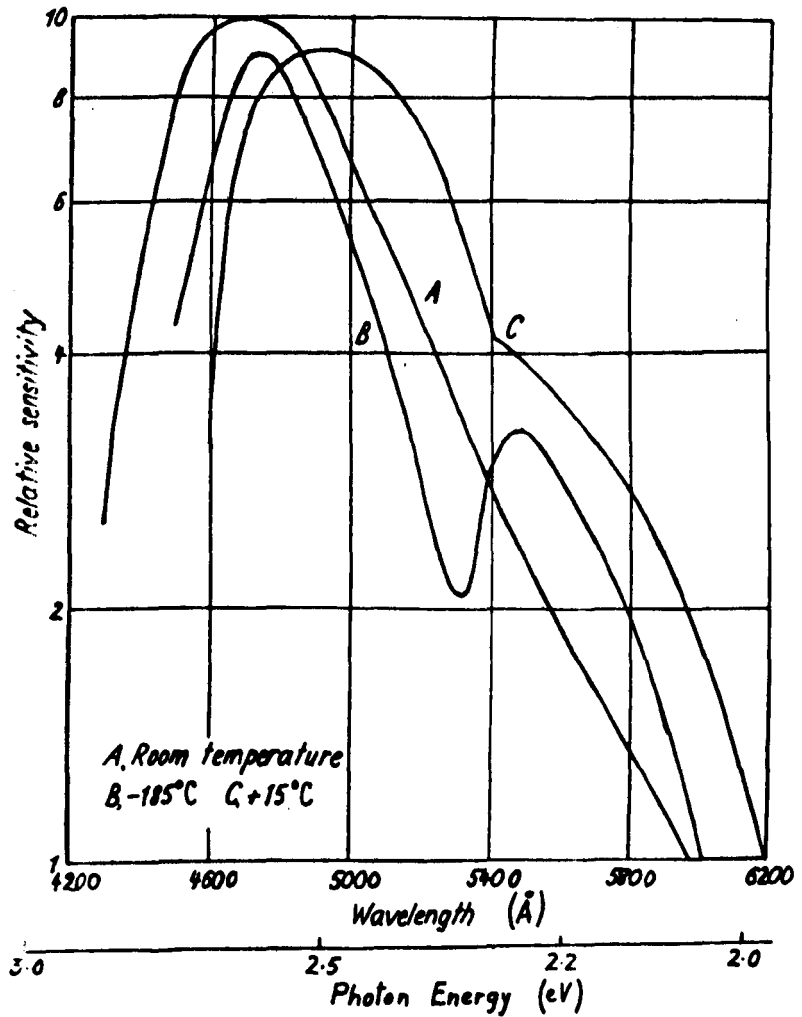


Figure 1.4. Spectral sensitivity of photocurrent after Kurrelmeyer, (A), and Tartakovsky & Rekalova, (B & C).

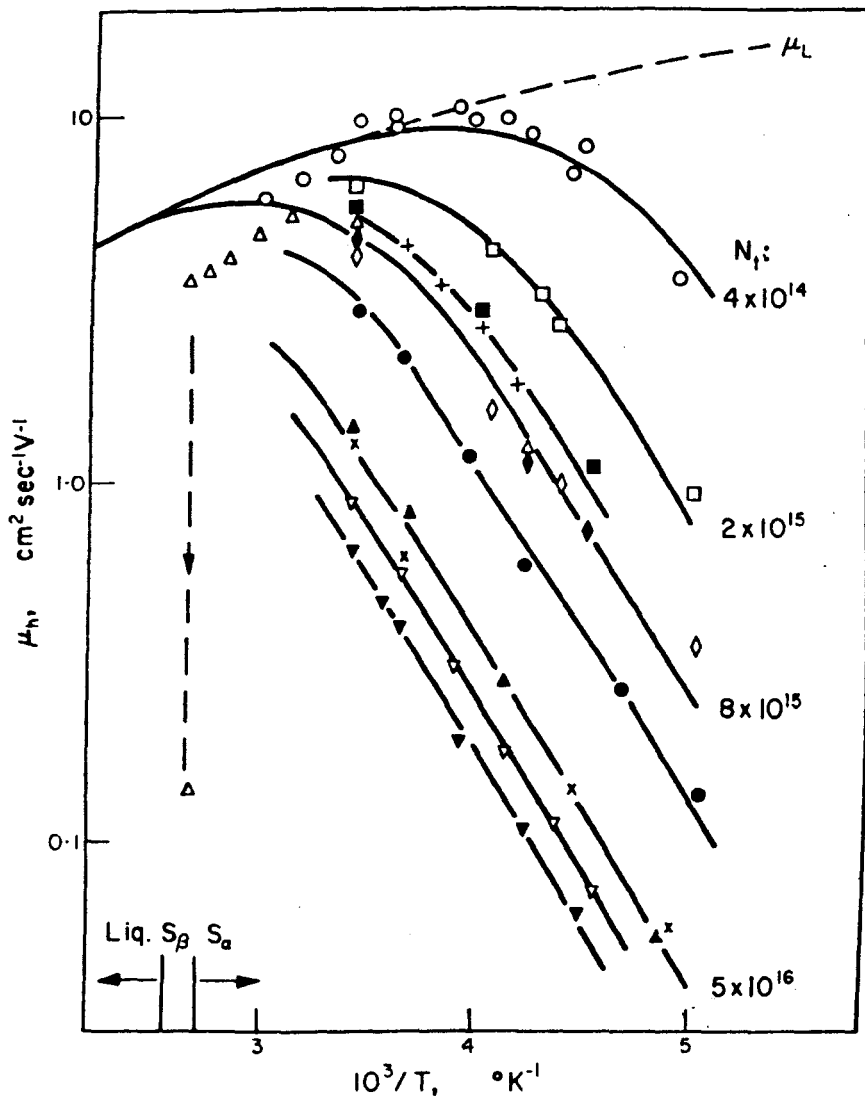


Figure 1.5 Temperature dependence of hole mobility μ_h according to Adams & Spear; μ_L is the lattice mobility. The solid curve was calculated using the values of N_t indicated.

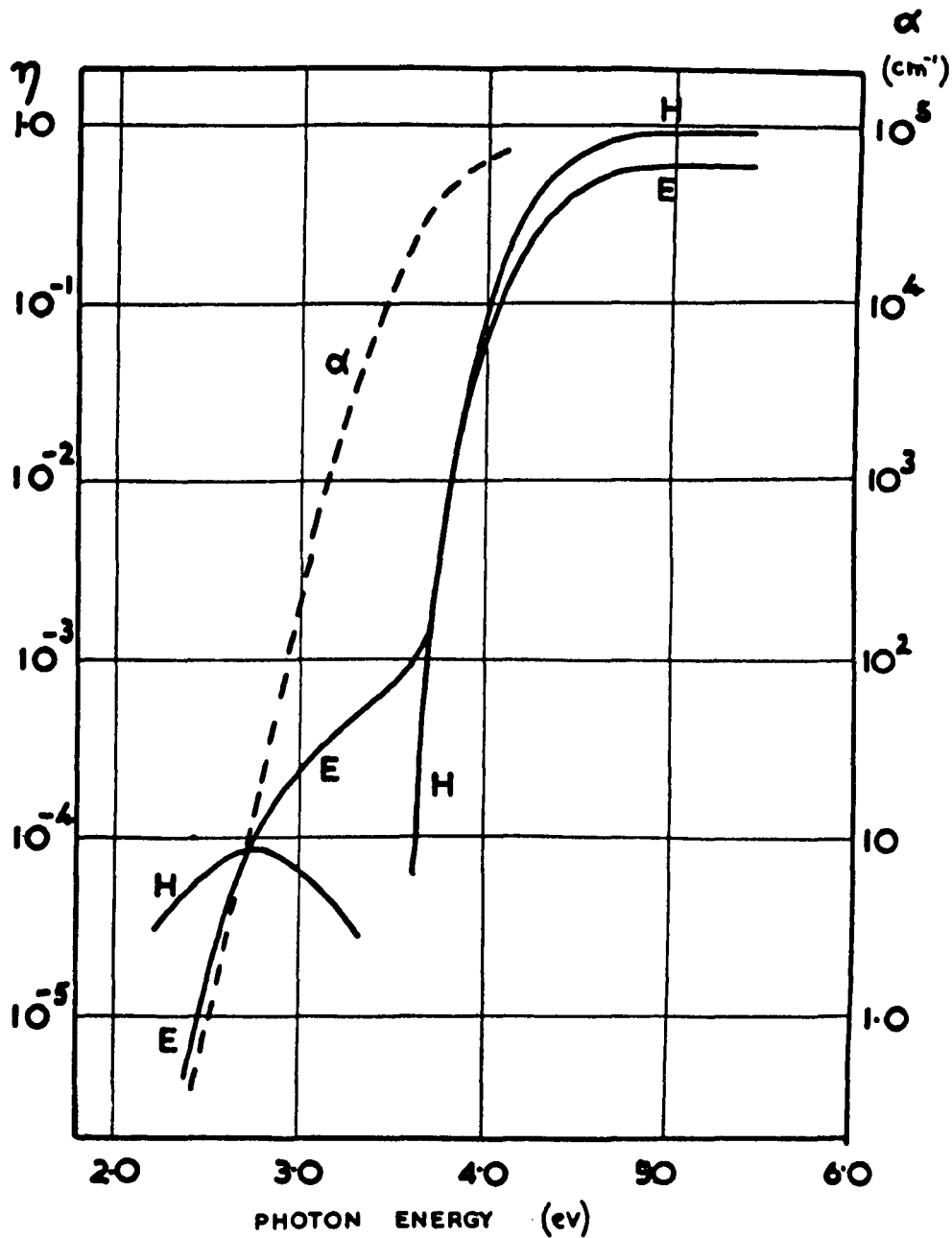


Figure 1.7 Optical absorption, α , and photoconductivity according to Spear & Adams. η is the generation efficiency for holes, (H), and electrons, (E), in carriers per incident photon.

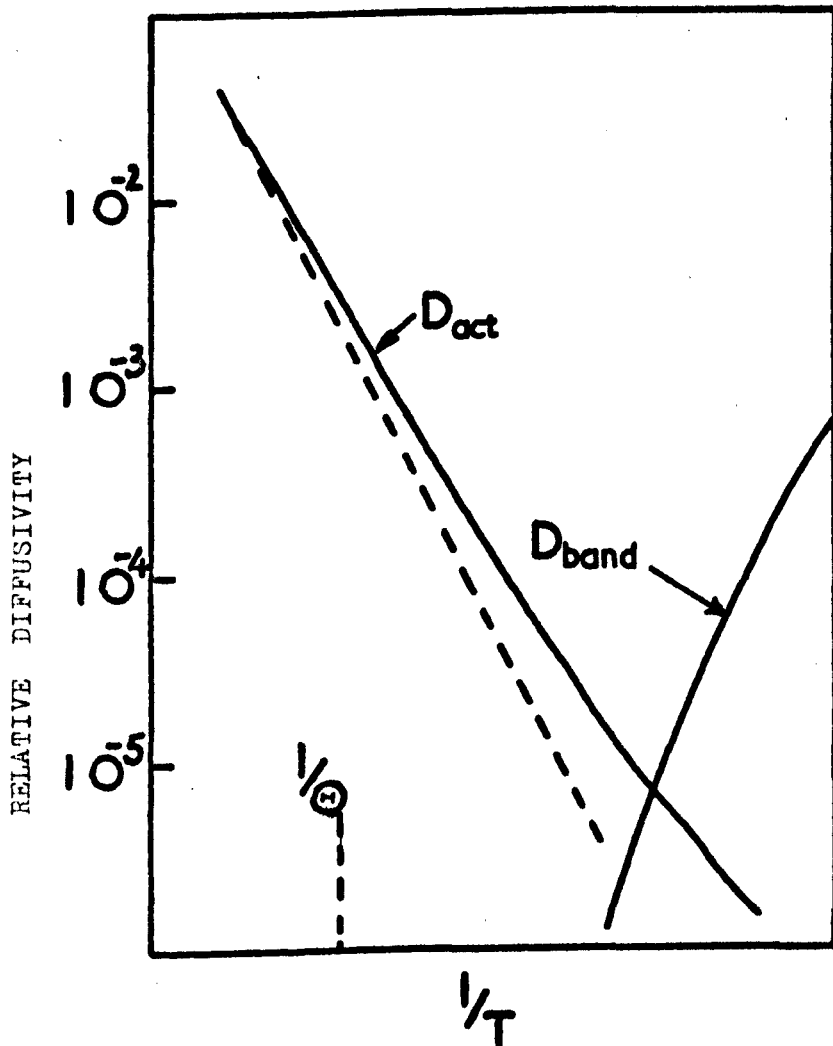


FIGURE 2.3

Polaron diffusivity versus temperature. The solid curves labelled ' D_{act} ' and ' D_{band} ' represent the contributions from random site jumps and polaron band motion respectively. The dashed curve gives the classical approximation to D_{act} .

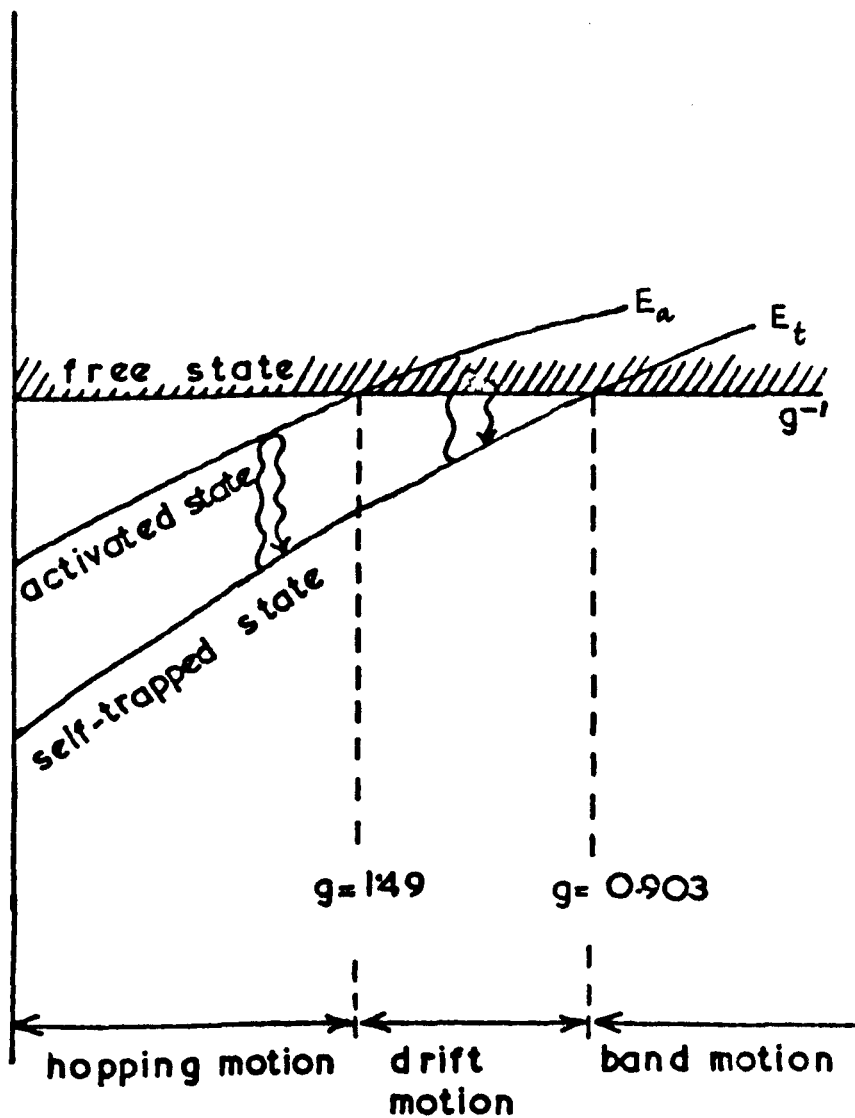


FIGURE 24

Energies of the self-trapped states relative to that of the free state according to Toyozawa.

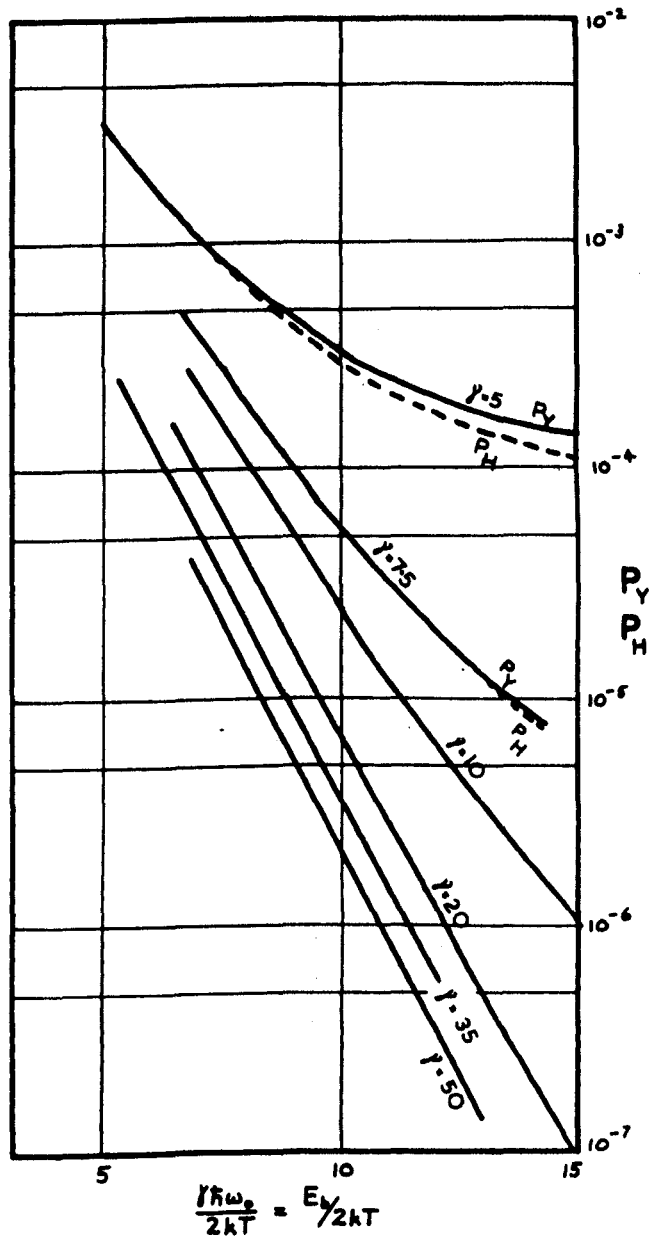


Figure 2.5 Carrier transition probability to an adjacent site as a function of temperature according to Holstein, (P_H), and Yamashita & Kurosawa, (P_Y), with γ as a parameter.

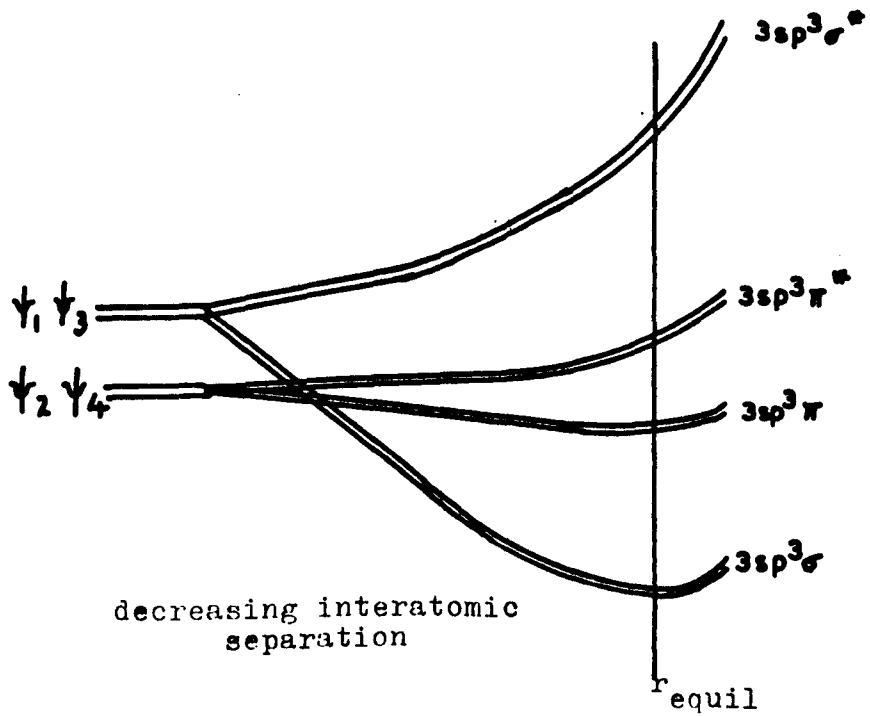


Figure 3.1

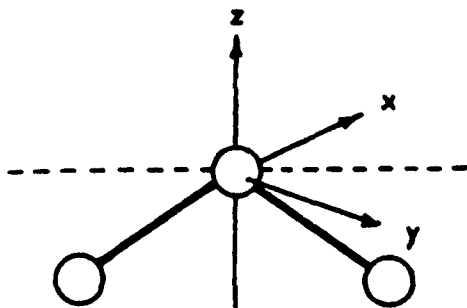


Figure 3.2

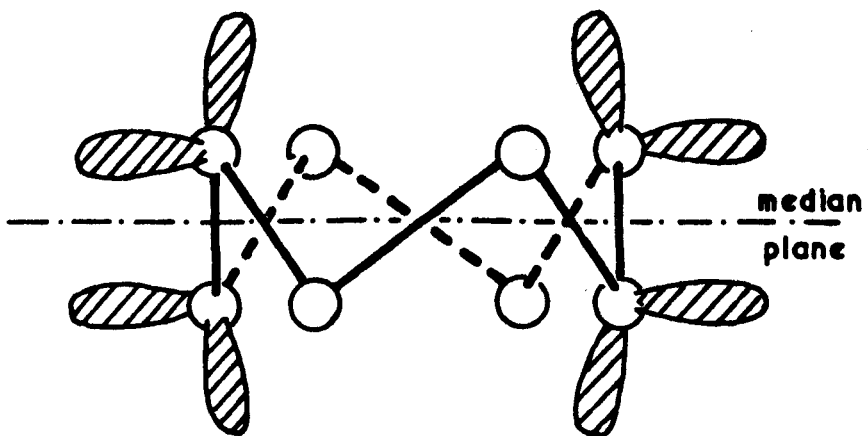


Figure 3.3 Diagram of S₈ molecule showing orientation of lone pair orbitals.

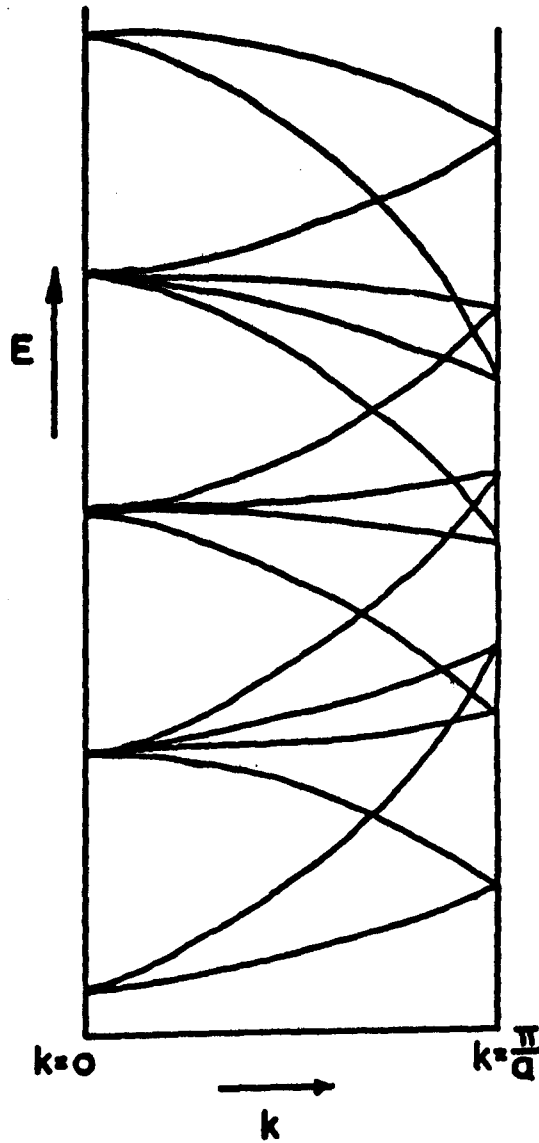


Figure 3.6 Energy band structure in a^{-1} direction of k space .

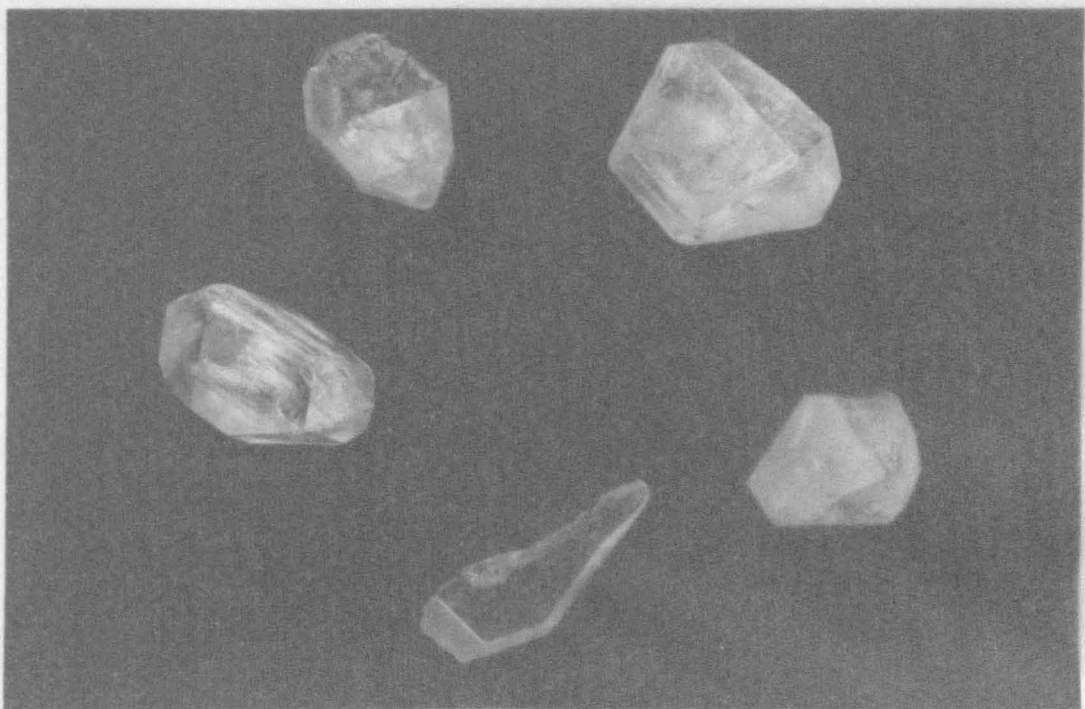
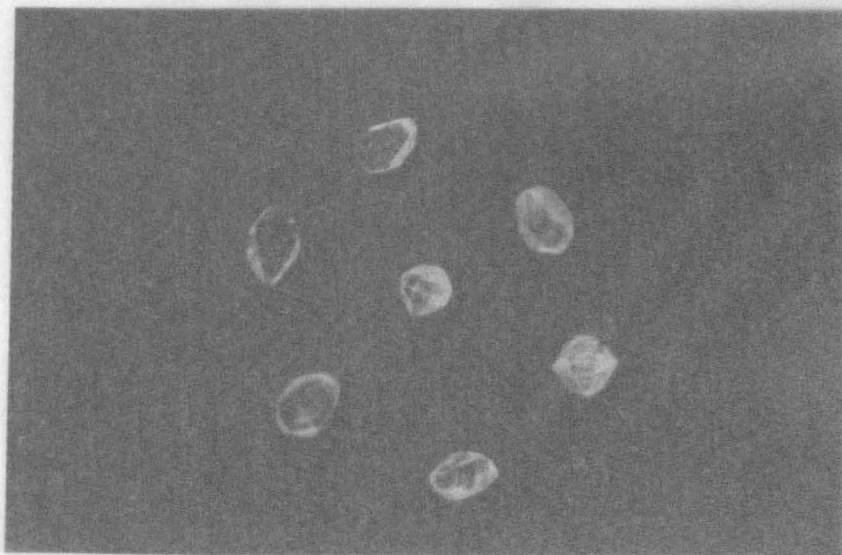
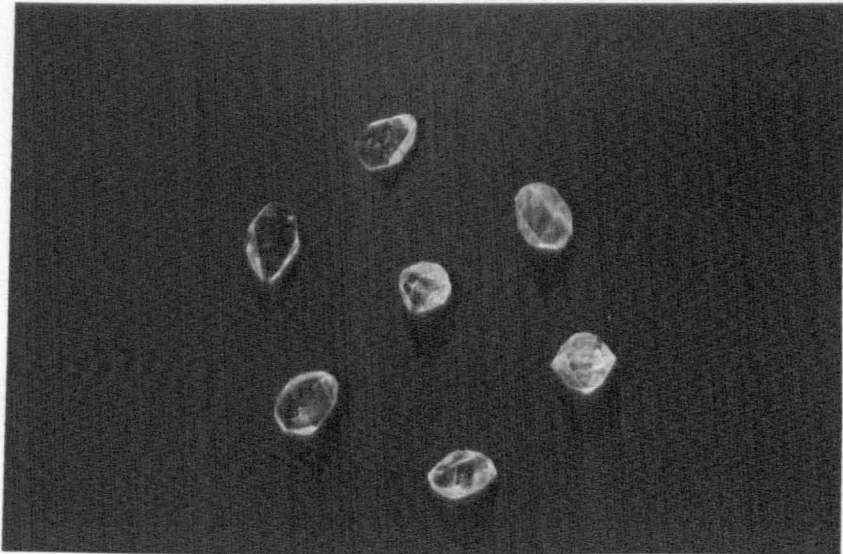
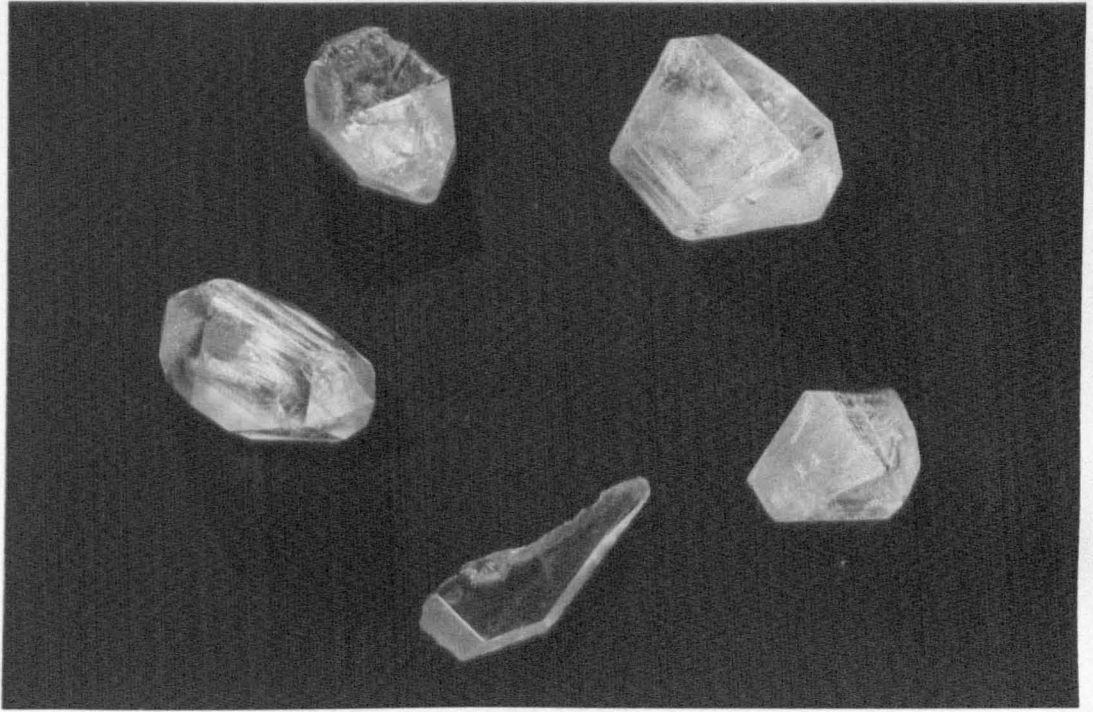


Figure 4.1. Photographs of crystals grown from solution in CS_2 showing well-developed (111) and (113) faces; (actual size).





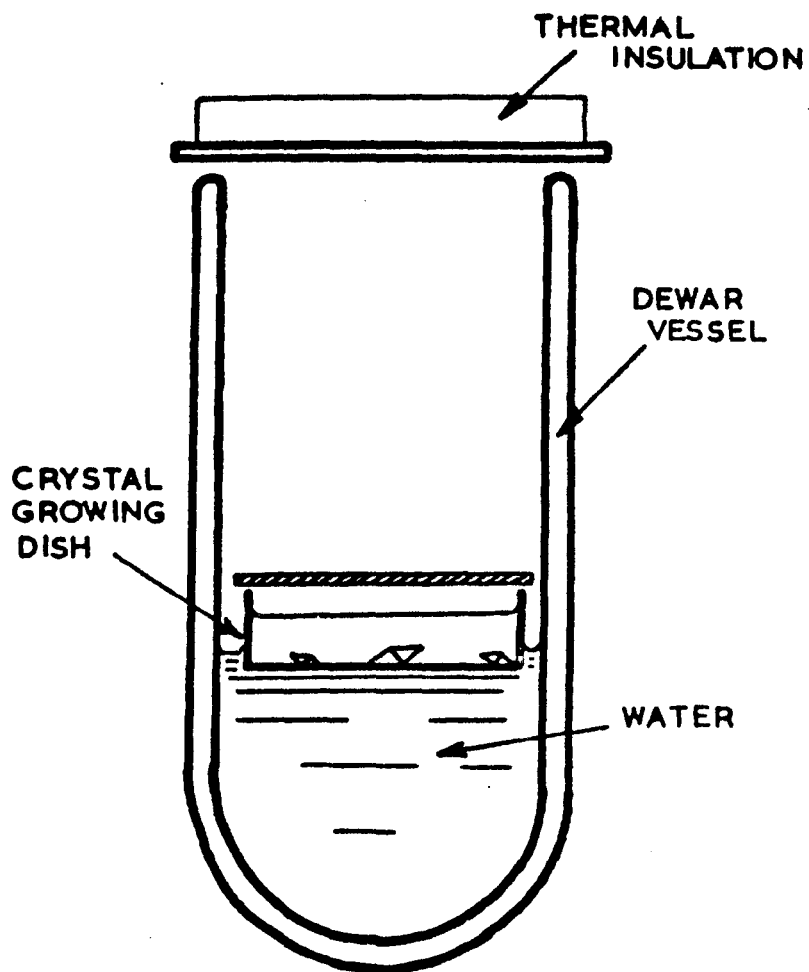
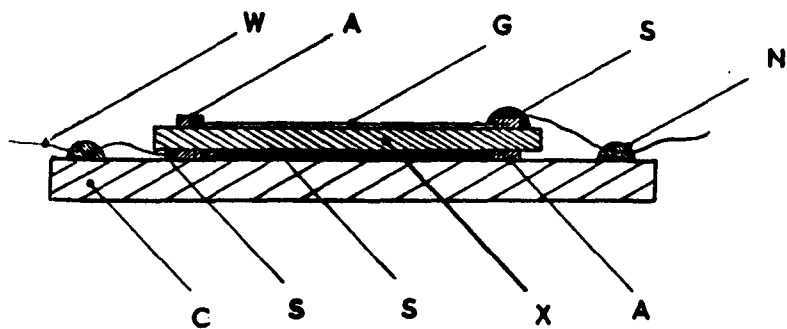


Figure 4.2 Apparatus used for growing single crystals from solution .



- A AQUADAG RING CONTACT
- C GLASS MICROSCOPE COVER SLIP
- G SEMITRANSSPARENT GOLD CONTACT
- N NITROCELLULOSE CEMENT
- S SILVER PASTE
- W THIN COPPER WIRE
- X CRYSTAL

Figure 4.4 Single crystal specimen
prepared and mounted for transport
measurements.

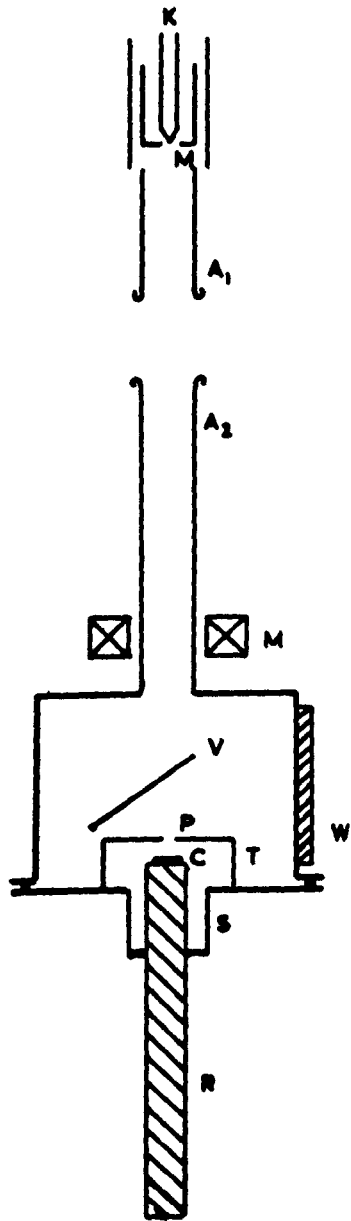


Figure 4.7 The electron bombardment gear and specimen holder

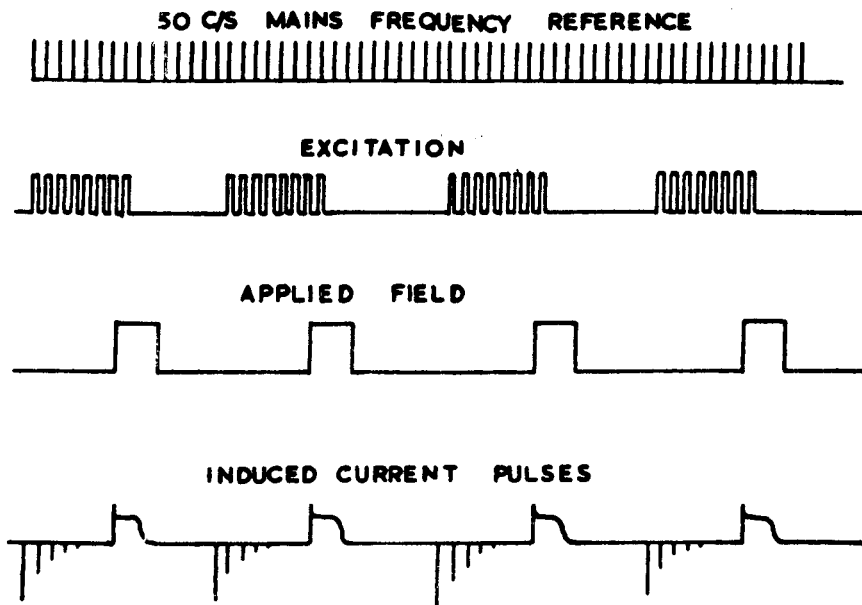


FIGURE 4-8

Relative positions of the field and excitation pulses for the observation of normal electron transits.

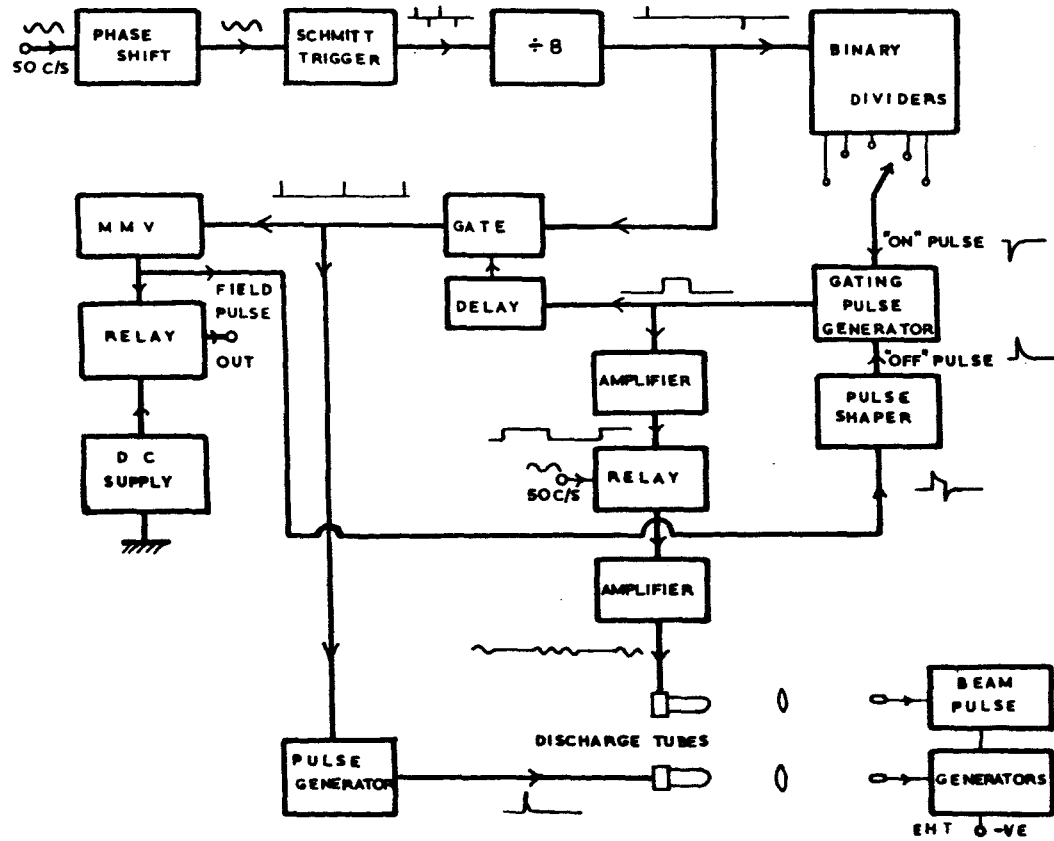


Figure 4.9 Block diagram of Master Pulse Unit

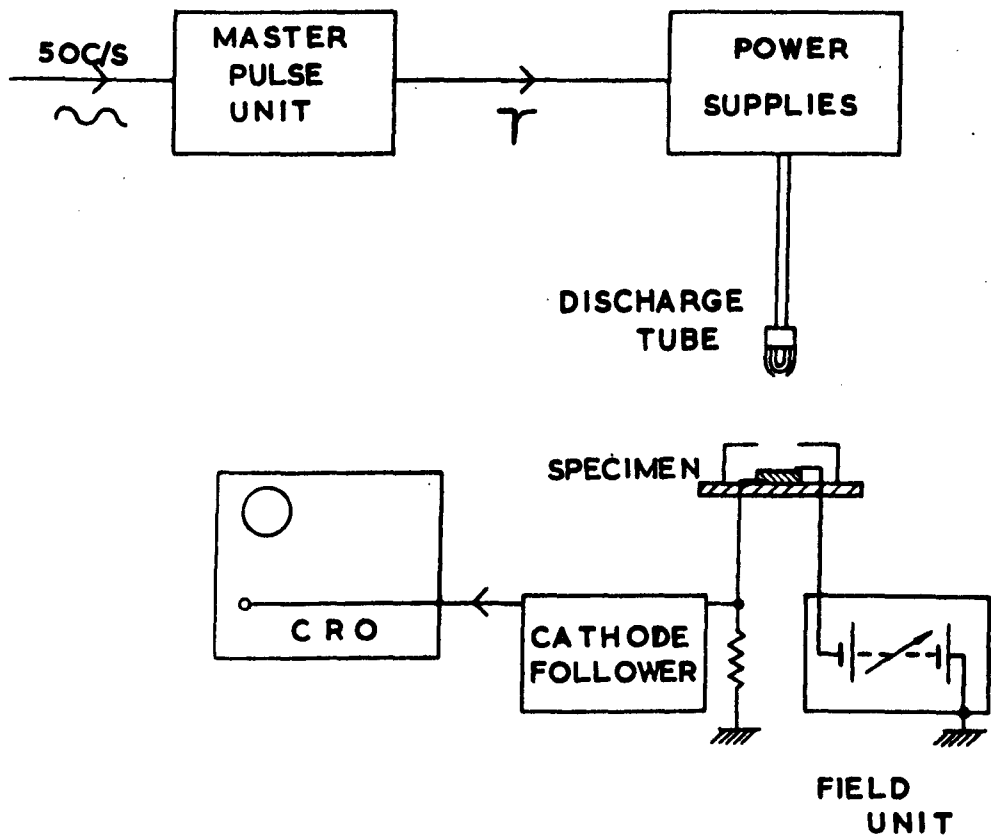


Figure 4.10 Block diagram of arrangement used for experiments employing photoexcitation.

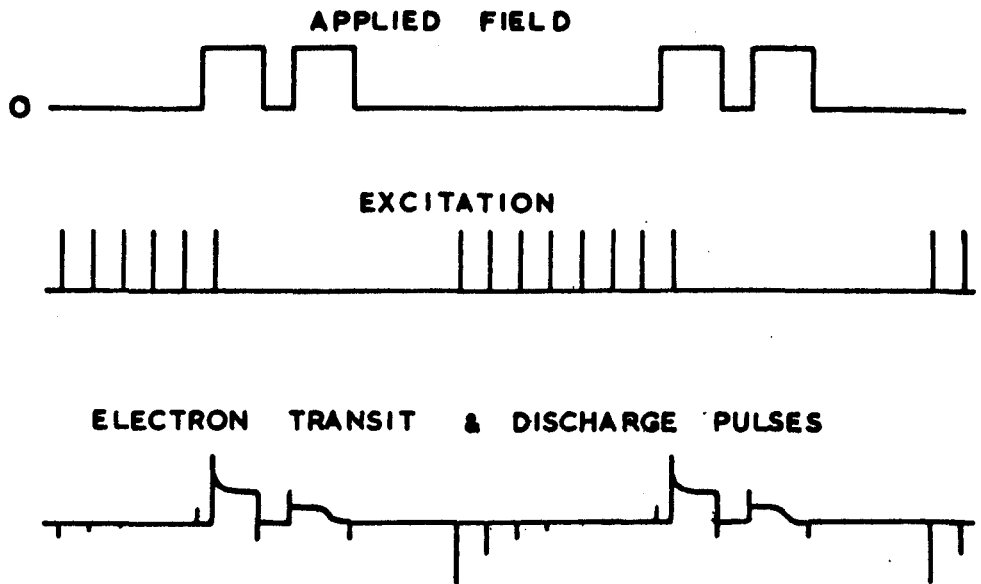


FIGURE 4-11

The relative positions of the field and excitation pulses for the observation of interrupted transits.

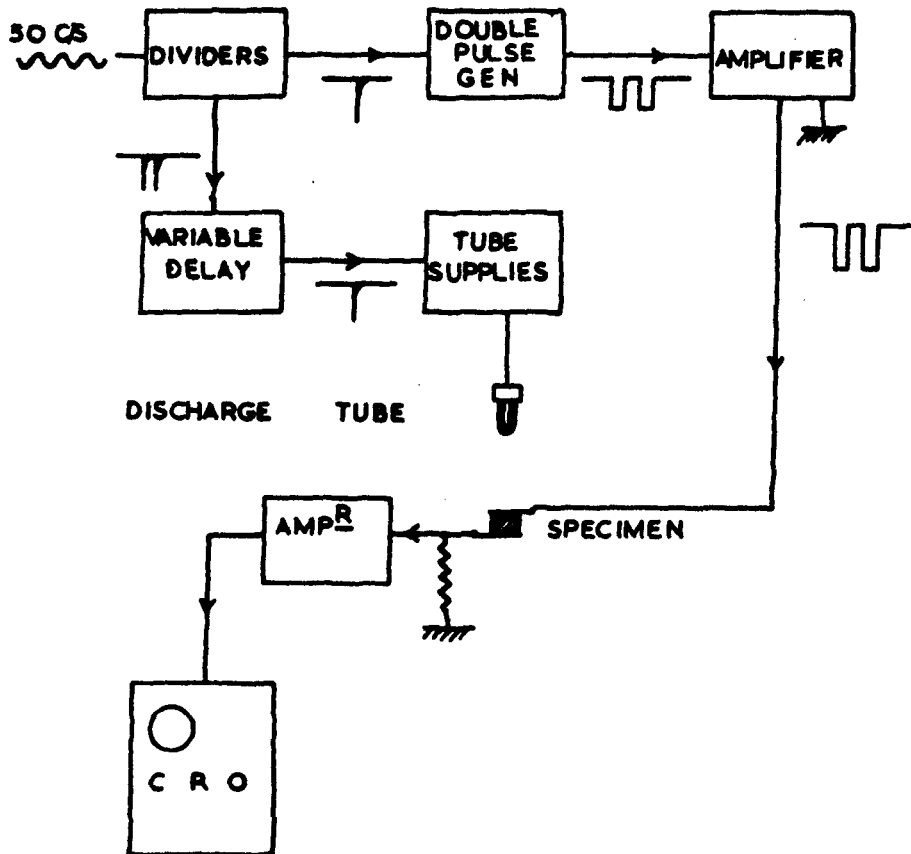


FIGURE 4-12

Block diagram of the circuit and experimental arrangement used for the observation of interrupted transits.

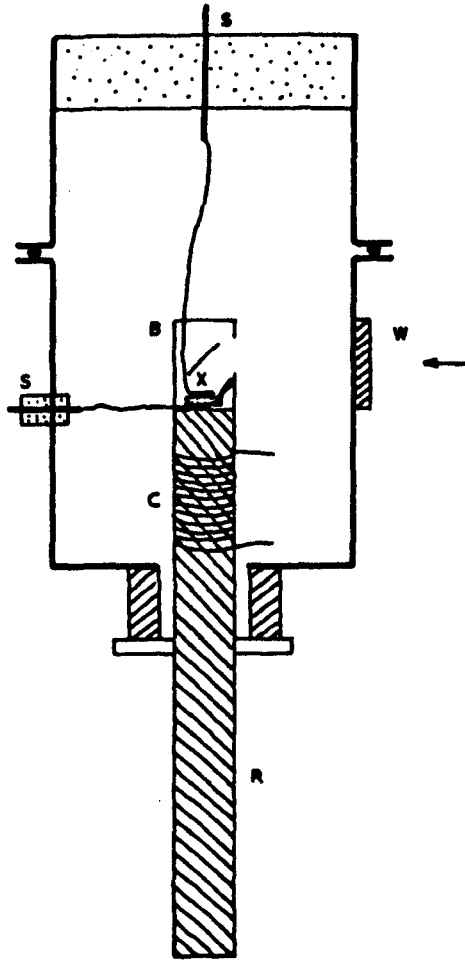


Figure 4.13 Specimen holder used for thermally stimulated conductivity. R, copper rod; C, heating coil; B copper box; X, crystal; W, silica window; S, insulated vacuum seals.

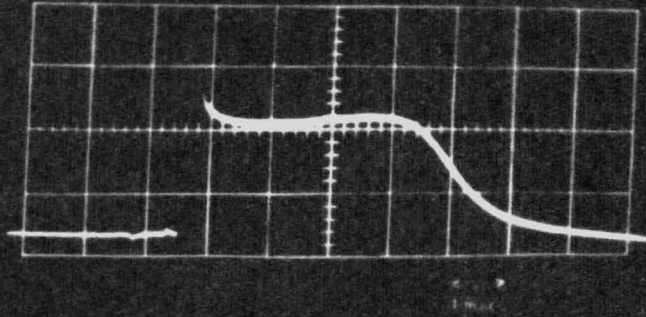


Figure 5.1. Typical electron transit current pulse for low intensity excitation.

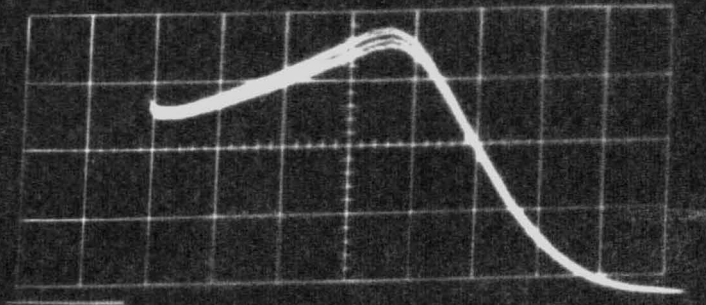


Figure 5.2. Transient SCL electron current pulse for high intensity excitation.

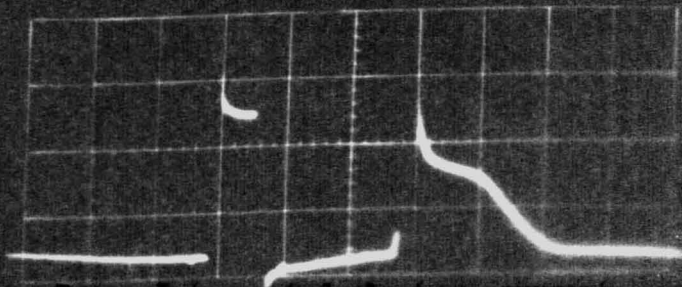
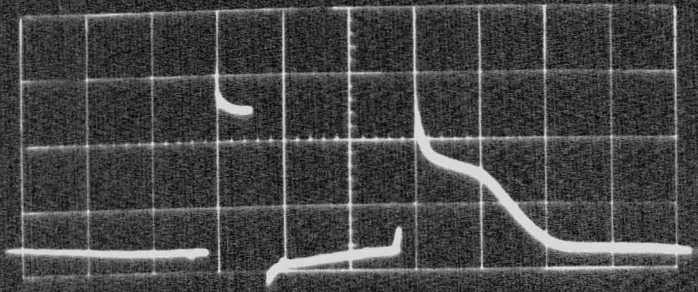
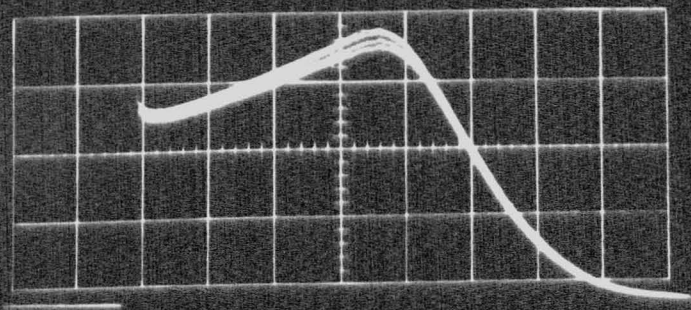
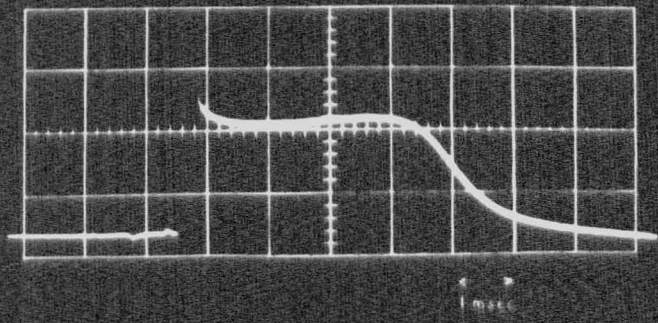


Figure 5.3. Interrupted electron current pulse.

Figure 5.1. Typical electron transit current pulse for low intensity excitation.

Figure 5.2. Transient SCL electron current pulse for high intensity excitation.

Figure 5.14. Interrupted electron current pulse.



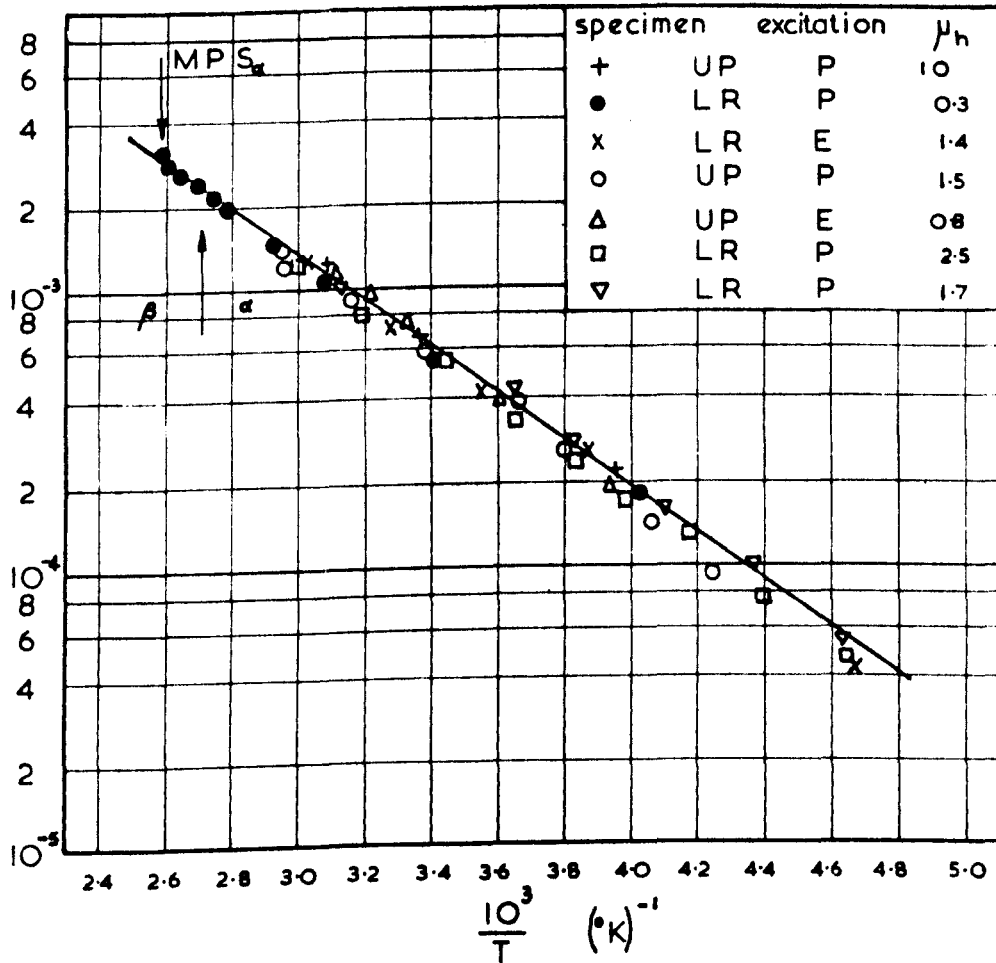


Figure 5.3 Temperature dependence of electron mobility in seven specimens of (111) orientation grown from ultra-pure, (UP), and laboratory reagents, (LR).
 E - electron excitation; P - photon excitation

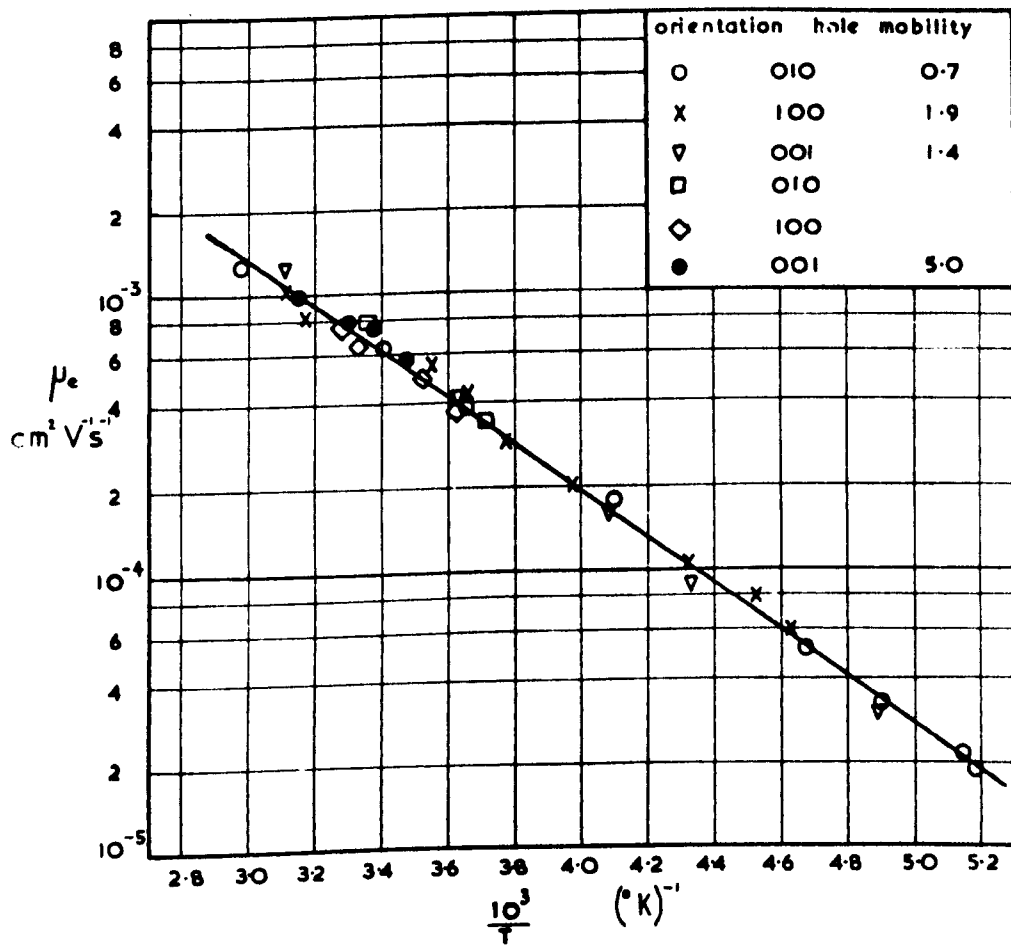


Figure 5.4 Temperature dependence of electron mobility in principal directions.

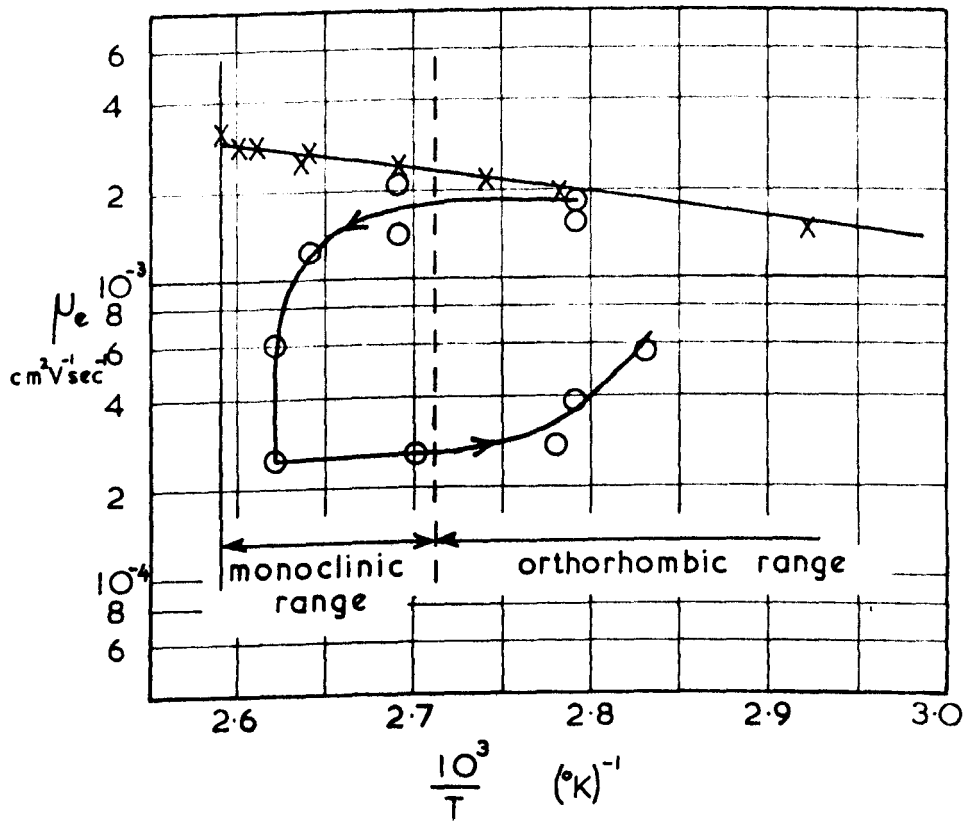


Figure 5.5 Electron mobility in the region of the monoclinic transition.

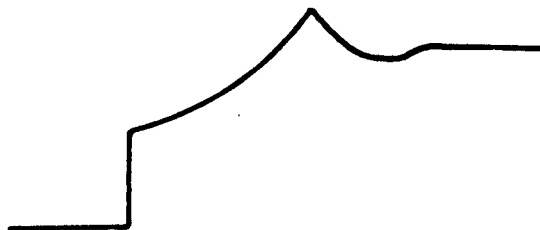


Figure 5.6 Shape of transient SCL current pulse in presence of continuous injection after $t = 0$ according to Many et al.

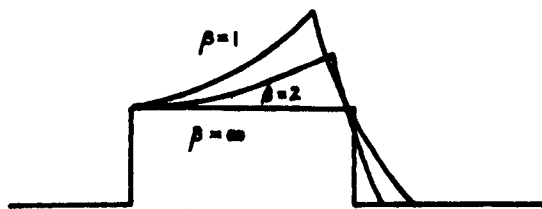


Figure 5.7 Shape of transient SCL current pulse in absence of injection from the electrodes according to Papadakis.

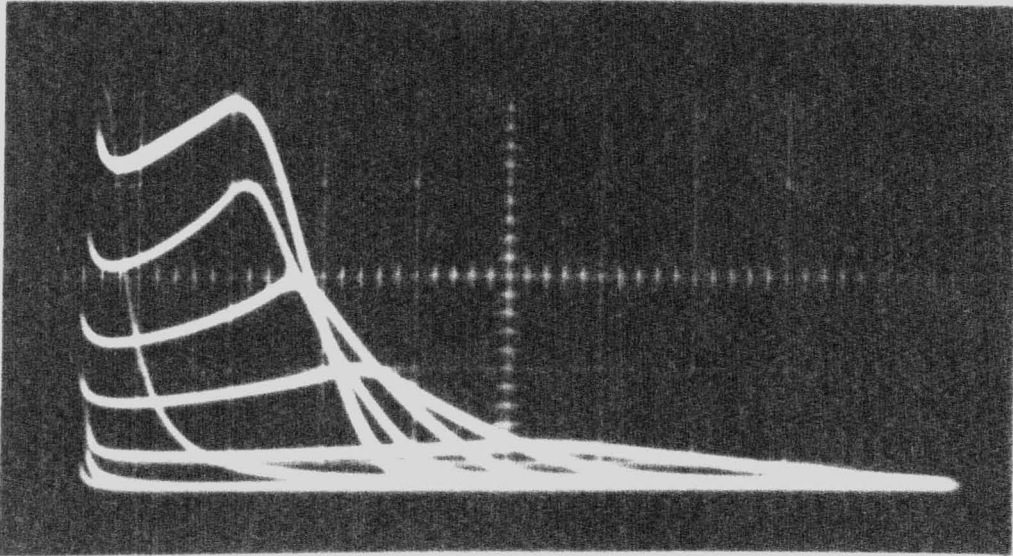


Figure 5.8(a) Transient SCL current pulses for several values of applied field.

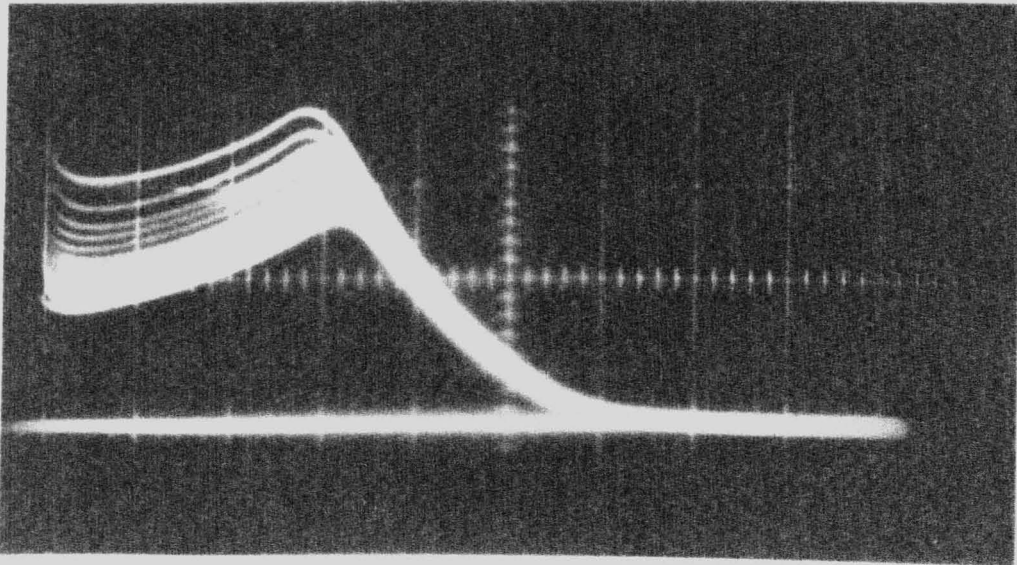
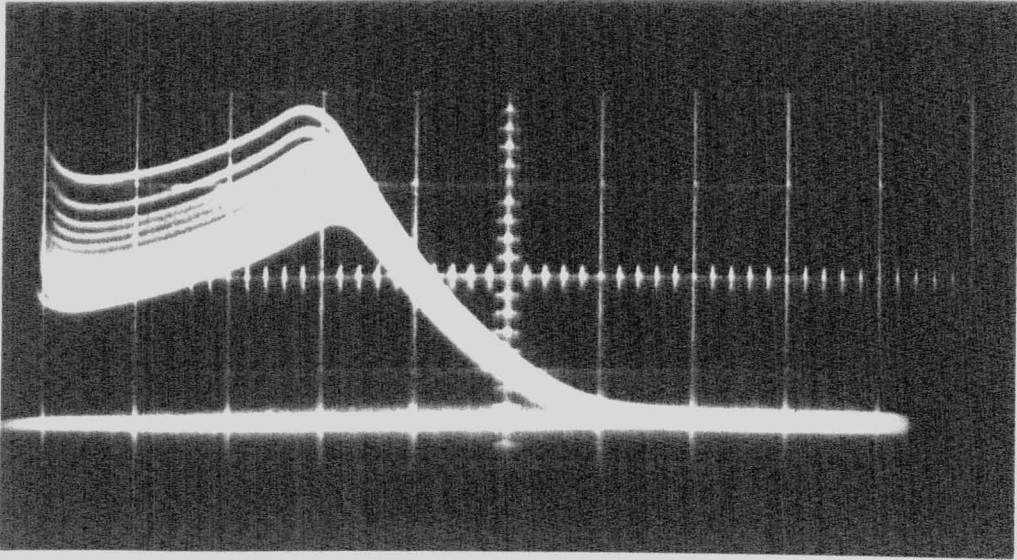
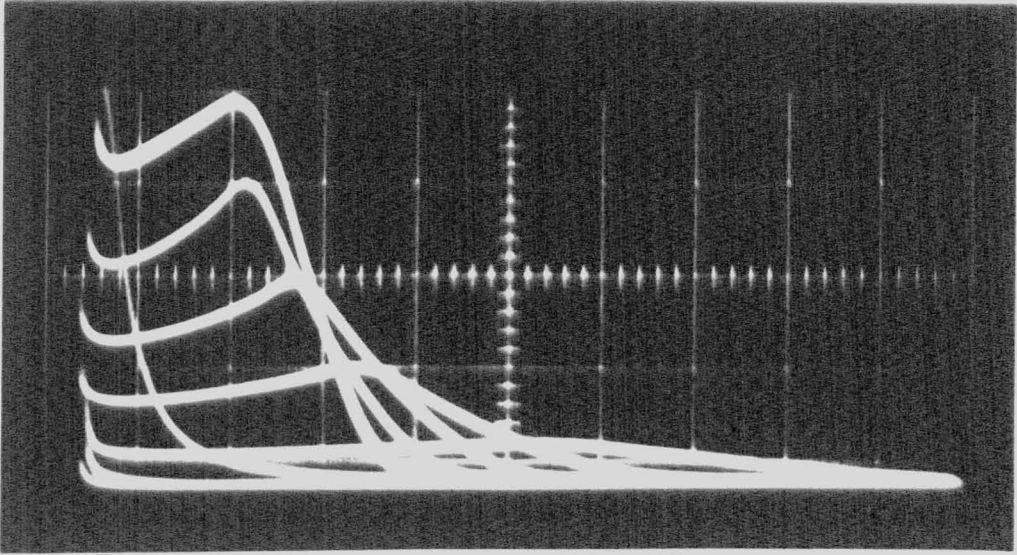


Figure 5.8(b) Successive transient SCL current pulses in absence of space-charge neutralization between pulses.



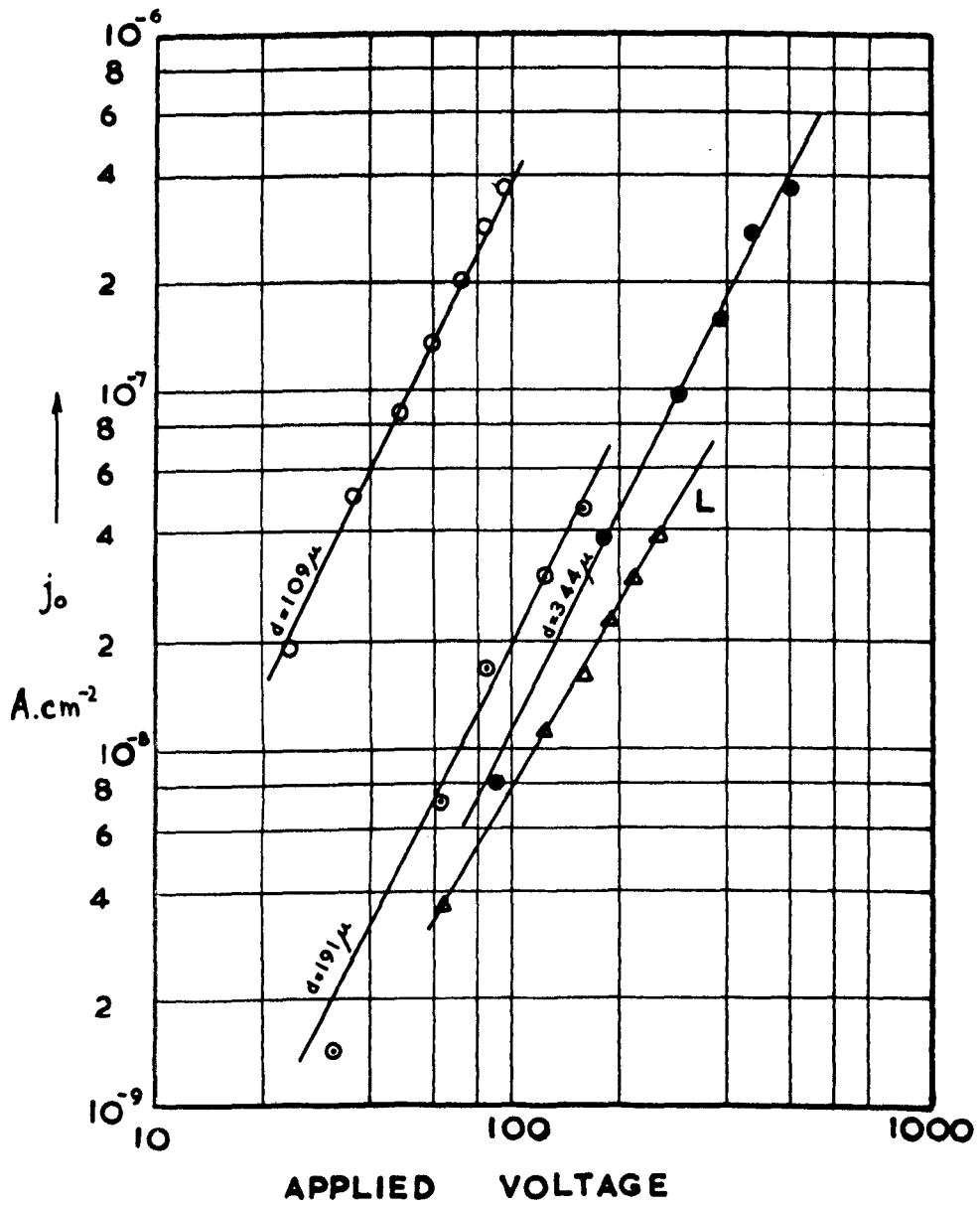


Figure 5.9 Initial value of SCL electron current density versus applied voltage after short flash excitation. L = low intensity flash.

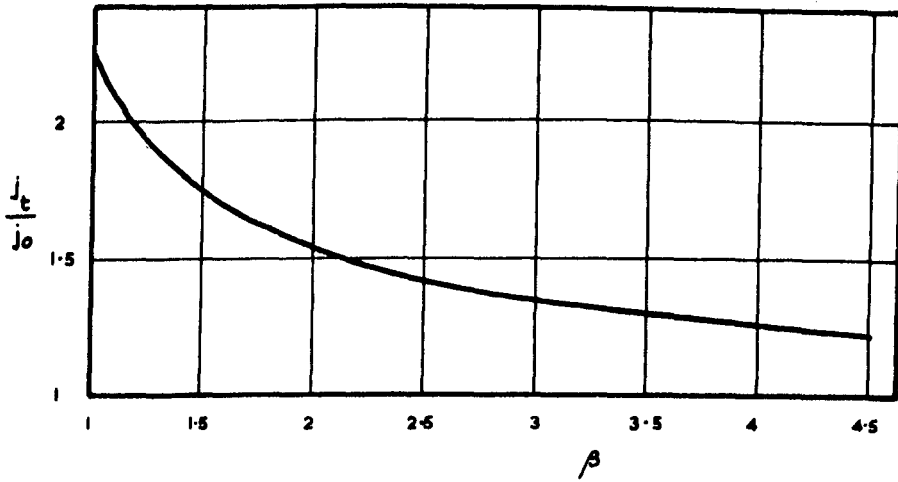


Figure 5.10 Ratio of peak to initial value of conduction current as function of parameter, β , according to Papadakis.

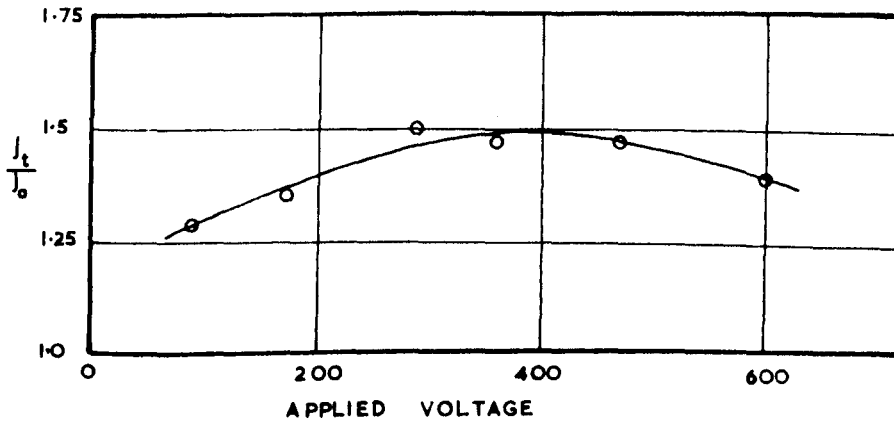


Figure 5.11 Experimentally determined ratio of electron current at peak to its initial value as a function of applied voltage.

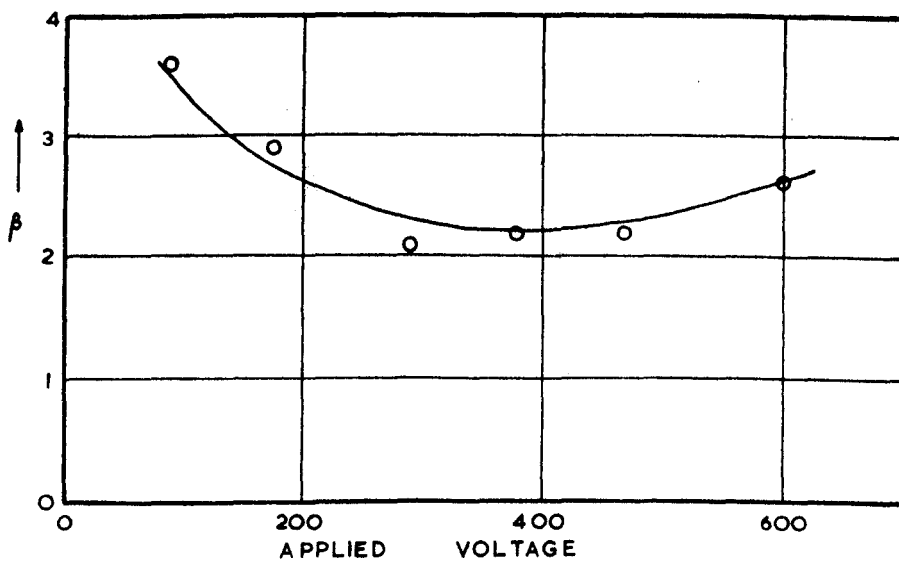


Figure 5.12 Ratio of applied field to space-charge field, β , as function of applied voltage derived from the results of figure 5.11.

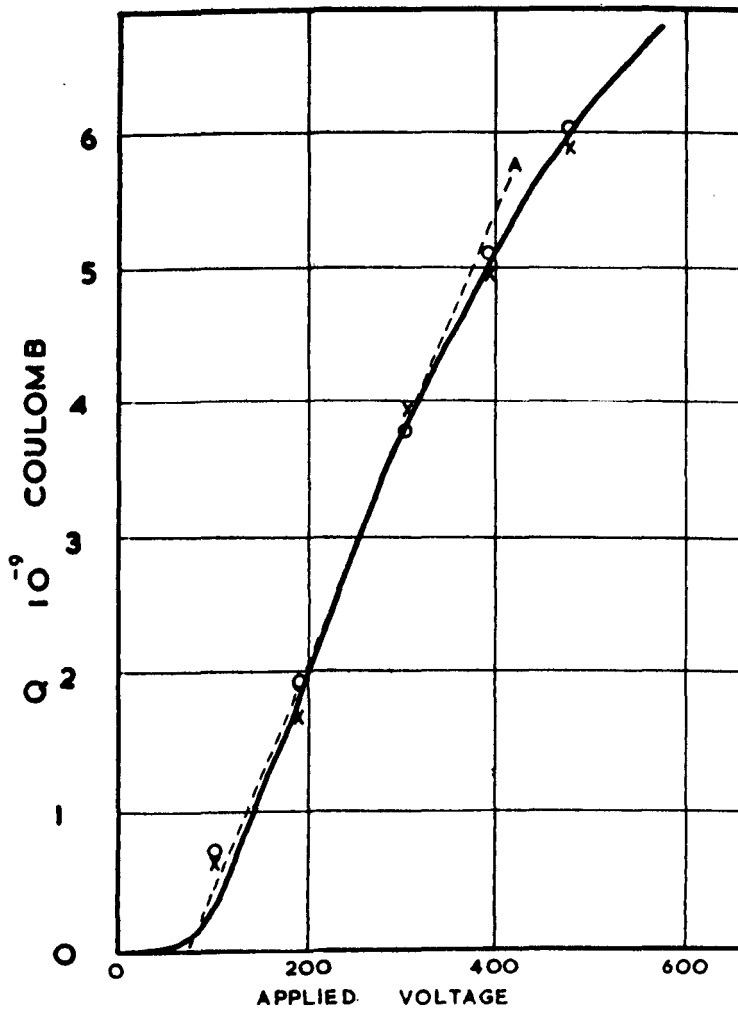


Figure 5.13 Total charge, Q , drawn out of generation region as function of applied voltage. X , obtained from area beneath current pulse; O , from derived value of β . The solid line is a plot of equation (5.3).

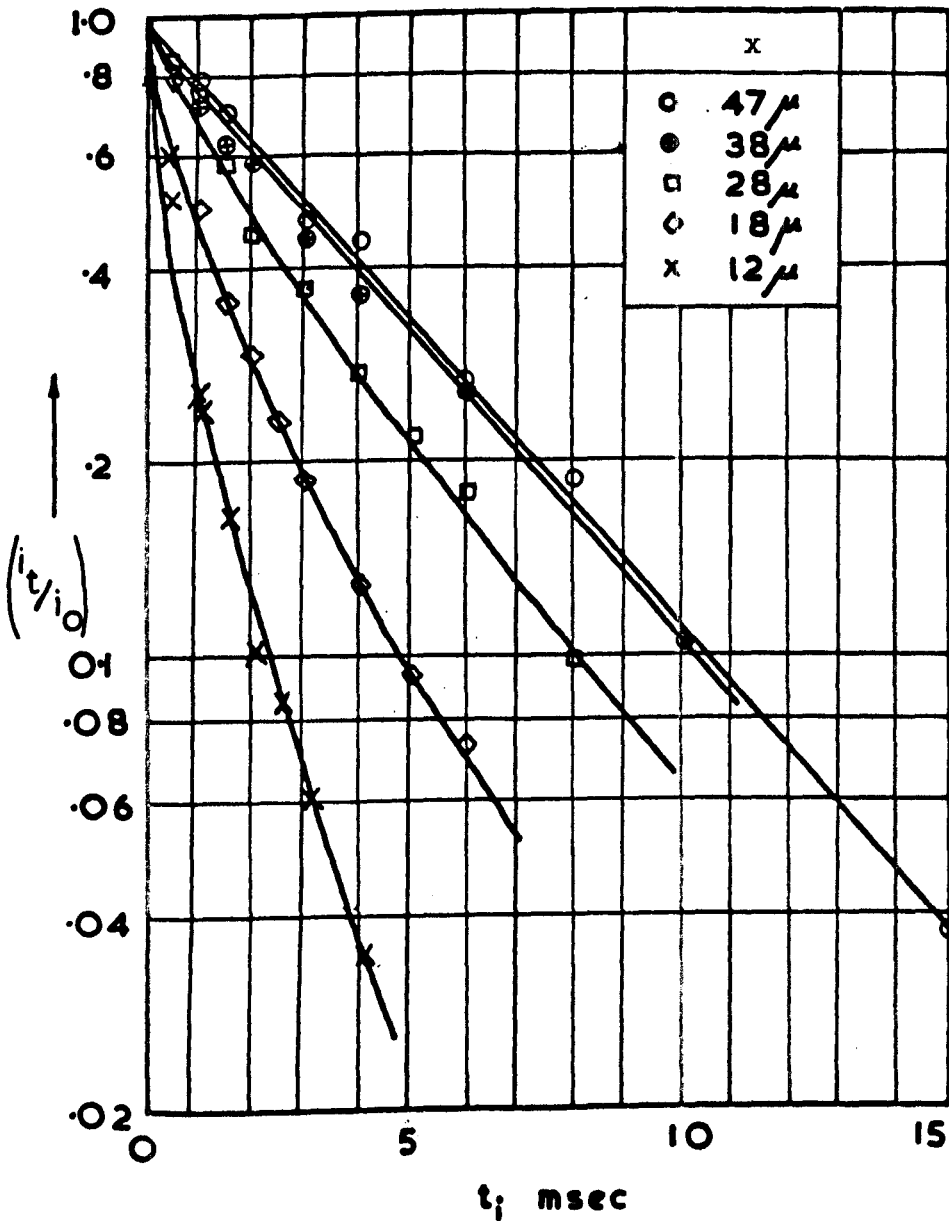


FIGURE 5-15

Electron decay as a function of time at various distances x from the surface region.

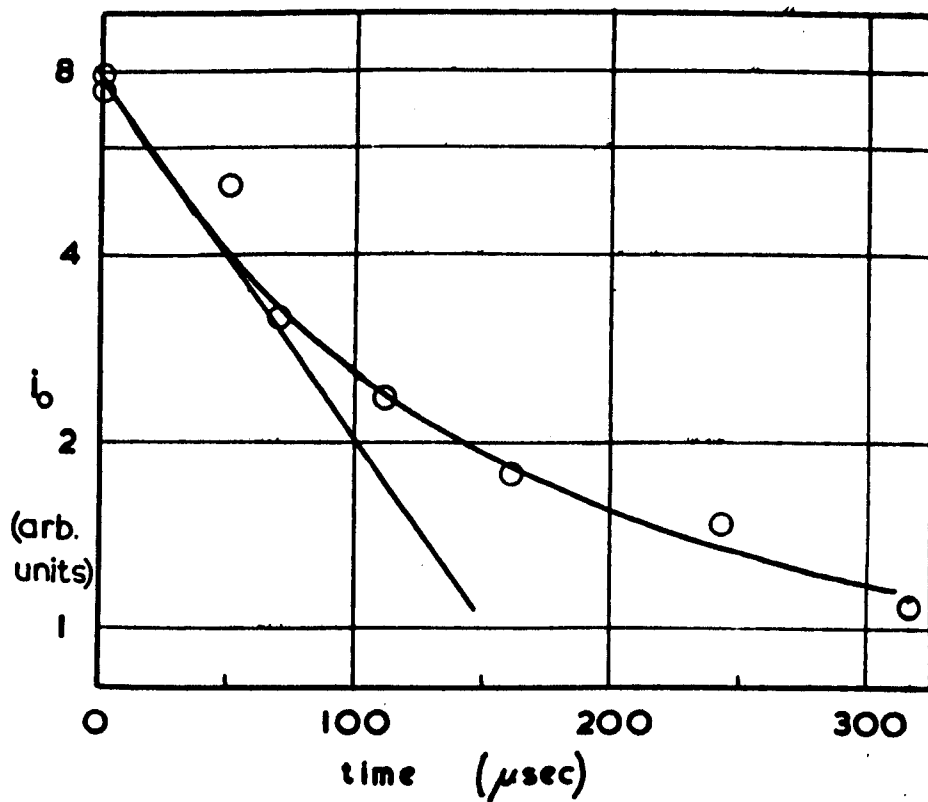


Figure 5.16 Initial value of electron current at various periods of time after surface excitation.

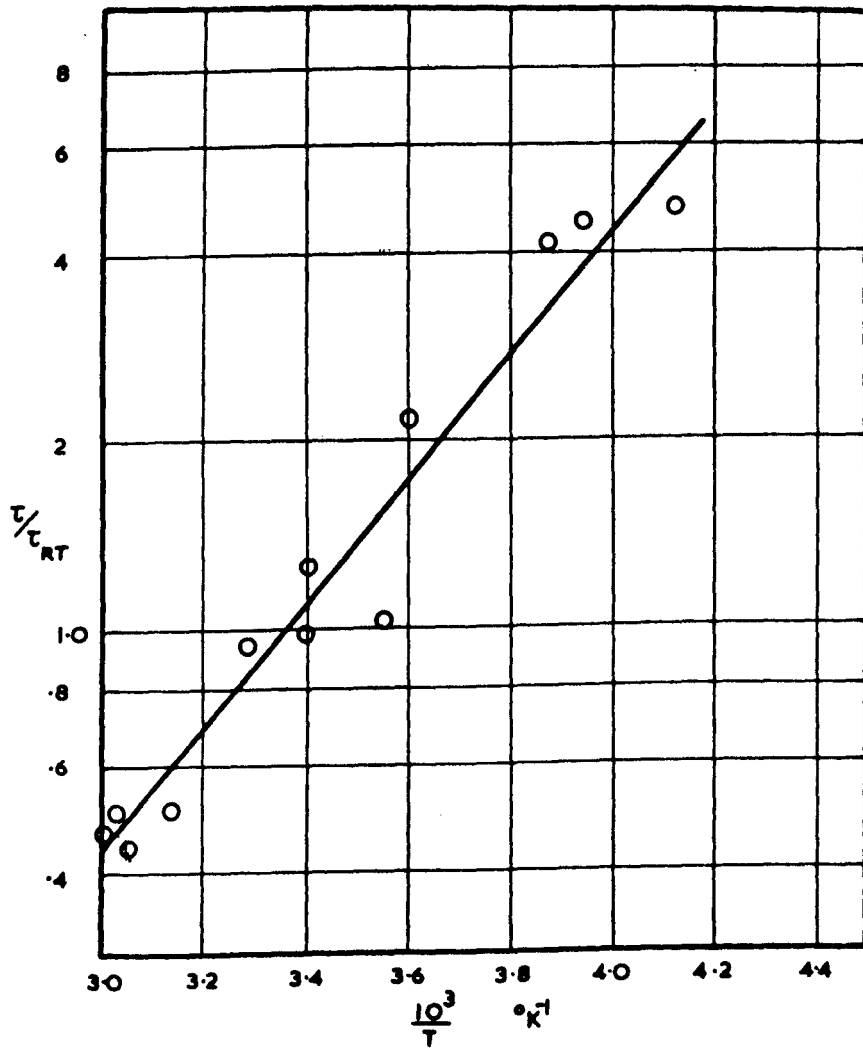


Figure 5.17 Temperature dependence of electron free lifetime in centre of a specimen 155 microns thick.

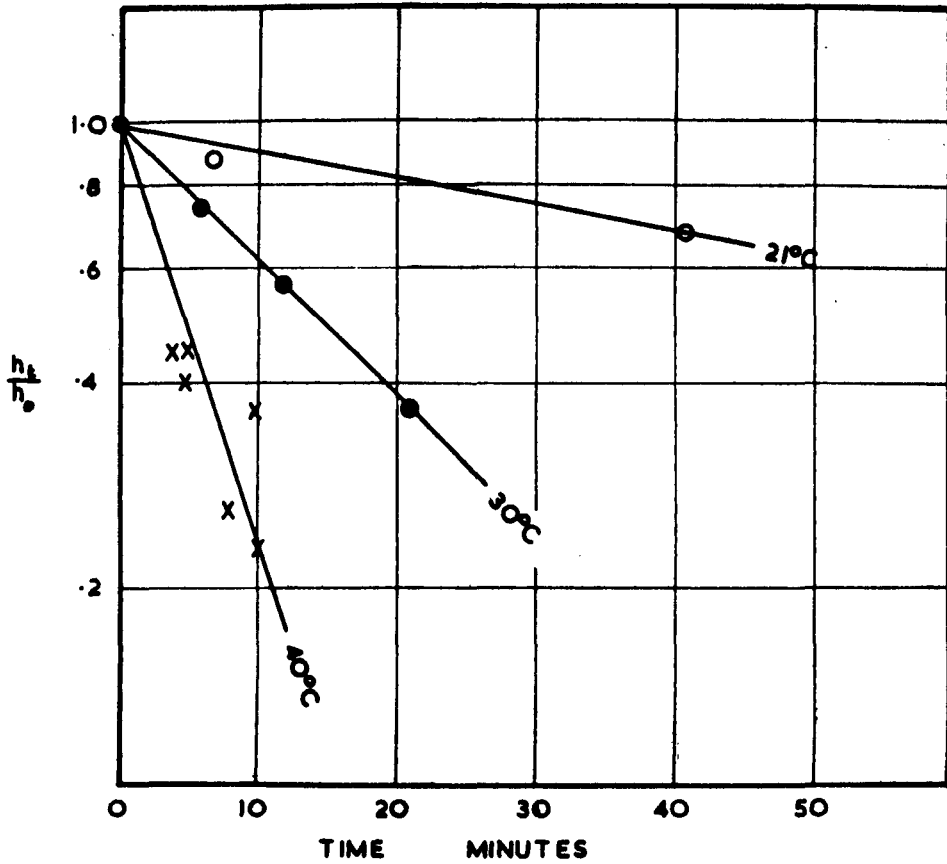


Figure 5.18 Polarization decay as a function of time. The vertical scale represents the ratio of the discharge pulse height to that obtained 20msec after polarization.

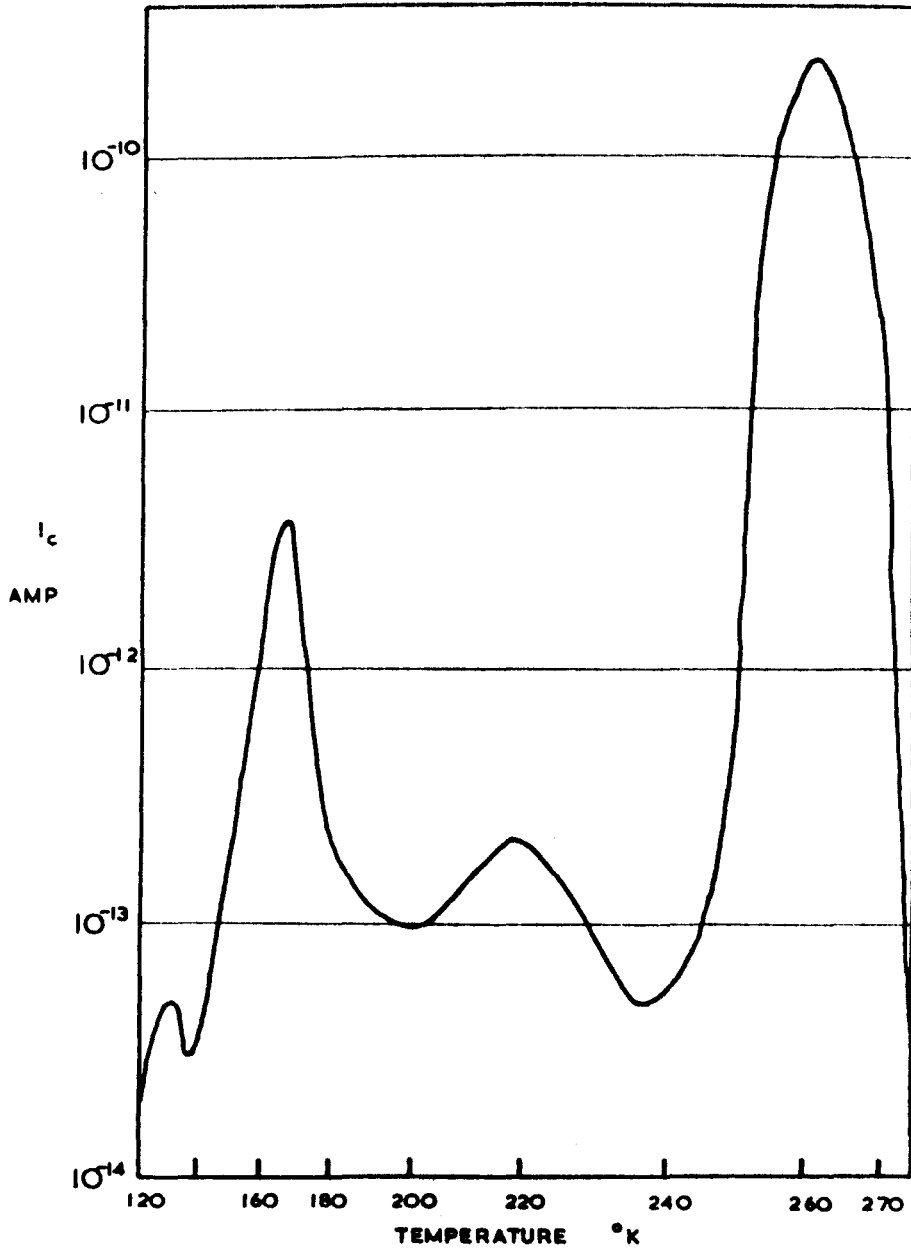


Figure 5.19 Representative conductivity glow curve for single crystal of S_u .

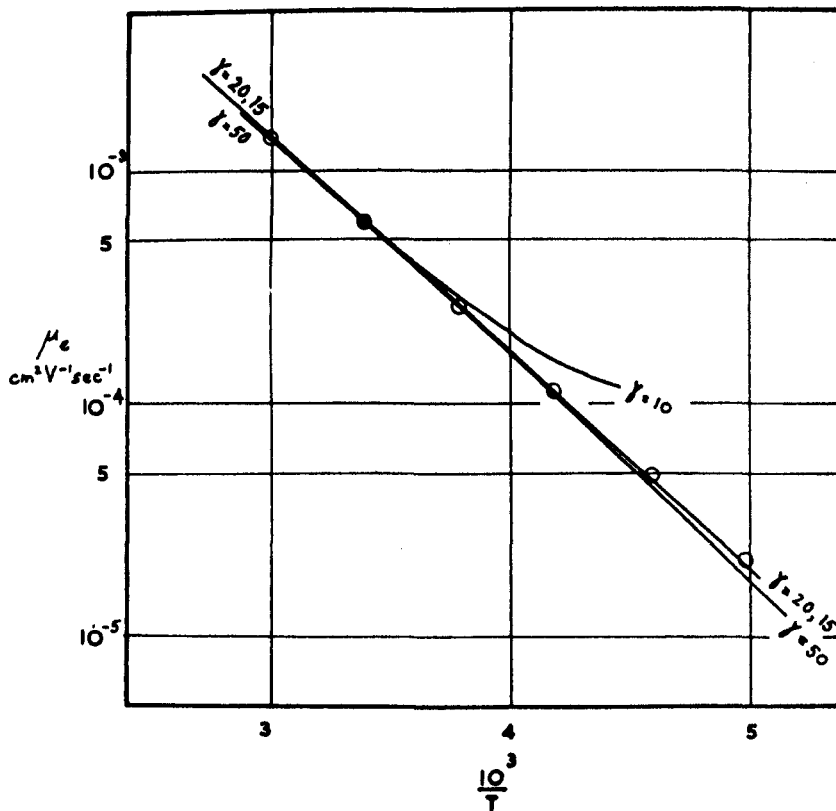


Figure 6.1 Form of the temperature dependence of mobility according to Holstein, equations (2.21) and (2.29), fitted to the experimental values at room temperature for four values of the interaction parameter, γ .

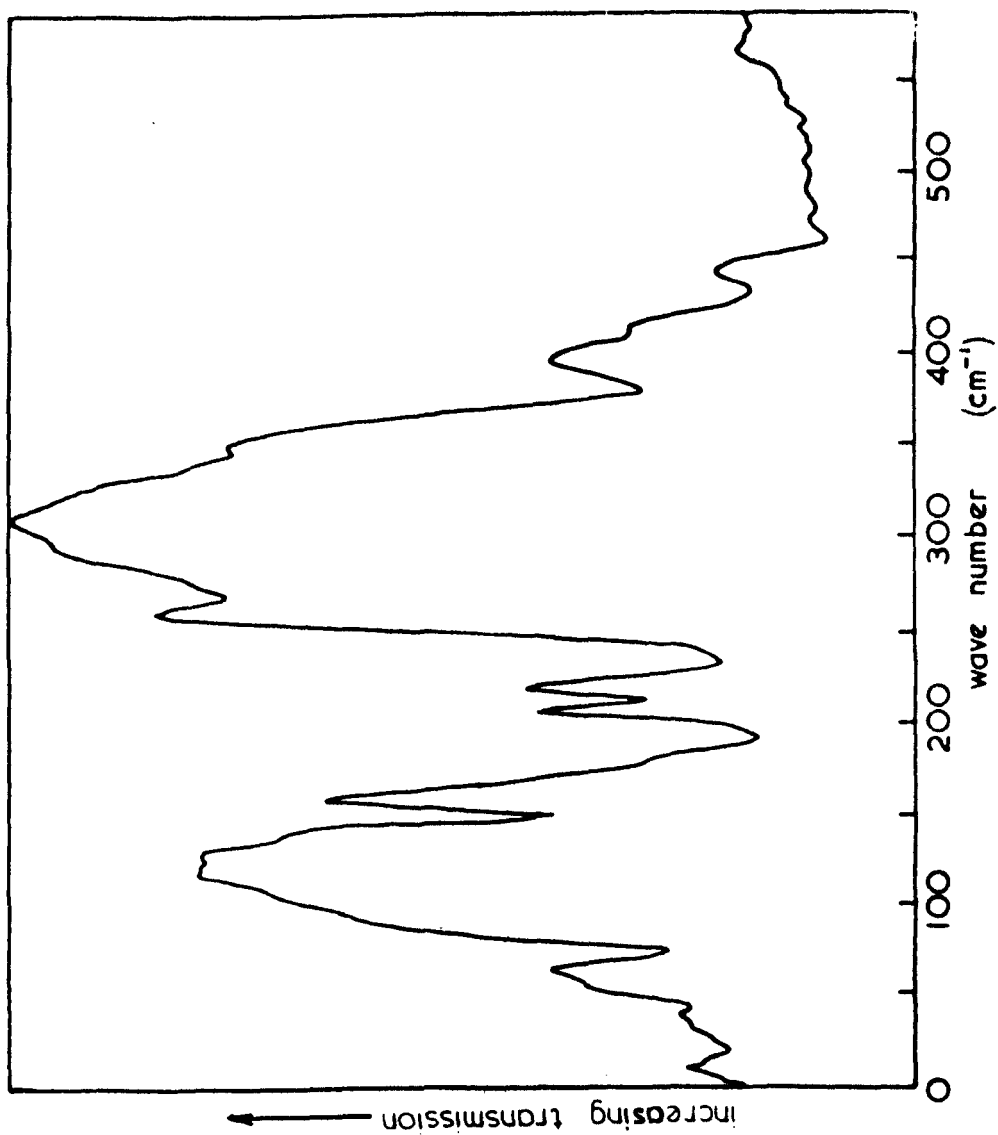


Figure 6.2 Infra red absorption spectrum of single crystal of orthorhombic sulphur.

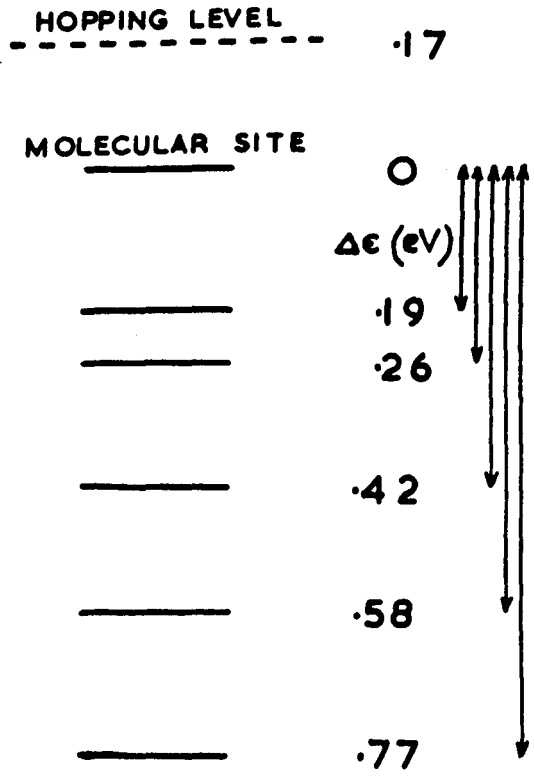


Figure 6.3 Positions of the electron traps relative to the energy of a molecular site.